VILNIUS UNIVERSITY

Gediminas Skvarnavičius

# Thermodynamic parameters in protein-ligand model systems: determination of binding volume and enthalpy

**DOCTORAL DISSERTATION**

Technological Sciences,
Chemical Engineering (T 005)

VILNIUS 2022

**Academic supervisor** – Dr. Vytautas Petrauskas (Vilnius University, Technological Sciences, Chemical Engineering –T 005).
**Academic consultant** – Prof. Dr. Daumantas Matulis (Vilnius University, Natural Sciences, Biophysics – N 011).

The doctoral dissertation will be defended in a public meeting of the Dissertation Defense Panel:

**Chairman** – Prof. Dr. Rolandas Meškys (Vilnius University, Technological Sciences, Chemical Engineering – T 005).
**Members:**
Dr. Rima Budvytytė (Vilnius University, Technological Sciences, Chemical Engineering – T 005),
Prof. Dr. Claus Czeslik (Technical University Dortmund, Natural Sciences, Biochemistry – N 004),
Dr. Kliment Olechnovič (Vilnius University, Natural sciences, Biochemistry – N 004),
Doc. Dr. Jolanta Sereikaitė (Vilnius University, Technological Sciences, Chemical Engineering – T 005).

The dissertation shall be defended at a public meeting of the Dissertation Defense Panel at 14:00 on 30th of August 2022 in auditorium R-401 of the Vilnius University Life Sciences Center.
Address: Saulėtekio 7, LT-10257, Vilnius, Lithuania
Tel. +37068646759; e-mail: gediminas.skvarnavicius@bti.vu.lt
The text of this dissertation can be accessed at the Library of Vilnius University, as well as on the website of Vilnius University:
www.vu.lt/lt/naujienos/ivykiu-kalendorius

https://orcid.org/0000-0003-2085-4313

VILNIAUS UNIVERSITETAS

Gediminas Skvarnavičius

# Termodinaminiai parametrai baltymų-ligandų modelinėse sistemose: jungimosi tūrio ir sąveikos energijos tyrimas

**DAKTARO DISERTACIJA**

Technologijos mokslai,
Chemijos Inžinerija (T 005)

VILNIUS 2022

**Mokslinis vadovas** – dr. Vytautas Petrauskas (Vilniaus universitetas, technologijos mokslai, chemijos inžinerija – T 005).
**Mokslinis konsultantas** – prof. dr. Daumantas Matulis (Vilniaus universitetas, gamtos mokslai, biofizika – N 011).

Gynimo taryba:
**Pirmininkas** – prof. dr. Rolandas Meškys (Vilniaus universitetas, technologijos mokslai, chemijos inžinerija – T 005).
**Nariai:**
dr. Rima Budvytytė (Vilniaus universitetas, technologijos mokslai, chemijos inžinerija – T 005),
prof. dr. Claus Czeslik (Dortmundo technikos universitetas, gamtos mokslai, biochemija – N 011),
dr. Kliment Olechnovič (Vilniaus universitetas, gamtos mokslai, biochemija – N 004),
doc. dr. Jolanta Sereikaitė (Vilniaus Gedimino technikos universitetas, technologijos mokslai, chemijos inžinerija – T 005).

Daktaro disertacija bus ginama atvirame Gynimo tarybos posėdyje 2022 m. rugpjūčio mėn. 30 d. 14 val. Vilniaus universiteto Gyvybės mokslų centro R-401 auditorijoje.
Adresas: Saulėtekio 7, LT-10257, Vilnius, Lietuva,
tel. +37068646759; el. paštas: gediminas.skvarnavicius@bti.vu.lt
Disertaciją bus galima peržiūrėti Vilniaus universiteto bibliotekoje, taip pat Vilniaus universiteto svetainėje asresu:
www.vu.lt/lt/naujienos/ivykiu-kalendorius

# Contents

# Abbreviations

| | |
|---|---|
| **GdmHCl** | guanidinium hydrochloride. |
| $^1\mathbf{H}-^{15}\mathbf{N}$ **HSQC** | $^1H-^{15}N$ heteronuclear single quantum coherence. |
| **ANS** | 8-Anilinonaphthalene-1-sulfonic acid. |
| **ASA** | accessible surface area. |
| **BSA** | bovine serum albumin. |
| **CAC** | critical aggregation concentration. |
| **CMC** | critical micelle concentration. |
| **DMSO** | dimethyl sulfoxide. |
| **DTAB** | dodecyltrimethylammonium bromide. |
| **FPSA** | fluorescent pressure shift assay. |
| **ITC** | isothermal titration calorimetry. |
| **NMR** | nuclear magnetic resonance. |
| **OCPS** | oppositely charged polymer-surfactant. |
| **PPC** | pressure perturbation calorimetry. |
| **SDS** | sodium dodecyl sulfate. |
| **TMAO** | trimethylamine-N-oxide. |
| **TSA** | thermal shift assay. |

# Introduction

Since the first conception of scientific method by Aristotle in the 4th century BCE, science was governed by the inseparable duality of inductive and deductive reasoning. To explain an empirical observation to the best of our capabilities, it is necessary to reduce it to the simplest components that are observable and understandable with the physical and theoretical tools currently available. This is because the overwhelming complexity of nature, which seems unimaginable to understand fully, is ultimately composed of surprisingly few fundamental elements. Understanding of these elements is attained by the deduction of empirical observations. Induction then can be employed to combine the fundamental understanding of elements into new shapes and forms. These forms accurately resemble the relevant systems of nature that we encounter in our lives. This duality of science has led the great minds of humanity, from the ancient thinkers to the great minds of the modern age to seek out the theory of everything. A hypothetical theory that is supposed to explain every encounter in nature from few principle elements. While the theory of everything might be an endlessly elusive ideal, the basic concepts from the duality of science have applications to every scientific field.

Computational efforts to predict the parameters of protein-ligand bind- ing in drug design are a perfect example of a complete scientific circle. Methods that predict ligand binding (docking) use scoring functions for affinity calculation. These functions rely heavily on thermodynamic data. Millions of compounds can be screened virtually, and promising lead compounds can be identified faster than any experimental methods would allow. Despite the exponential breakthrough in computational power in recent years, the values of docking scoring functions do not correlate ideally with experimental data [1]. This is partly because the mechanism of ligand binding is not fully understood, and all the thermodynamic contributions can not be determined accurately [2]. Many unexplored areas in binding thermodynamics have lagged behind the development of novel drug design methods. This thesis explores a couple of these areas.

Historically docking was based on rigid structures of the protein and ligand obtained from X-ray crystallography. Attempts to account for the plasticity and dynamics of protein structure have started only recently. Consequentially, adding additional variables into the algorithms,

which are not constrained based on experimental data, is bound to add additional uncertainty. The role of water in protein-ligand binding is also poorly understood. Changes in hydration shells of the protein and ligand undoubtedly have significant consequences to binding as well as the possible entrapment of water molecules in the binding site. Protein conformation fluctuations and changes in hydration are closely related to changes in volume and compressibility upon ligand binding [3–5]. However, these parameters are determined for very few protein-ligand systems. The impact of solvent composition and local environment on the forces governing ligand binding is also not clear. For example effects of different cosolvents and molecular crowding on protein-ligand binding are still being researched. Determination of these volumetric parameters for several protein-ligand systems, alongside the effects of commonly used denaturants are presented in this thesis.

The effects of hydrophobicity on the contributions of ionic interactions is an ongoing topic as well. The complexity of the systems mentioned above leads to knowledge on these forces that is often not applicable universally and can not be transferred to different systems. The dissection of elementary interactions can be obtained in simplified model systems that represent the desired properties of the real system. Several oppositely charged model systems have been already researched (Figure 1), yet gaps in this ongoing topic need to be filled [6–8]. In this thesis, two model systems are used to determine the changes in protein volume upon binding a ligand and the contribution of electrostatic interactions towards the overall energy of protein-ligand binding.

**Thesis Objectives:**

- To explore the role of volume changes upon primary sulfonamide inhibitor binding to three carbonic anhydrase (CA) family proteins.

- To investigate thermodynamic binding parameters of ion-pair formation in a protein-ligand model system composed of charged poly(amino acid)s and oppositely charged surfactants.

**Thesis Tasks:**

- To develop the fluorescent pressure shift assay (FPSA) method for the determination of $\Delta V_{\mathrm{b}}$ in strongly interacting protein-ligand systems.

- To obtain changes in volume that arise upon the interaction between carbonic anhydrase family proteins and primary sulfonamides, using FPSA and high pressure nuclear magnetic resonance (NMR) techniques.

- To assess the advantages and limitations of the $\Delta V_{\mathrm{b}}$ determination methods.

- To interpret the sign and magnitude of $\Delta V_{\mathrm{b}}$ in the CA-sulfonamide system.

- To perform isothermal titration calorimetry (ITC) experiments on the oppositely charged poly(amino acid)-surfactant systems, varying surfactant chain length, temperature, and ionic strength.

- To analyze ITC data and determine the contribution of charged chemical groups to the binding energy of the overall system.

**Novelty and Significance.** Protein-ligand binding volume has been studied for several decades [9–12]. Despite the interest, the results are scarce and obtained in several inconsistently related protein-ligand systems. This is mainly because binding volume determination is practically laborious and often requires high pressure techniques that are not readily available to most researchers. In this thesis, research of binding volume in an otherwise well researched system is presented. The features of CA-sulfonamide model systems (further discussed in the thesis) provide a solid framework for understanding binding volume. The effects of guanidinium hydrochloride (GdmHCl), a common destabilizing agent in pressure unfolding studies, were explored. CA XIII unfolding pathway using GdmHCl was determined for the first time. The linearity of melting pressure ($p_{\mathrm{m}}$) shift with increased GdmHCl concentration was evaluated for three CA isoforms (CA I, CA II, CA XIII). This led to a concept of fluorescent pressure shift assay (FPSA) technique using different GdmHCl and ligand concentrations for strong ligand binding volume determination. High pressure $^{1}\mathrm{H}-^{15}\mathrm{N}$ HSQC NMR technique was employed to determine primary sulfonamide inhibitor and CA isoform I

and II binding volume. NMR data also revealed detailed information on which amino acids are affected by binding of a ligand and pressure. A method for determining changes in volume upon protein-ligand binding from a single series of $^1H-^{15}N$ HSQC spectra was described for the first time.

A model system consisting of oppositely charged amino acid homopolymers and surfactants was used to determine the contributions of chemical modifications and ionic interaction towards protein-ligand binding. Contributions of alkyl chain lengthening and head group make up towards enthalpy and heat capacity of interactions were determined for the first time in an oppositely charged poly(amino acid)-surfactant system.

**Defense statements:**

- In a low concentration range, GdmHCl reduces the melting pressure ($p_m$) values of carbonic anhydrases linearly. The $p_m$ value obtained in this range of GdmHCl concentrations can be used for determination of $\Delta V_b$ by the FPSA method in strongly interacting protein-ligand systems.

- High pressure $^1H-^{15}N$ HSQC NMR can be used to determine changes in volume due to protein-ligand binding not only for interactions that are fast on the NMR timescale but for those that are slow as well.

- Changes in volume upon protein-ligand interaction can be calculated from a single series of NMR spectra registered using constant protein and ligand concentrations but with varying pressure if the dissociation constant is in a similar value range as the protein concentration used.

- Carbonic anhydrase interaction with sulfonamide inhibitors exhibit a small negative binding volume.

- Charged surfactants bind to oppositely charged poly(amino acid)s by forming ion pairs between the head-group of the surfactant and the charged moieties of the polymer with a one-to-one ratio.

- Interaction of bound surfactant alkyl chains with each other is an important contributor to the interaction and depends on chain length.

- The affinity between surfactant head-group and poly(amino acid)'s charged moiety can differ based on the chemical structure of the charged groups, while the difference in binding enthalpy due to aliphatic chain lengthening is similar in all poly(amino acid)-surfactant systems.
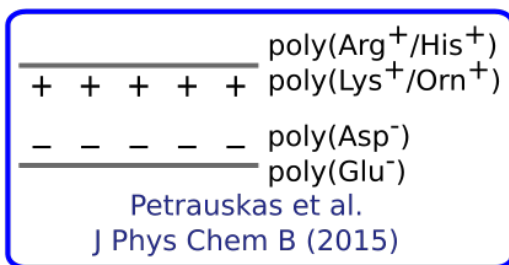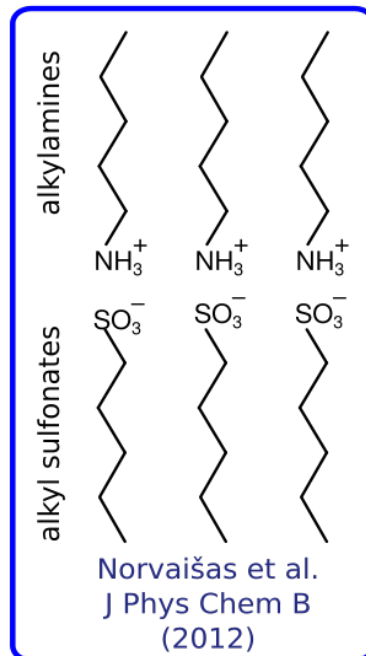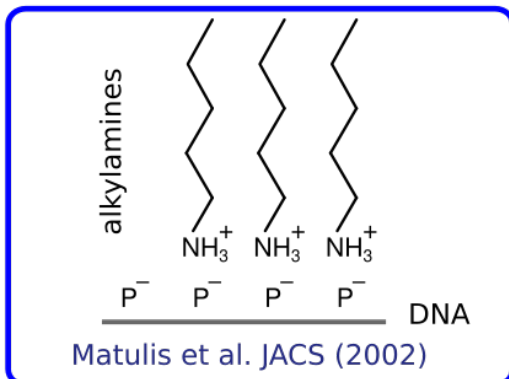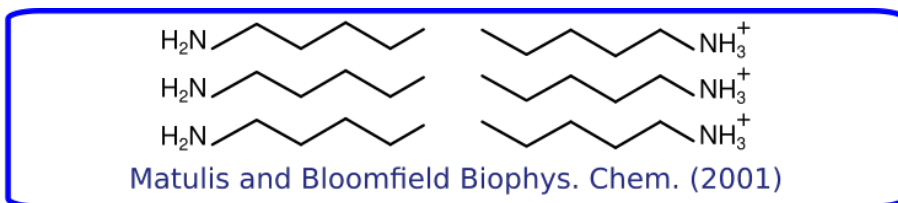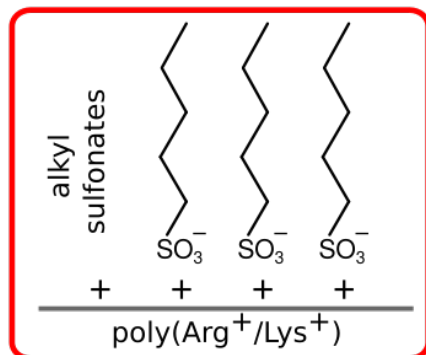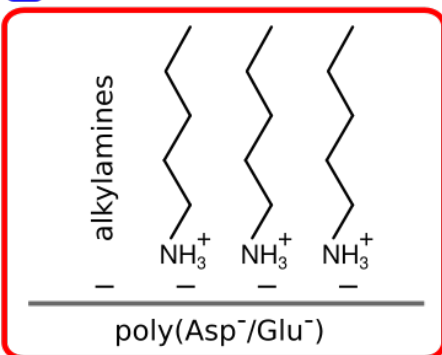
Figure 1: Opposite charge interaction model systems. Research on model systems within blue borders have been published previously. Model systems within red borders are a part of this thesis.

# Literature overview

# Chapter 1

# Thermodynamics of protein-ligand interaction

In this chapter, the basic mathematical description of chemical equilibrium, along with common thermodynamic parameters used in drug design are described.

## 1.1 The Gibbs energy and equilibrium

Following the second law of thermodynamic, a process is spontaneous if the overall entropy change of the process is positive. Josiah Willard Gibbs has combined entropy change of the system and its surroundings into a single state function that describes the overall entropy change. This state function is now known as the Gibbs energy, $G$, and is expressed as:

$$G = H - TS \tag{1.1}$$

Where $T$ is the temperature, $S$ is entropy, and $H$ is enthalpy. Enthalpy is expressed as the sum of internal energy $U$ and the product of pressure and volume $V$:

$$H = U + pV \tag{1.2}$$

The changes in the Gibbs energy is of particular importance in the fields of biological and chemical thermodynamics. The full differential can be

expressed as a sum of two partial derivatives:

$$\mathrm{d}G = \left(\frac{\partial G}{\partial p}\right)_T \mathrm{d}p + \left(\frac{\partial G}{\partial T}\right)_p \mathrm{d}T \qquad (1.3)$$

This expression means that the Gibbs energy depends on both temperature and pressure; therefore, both variables are essential.

The change in the Gibbs energy holds the information whether the process is spontaneous and how much energy will be released in the process. It is an important state function in chemistry and biology since it is directly related to chemical equilibrium. For example, if the reactants are in their standard states, the equilibrium constant of a reversible reaction $A \rightleftharpoons B$ can be expressed as:

$$K_{\mathrm{eq}} = \frac{[B]}{[A]} = \mathrm{e}^{-\Delta G^\circ / RT} \qquad (1.4)$$

where [A] and [B] are concentrations of both substances at equilibrium, $\Delta G^\circ$ is the standard Gibbs energy change, and $R$ is the universal gas constant.

The relationship between $\Delta G^\circ$ and pressure can be expressed in terms of changes in volume, $\Delta V$, and isothermal compressibility coefficient, $\Delta\beta$, between two states of the system:

$$\Delta G^\circ = \Delta G^\circ{}_0 + \Delta V (p - p_0) + \frac{\Delta\beta}{2}(p - p_0)^2... \qquad (1.5)$$

The $\Delta G^\circ{}_0$ term denotes the change in the Gibbs energy of the process at reference pressure.

If the pressure is held constant the change of Gibbs energy in terms of temperature can be expressed as:

$$\Delta G^\circ = \Delta H_0^\circ - T\Delta S_0^\circ + \Delta C_p^\circ \left[ (T - T_0) - T\ln\left(\frac{T}{T_0}\right) \right], \qquad (1.6)$$

where $\Delta H_0^\circ$ and $\Delta S_0^\circ$ are changes in standard enthalpy and entropy at reference temperature $T_0$, respectively, and $\Delta C_p^\circ$ is the change in constant pressure heat capacity. From these equations, it is evident that variation of temperature and pressure can give information about distinct parameters of the system, and ideally, both variables must be utilized for a full thermodynamic description.

## 1.2 Description of relevant thermodynamic parameters

From an outsider's point of view, it is sometimes easy to overlook the necessity of drug candidate thermodynamic profiling in the whole process of drug design. Knowing that biological effects of the potential drug are the end result, one may ask, "Why not skip thermodynamic profiling and proceed straight to *in vitro* and clinical trials? As all candidate's effects on the organism can not be foreseen from thermodynamic data alone, why bother?" The answer is simple – cost. Indeed, thermodynamic parameters can not foresee many processes that involve side interactions, toxicity, bioavailability, and others. However, they can give enough insights into the actions of potential drug candidates. Thermodynamic research can narrow down the selection of optimized candidates and save millions in currency and years in time for the development of a single drug compound. Many authors have reviewed the importance of thermodynamic profiling [13–15]. Here, I describe what insights can be made by obtaining the thermodynamic parameters of the system.

### 1.2.1 The enthalpy change upon protein-ligand interaction

Enthalpy is one of the most investigated thermodynamic parameters. This is in part because the conception and spread of isothermal titration calorimetry (ITC) [16] made its determination simple, fast, and relatively cheap. Calorimetric methods measure the heat released or absorbed during the process, which is proportional to the enthalpy change of the reaction. $\Delta H^\circ$ can also be measured indirectly by the van Hoff relationship:

$$\Delta H^\circ = -R \left( \frac{\partial \ln K_b}{\partial (1/T)} \right) \tag{1.7}$$

The enthalpy that is measured directly or indirectly is the apparent enthalpy of the process ($\Delta H^\circ_{app}$) and is composed of the intrinsic enthalpy ($\Delta H^\circ_{int}$) and several additional constituents. $\Delta H^\circ_{int}$ is the enthalpy value arising from direct non-covalent interactions between the ligand and its target. Additions to the apparent enthalpy come from coupled equilibria, such as changes in solvation or conformation of the binding participants, exchange of additional ligands, or ionization of

reacting species and buffering agents.

Enthalpy is a thermodynamic parameter of particular interest due to a common practice in ligand design – enthalpic optimization. It is a process where ligands, whose binding is primarily driven by enthalpy, are preferably selected. Perhaps the first example of this process was described byVelazquez-Campoy *et al.* [17]. Based on the study and design of HIV-1 protease inhibitors, the authors deduced that enthalpic contributions to binding come mostly from polar interactions (hydrogen bonds, ionic interaction, van der Waals interactions). These interactions lead to better specificity of the inhibitor. Favorable enthalpic contribution allows flexibility of the ligand by compensating for the negative entropic contribution which comes with this feature. This makes the ligand more likely to adapt to mutations of the target, therefore lowering the chances of drug resistance. An additional benefit of enthalpy favored ligands is solubility. Enthalpic ligands favor polar interactions; they are much more likely to have a higher number of polar groups and therefore be water soluble. The opposite is true for entropy driven ligands as they tend to bind with large hydrophobic patches. Optimizing a ligand towards more hydrophobic interactions usually leads to poor solubility in water, which is often undesirable for a potential drug candidate.

### 1.2.2   The entropy change upon protein-ligand interaction

Entropy is a parameter that is associated with the number of degrees of freedom in the system. An increase in entropy means that the system has gained degrees of freedom. A positive gain in entropy upon binding is observed due to several contributions. Desolvation of molecules that usually accompanies binding is associated with an increase in entropy [18]. A change in entropy can arise due to changes in the conformation of the ligand and target upon binding. Both positive and negative contributions can be observed upon ligand binding [19]. Ligand binding is also associated with a loss of translational entropy [20]. This is because the movement of each separate component is restricted.

### 1.2.3 Change in constant pressure heat capacity upon protein-ligand binding

Change in heat capacity upon ligand binding is usually determined by measuring enthalpy values at different temperatures using the ITC technique. The heat capacity of binding is a characteristic that can give insights into the mechanism of binding. A negative change in heat capacity can signify that nonpolar groups are shielded from water upon binding, indicating that hydrophobic effects are in play [21]. Due to these early findings, changes in heat capacity are linked to changes in accessible surface area (ASA). Because of this, heat capacity is a good indicator of conformational changes upon ligand binding. This relationship gives insights on allosteric effects and cooperativity of ligand binding, which translates into biologic function [22]. A small positive change in heat capacity can indicate electrostatic interactions, as shown by Gallagher and Sharp in a study of DNA binding to various ligands [23]. Cooper also argues that a variety of weak interactions and processes should be considered as contributors to heat capacity, including the effects of water displacement upon binding [24].

### 1.2.4 Change in volume and compressibility upon protein-ligand binding

Change in volume upon protein-ligand binding is the difference in the total volume between two states of a system. In the first state, the protein and ligand are free; in the second state, the ligand is bound to the protein (Figure 1.1). This volume difference between the two states is further referred to as binding volume ($\Delta V_b$) in this thesis. The second term of Gibbs energy pressure dependence (equation (1.5)) is compressibility. The compressibility coefficient of binding – $\Delta \beta_b$ describes how $\Delta V_b$ changes with pressure. A significant $\Delta \beta_b$ value could indicate that one of the states (bound or unbound) changes its volume with pressure. As the determination of binding volume and its origins is a significant part of this thesis, the origins of $\Delta V_b$ and its relation to ligand binding are discussed more extensively degree in the discussion and summary portions of this thesis.

$$\Delta V_b = \left( V \left( {}^{\text{Hydrated}}_{\text{PL complex}} \right) \quad + \quad V \left( {}^{\text{Excess}}_{\text{bulk water (W)}} \right) \right) - \left( V \left( {}^{\text{Hydrated}}_{\text{protein (P)}} \right) \quad + \quad V \left( {}^{\text{Hydrated}}_{\text{ligand (L)}} \right) \right)$$



Figure 1.1: Illustration of the volume change upon protein-ligand binding. The change in volume can come from rearrangements of the protein 3D structure, that lead to differences in solvent inaccessible voids, as well as the difference due to rearrangement of water molecules.

### 1.2.5 Enthalpy-entropy compensation

When talking about binding related thermodynamic parameters, the topic of enthalpy-entropy compensation (EEC) always arises. EEC is a phenomenon observed in various processes, described as a linear correlation between enthalpy and entropy contributions to changes of the Gibbs energy. For example, if a particular chemical group of a ligand is modified to produce a large range of $\Delta H^\circ$ values, this often results only in a narrow gain in $\Delta G^\circ$. This is because the same modification causes an increased contribution of $-T\Delta S^\circ$, in a direction that counteracts the gain from $\Delta H^\circ$.

There are many attempts to explain this phenomenon. Some authors propose that this is due to rearrangements of solvent water molecules and that EEC is universal for all processes in aqueous solutions [25]. Others argue that the origin of EEC lies in the flexibility and small conformational fluctuations of the macromolecule [26].

Counter arguments to the existence of this phenomenon mostly rely on the experimental errors and limitations of biophysical methods and on confirmation bias. ITC is the main method for determining the contributions of enthalpy and entropy to Gibbs energy. This method has a significant amount of uncertainty and systematic errors, which can falsely contribute to the appearance of EEC [27]. On top of that, ITC has its limitations. By ITC, $\Delta H^\circ$ is determined directly from the heat released upon binding. In contrast, $\Delta S^\circ$ is determined by calculation, using the $\Delta H^\circ$ and $\Delta G^\circ$ values determined by the experiment. Using ITC $\Delta G^\circ$ can only be accurately determined by in a narrow range limited by the Wiseman factor [16] also called *c*-factor. This limitation reduces the data available for verification of EES since a large gain in

enthalpy for a certain modification would push the $\Delta G°$ to the boundary of determination. A large enthalpy value and a $\Delta G°$ value that is beyond ITC limits would be the result of this modification. As a result, the calculated contribution of entropy would be falsely large. Some evidence of data selection and publication bias is also considered as a possible contributor to EEC [28, 29].

Despite the controversy, the phenomenon of EEC is still rigorously researched due to its relevance in drug design. Understanding these effects would help to design more potent ligands that break the EEC rule.

# Chapter 2

# Carbonic Anhydrases as a Model System

Carbonic anhydrases (CAs) are a family of metalloenzymes that catalyze the reversible hydration of $CO_2$:

$$CO_2 + H_2O \rightleftharpoons HCO_3{}^- + H^+$$
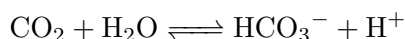
Carbonic anhydrases were discovered 80 years ago and since then have been extensively studied due to their relevance in biology, human physiology, and drug design [30]. This section will explore the basic classification and structural properties of the studied CA isoforms, the mechanism of action, and their use as a model system in molecular biophysics.

## 2.1 Classification and role of CAs in the human physiology

Based on their primary sequence and tertiary structure CAs are categorized into five distinct classes – $\alpha, \beta, \gamma, \delta, \zeta$. The only carbonic anhydrase class found in mammals is the $\alpha$-CA. In humans so far, sixteen isoforms of CAs have been identified. Based on their subcellular location, these isoforms are cytosolic (CA I-III, CA VII, CA VIII, CA X, CA XI, CA XIII), mitochondrial (CA V-A, CA V-B), secreted (CA VI), membrane-bound (CA IV, CA XV) and transmembrane (CA IX, CA XII, CA XIV) [31].

CA I and CA II are expressed by human red blood cells in high quan-

tities. Their presence in blood plays a crucial role in $CO_2$ exchange. They catalyze the hydration of $CO_2$ in the blood – this is how it can be transported. At the other end of the $CO_2$ cycle, these isoforms help release $CO_2$ by dehydrating bicarbonate in the respiratory system, where $CO_2$ then can be excluded from the organism [32]. CA II is expressed in abundance in kidney cells where it is responsible for bicarbonate reabsorption [33] and is believed to modulate the cell type profile [34]. CA III is expressed in muscle and adipose tissue. Its activity is low, and the exact functions in muscle tissue are not clear yet. In adipose tissue, it likely plays an essential role in adipogenesis, and fatty acid metabolism [31]. CA VII is expressed in the colon, liver, skeletal muscle, and brain, where it is suspected to play a role in neuronal excitation by aiding the GABA receptor and channel system [35] CA XIII is a widely expressed isoform found in the thymus, kidney, submandibular gland, small intestine, and reproductive organs of both sexes. It is likely to contribute to pH regulation in reproductive processes, e.g., sperm mobility [36].

The mitochondrial CA – CA VA is found mainly in liver tissue while CA VB has a broad distribution. Mitochondrial CAs supply bicarbonate for carbamoyl phosphate synthetase catalyzed synthesis of carbamoyl phosphate, which is a participant in ureagenesis. Based on CA inhibition studies, mitochondrial CAs likely also play an important role in biosynthetic reactions gluconeogenesis and lipogenesis by aiding precursor synthesis [31].

CA VI is an excreted CA found mainly in saliva. As the buffering capacity of saliva mostly depends on bicarbonate ions CA I most likely plays a primary role in salivary secretions. This is linked to the neutralization of acid produced by bacteria on the dental biofilm. CA VI is also closely related to the sensation of taste [37].

CA IV is a membrane attached protein found mainly in the kidneys and the heart, brain, eyes, erythrocytes in smaller amounts. Along with CA II and another membrane-bound CA isoform XII it is responsible for the reabsorption of bicarbonate [31]. CA IX and CA XII isoforms are tumor-related. CA IX expression in healthy cells is limited. It is known to be overexpressed in tumors and contribute to tumor cell migration, proliferation, and pH control. CA IX, therefore, is a popular target for treatment and diagnostic techniques [38]. CA XII is expressed in a variety of tissues. It is regulated by estrogen and is a good predictor

of breast cancer [39]. CA XIV is the least studied isoform, which is expressed mostly in the brain. CA XIV mediated pH regulation likely plays a role in electrical brain activity [40].

## 2.2   Mechanism, activity and inhibition of CAs

The catalytic site of CA is located deep in its globular structure and is solvent-accessible trough a 15 Å cleft [41]. A $Zn^{2+}$ ion is positioned by tetrahedral coordination to three histidine residues and a water molecule at the catalytic site. The zinc coordinated water molecule must be deprotonated to a hydroxy ion for the catalysis event to begin. Then the hydroxy ion can carry out a nucleophilic attack of the carbon atom in the $CO_2$ molecule, forming a $HCO_3^-$ bicarbonate ion that is attached to the coordinated zinc ion. Bicarbonate is then released by replacement with another water molecule. The deprotonation of coordinating water molecules is the rate-limiting step of this reaction [42]. A simple scheme of catalysis by carbonic anhydrase is presented in Figure 2.1. Alongside hydratase activity, carbonic anhydrases exhibit esterase activity [43]. The catalytic site of CA esterase activity is the same as hydratase, and the mechanism involved is similar. The CA esterase activity is generally slower than $CO_2$ hydration, but as both activities share inhibition mechanisms, it is often used for high throughput screenings. The reason for esterase activity preference is that 4-nitrophenyl acetate, a popular esterase substrate, can be easily observed by colorimetric methods. On top of that, the use of gaseous substrate – $CO_2$ comes with its own set of experimental difficulties [44, 45].

Carbonic anhydrases can be inhibited through several mechanisms. These include binding to the zinc ion or the coordinated water/hydroxy ion, occlusion of the cleft in the catalytic site, allosteric effects [46]. The most important and extensively studied class of CA inhibitors is primary sulfonamides. The $SO_2NH^-$ moiety of sulfonamides, in their deprotonated state, bind directly to the zinc atom, replacing the bound hydroxide ion. In addition, the sulfonamide inhibitors interact with conserved residues in the catalytic site of $\alpha$-CA, that is Thr 199 and Glu 106. In a normal state, Thr 199 is hydrogen-bonded to the coordinated water molecule, and Glu 106 is hydrogen-bonded to Thr 199. The selectivity and effectiveness of sulfonamide inhibitors depend primarily on the
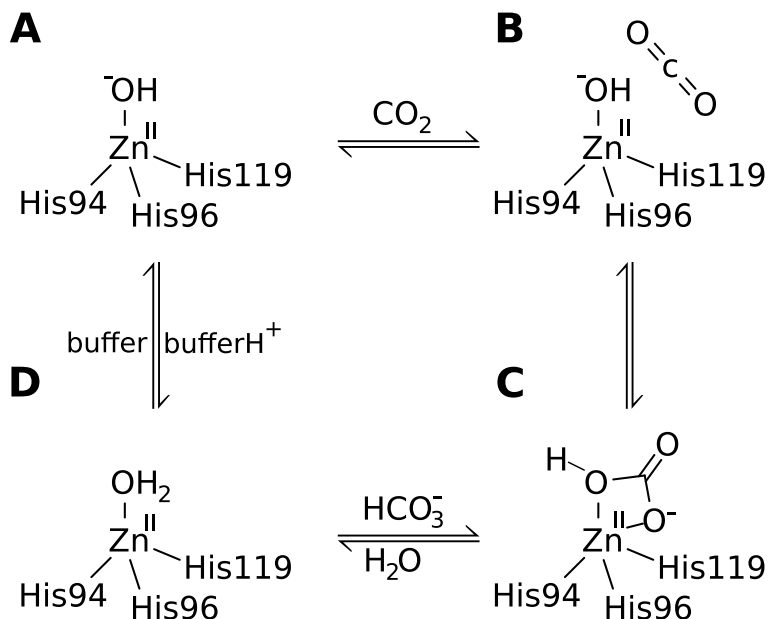
Figure 2.1: General mechanism of $CO_2$ hydration catalyzed by CA. A – CA catalytic site with the water molecule deprotonated. B – nucleophilic attack of the hydroxy ion by $CO_2$. C – Formed bicarbonate ion in the catalytic site. D – the bicarbonate is excluded, and a protonated water molecule is left in the catalytic site. The illustration is adapted from [42].

structure of the rest of the molecule on which the sulfonamide group resides [47]. The catalytic site has a hydrophobic and a hydrophilic side; ideally, a good inhibitor has a structure accommodated by both sides. At least 20 sulfonamide inhibitors targeting carbonic anhydrases are used in clinical practice, and more are awaiting clinical trials [38, 46]. In addition to zinc binding sulfonamides, a variety of compounds bearing OH, COOMe, $SO_3H$, and primary amine groups can anchor to the coordinated water molecule or hydroxy ion [46]. The rest of the structure of these inhibitors should compliment both sides of the catalytic site, similarly to zinc binders. Several classes of compounds are thought to occlude the catalytic site further away from the zinc atom, as well there are indications that specific molecules can inhibit CAs by attaching further away from the catalytic site [46].

## 2.3 Carbonic anhydrases as model systems

Carbonic anhydrases are used or reviewed as a model system for ligand binding and other studies [48–50]. Besides the clinical relevance of CAs, several carbonic anhydrases – human CA I, CA II and bovine CA II – have gained popularity as model systems due to several characteristics. These proteins are relatively small monomers that are highly soluble in water. These properties simplify various universal steps in biophysical and biochemical methods. They are readily available for purchase or can be easily expressed in *e.coli* and purified in a laboratory with standard equipment [51].

The CA model isoforms are well characterized by various methods. Structural data are abundant on these CAs. For example, CA II produces good crystals for X-ray crystallography. Currently there are over 700 structures of CA II in PDB [52]. Recently, neutron diffraction data on CA II and its complexes with sulfonamides have been published as well [53, 54]. Chemical shift assignments of CA I and CA II sequences are available for NMR studies [55, 56]. Although the size of carbonic anhydrases makes structure determination by solution NMR difficult, recently, there has been a successful attempt to solve CA II structure by NMR (PDB ID: 6HD2).

Among other advantages of CAs as a model system is that the reaction they catalyze is relatively simple. As mentioned in the previous section, CAs have many well-studied and commercially available inhibitors. The catalytic site does not undergo major structural rearrangements upon ligand binding. This allows the measurement of how small structural changes in the ligand affect binding thermodynamics and enzyme catalysis. CA's have been used as a standard for calorimetric studies of ligand binding thermodynamics and kinetics [49, 50, 57].

# Chapter 3

# Thermodynamics of Interaction Between Oppositely Charged Polymer-surfactant

An oppositely charged polymer-surfactant (OCPS) system consists of a polymer with ionic residues (e.g., polyacrylic acid, poly-L-arginine) and surfactant molecules bearing an opposite charge (e.g., alkylamines, alkyl sulfates). In this chapter, historical and current research on the binding thermodynamics of this system are discussed. The chapter is divided into two sections: the first describes the general binding mechanism and forces that govern the interaction and, the second overviews the research on OCPS interaction thermodynamics by focusing on variables that affect binding.

## 3.1 General binding mechanism of oppositely charged surfactants and polymers

### 3.1.1 Binding stages revealed by surface tension

By definition, surfactants lower the surface tension of aqueous solutions. Therefore, the general polymer titration with surfactant model is easy to describe by showing surface tension trends. If no polymer is present
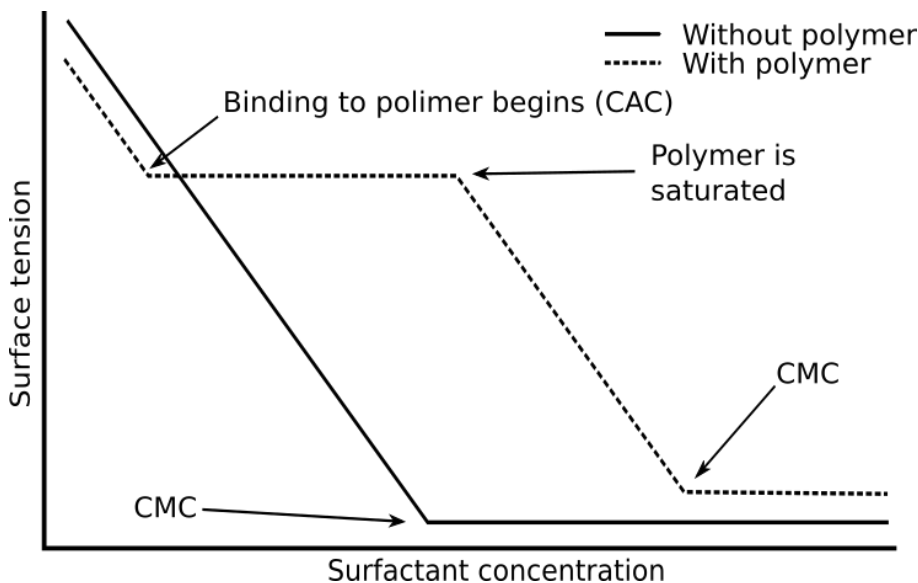
Figure 3.1: Sketch of the expected change in surface tension when the concentration of an ionic surfactant is increased. Two cases are presented, solid line – when no polymer is present and dashed line – an oppositely charged polymer that binds the surfactant is present.

and more surfactant is added, the surface tension decreases as the surfactant molecules position themselves at the solution-air interface. At a specific surfactant concentration, this relationship stops. When enough surfactant is present, their hydrophobic tails interact with each other, shielding themselves from water, forming spherical shapes. This structure is called a micelle, and the concentration at which it occurs is called critical micelle concentration (CMC).

If an oppositely charged polymer is present and surfactant interaction with the polymer is preferential to micelle formation, the surface tension reduction stops before the CMC as shown in Figure 3.1. This halt happens because the binding of charged surfactants to oppositely charged polymer is cooperative. When a specific surfactant concentration is reached, most of the added surfactant molecules bind to the polymer. This concentration is called critical aggregation concentration (CAC). As the surfactant is binding to the polymer, the concentration of free surfactant is not increasing; the surface tension becomes constant. When the polymer is saturated, further added surfactant remains

unbound and starts to reduce surface tension again until it reaches a CMC and micelles, which are independent of the polymer, start to form. This general tendency was observed for various OCPS systems such as polyacrylamide sulfonate and alkyl trimethyl ammonium bromides [58], polystyrene sulfonate and dodecyltrimethylammonium bromide (DTAB) [59], many others.

Each binding stage is of particular interest. However, in this thesis, surfactants and polymers are mainly used as model systems for protein-ligand binding. Therefore, further in this thesis, only research related to surfactant binding at the stoichiometric surfactant/monomer ratio at relatively dilute solutions is reviewed.

### 3.1.2 Hydrophobic effect contribution to the interaction

As the name infers, hydrophobicity is the aversion of certain groups towards water, or more generally, polar environment. Historically, the hydrophobic effect was quantified as the energy of transfer from a reference non-polar solvent to water [60], or more recently as the energy of transfer from the gas phase to water [61]. Hydrophobic interactions are essential in the micellization of surfactants. As the length (hydrophobicity) of the non-polar chain of a charged surfactant increases, its CMC decreases drastically. The CMC decreases because the energy penalty of a hydrophobic tail exposure to water increases with added hydrophobicity. The "necklace and beads" model is often used to model charged surfactant-polymer interaction. This model assumes that surfactants bind with polymers head first, and due to the hydrophobic effects, the tails assemble with each other forming micelle like structures with the polymer wrapped around them.

### 3.1.3 Electrostatic contribution to the interaction

The attraction between opposite charges of a polyelectrolyte and surfactant plays a role in their interaction. Although there are several stages and modes of surfactant binding, there is substantial evidence on many OCPS systems that the stoichiometric ratio of charges signifies a certain critical point. The interaction in these systems can be shifted by changing the number of charges in the polymer via pH [62] and chemical modification [63]. Furthermore, it has been shown that neutralizing

the charge on the polymer changes the mechanism of binding [64]. The role of electrostatic interaction in surfactant binding was even shown by dielectric spectroscopy [65].

Hydrating water molecules and small counterions stabilize charged groups on the polymer in aqueous solutions of polyelectrolyte salts. The degree of counterions attached to the polymer chain varies [66]. Similarly, the head groups of surfactants have a hydration shell of their own. Therefore, the association of surfactant head groups with charged sites of the polymer can be viewed as a competition between small counterions and large molecules. It is thought that hydration of ionic groups comes with an entropic penalty, as the water molecules surrounding the charge are orientated uniformly.

## 3.2   Factors affecting the interaction

### 3.2.1   Temperature

The temperature has significant effects on ionic surfactant binding to oppositely charged polymers. As discussed previously, hydrophobic effects play a role in surfactant – polymer interactions. The hydrophobic effect is highly related to temperature as its signature is a negative $\Delta C_p^\circ$ value. As the temperature increases, the enthalpy contribution to hydrophobic effects becomes greater [21].

Publications that have direct measurements on surfactant interaction in relation to temperature are not numerous in the literature. Santerre *et al.* tested the effects of temperature on DTAB binding to dextran sulfate. The Gibbs energy of binding shifted slightly with the temperature reaching a peak at around 30 °C, and the process became more exothermic with the increase in temperature [67]. Chakraborty *et al.* showed that the concentration of cetyltrimethylammonium bromide needed to saturate sodium carboxymethylcellulose decreases with higher temperature [68]. The authors found binding to be more enthalpy driven with increased temperature. A similar increase, peak, and reversal in binding strength were observed in the interaction of dodecyltrimethylammonium chloride and DNA [69], and diallyldimethylammonium chloride – sodium dodecyl sulfate (SDS) interaction as well [70]. Matulis *et al.* observed a high degree of enthalpy-entropy compensation in the study

of alkylamine binding to DNA [6]. Similar to other systems, the binding strength remained primarily unchanged with increasing temperatures, but the exothermic contribution of enthalpy became larger in magnitude.

Similar forces govern the micelle formation of charged surfactants as OCPS interaction and, therefore, in some ways, the processes are analogous [71]. The thermodynamics of micelle formation seems to be affected by temperature very similarly. Majhi *et al.* observed a peak in Gibbs energy of micelle formation at a specific temperature along with a constant decrease in enthalpy, analogous to previously described reports on OCPS interaction-temperature relationship [72].

### 3.2.2   Ionic strength

The ionic strength of the solution is of particular importance to interactions where charge effects are significant.marged polymer but increases the cooperativity of the interaction [73, 74]. Since then, numerous studies have been devoted to salt effects on OCPS interactions. Hayakawa *et al.* showed that increasing the valency of negatively charged polymer counterion means that a larger concentration of positively charged surfactant is needed for the binding to occur [75]. Wang *et al.* has studied the effects of sodium bromide on the complex formation of dextran sulfate with DTAB. At low concentrations of NaBr, the complexation follows the traditional mechanism – surfactant binds onto the polymer and forms of micelles with the polymer warped around them. At NaBr concentration of 0.23 mM, first, polymer independent micelles are formed. Only when more surfactant is added, the micelles aggregate with the polymer. At even larger salt concentrations, no interaction with the polymer occurs. A decrease in the electrostatic contribution towards binding strength between DNA and alkylamines with added NaCl was observed by Matulis *et al.* [6]. The increase in the entropy of the electrostatic component led to this decrease; the enthalpy remained unaffected by the increase in ionic strength. The tendency for binding constant to decrease and cooperativity to increase with electrolyte addition was also observed in poly(diallyldimethylammonium chloride) – SDS system by Nizri *et al.*, using conductometry, calorimetry and *ab initio* calculations [77].

### 3.2.3 Contribution of the ion pair composition to the interaction

The general mechanism of OCPS interaction involves the surfactant head group binding to polymer side chains; therefore, the chemical composition of ionic groups involved has a significant influence. Ahmadova *et al.* studied the head group effects in the system of polyachrylic, and polymethacrylic acids and their surfactants containing dodecyl chain and different hydrophilic groups [78]. The authors observed that the $\Delta G°$ of interaction was small and not influenced by the head group pair to a large degree. The values ranged from $-0.21\,\mathrm{kJ\,mol^{-1}}$ to $-5.71\,\mathrm{kJ\,mol^{-1}}$. The authors conclude that the steric effects of bulky fragments around charge hinder ion attraction and other effects govern the interaction. Petkova *et al.* studied the foaming properties of SDS and sodium dodecyl oxyethylene sulphate in the presence of polyvinylamine and found that the addition of an ethoxy fragment to SDS increased the binding properties of the surfactant [79]. Quaternary ammonium surfactant binding to sodium poly(acrylate) decreased with the size of alkyl groups attached to the nitrogen in the head group by Yan *et al.* [80]. So far, most studies on head group comparisons have mainly focused on the influence of chemical modification of the head groups, particularly the addition of hydrophobic fragments. On the other side, differences between surfactant binding to different polymers were also observed [73]. So far, to my knowledge, no extensive comparisons of head groups with entirely different charged groups were made.

### 3.2.4 Surfactant tail length contributions to the interaction

CMC of surfactants depends on chain length, generally longer chain surfactants for micelles more readily. Similarly OCPS binding is also influenced by chain length. Goddard *et al.* pioneered the research on surfactant chain length contribution to OCPS interaction. The authors showed that a lesser concentration of alkyl sulfate was needed to keep a cationic polymer precipitated (precipitation is associated with a single layer of surfactant bound to the polymer) [81]. Authors also showed that the surfactant $CH_2$ group contribution to binding on to a polymer is larger than its contribution to micelle formation. Early extensive studies

of chain length effects were conducted by Malovikova *et al.*. The authors observed a linear relationship between alkylpyridinium tail length and the overall binding parameter of interaction with dextran sulfate [74]. Later Okuzaki *et al.*, using a more extensive selection of alkylpyridinium surfactants, showed that both their binding constant and cooperativity of binding to a sulfonate group-containing polymer increases exponentially with surfactant alkyl chain length [82]. These tendencies have also been confirmed by Monte Carlo simulations, which show that the CAC/CMC ratio decreases with increased surfactant chain length [83]. An increase in the binding strength and specifically the hydrophobic contribution with increasing alkyl tail length was observed in the alkylamine – DNA system [6]. So far, all studies reviewed in this subsection are in consensus that increased surfactant chain length increases the strength and cooperativity of OCPS binding.

### 3.2.5 Influence of polymer properties on the interaction

The effects of poly(acrylic acid) and poly(methacrylic acid) charge density towards binding of tetradecyltrimethylammonium bromide were studied by Kiefer *et al.* [84]. No interaction occurs when the polymer is electrically neutral. Surprisingly lower concentrations of surfactant required for cooperative binding were observed when the ionization degree was lower. This effect reached a plateau at a certain critical ionization degree which was 0.4 in this case. This effect was attributed to conformational effects of the polymer since higher charge density uncoils and constrains the polymer disallowing some conformations. Li *et al.* has analyzed the data of numerous studies with different OCPS systems and found a linear correlation between the ideal polymer charge density and binding strength [85]. This study also analyzed the effects of polymer chain stiffness and hydrophobicity but found no strong dependence. Monte Carlo simulations showed that increased chain rigidity has adverse effects on binding due to internal stress caused by the formation of micelles with the polymer wrapped around them [86]. Furthermore, the morphology of OCPS complexes are dependent on polymer chain flexibility [87].

# Chapter 4

# Changes in Protein Volume upon Interaction and Unfolding

## 4.1 Protein volume and pressure-induced unfolding

Perhaps the first description of protein volume was done by Richards, it is used as a starting point for many protein volume-related publications to this day [88]. Protein volume is defined as the volume that the molecule occupies in a solution and can be decomposed into two main terms: geometric (solvent excluded) volume, $V_{\text{SE}}$, and the volume changes in solvent, $V_{\text{Hyd}}$, due to the interactions with the protein surface. The solvent excluded volume is composed of the intrinsic protein volume. The van der Waals volume of the protein's atoms ($V_{\text{vdW}}$) and solvent inaccessible void volume ($V_{\text{void}}$) makes up the intrinsic protein volume [89]. The thermal volume ($V_{\text{T}}$), which describes the volume of the dividing surface between solute and solvent, is also often separated as a composite [90].

By definition, if the protein unfolds at high pressure, the volume of the system where the protein is unfolded is lower than the volume of the system where the protein is in its native conformation. Since this thesis offers no dissection of the volumetric contribution of aqueous protein solution system's constituents, the protein unfolding change for

the purposes of this thesis is defined as the difference in volume between two systems in one of which the protein is unfolded and in the other the protein is in its native form. When the protein unfolds, several of its volume-affecting characteristics change. The most intuitive difference between volumes of folded and unfolded states comes from the hydration of previously solvent inaccessible voids. Perhaps the most convincing evidence of this was done by Ando *et al.* [91]. Extra cavities in T4 lysozyme were induced by mutation. The existence of induced cavities increased the negative volume of unfolding. However, the $\Delta V_\mathrm{u}$ values in most proteins are smaller in magnitude than the volume of cavities. This means that other effects compensate for the negative volume change of void removal.

Protein unfolding exposes more surfaces to water, which means increased ASA. Larger ASA means that more water molecules that previously were in the bulk solvent now interact with the protein surfaces. The questions "whether the volume of interacting water differs?" and "whether this contributes to changes in volume?" arise. The sign and magnitude of solvent interaction effects on volume are still being debated. One school of thought is that exposing polar and non-polar groups to water results in a decrease in volume [92–95]. Chen *et al.* argues that the transfer from solution to gas phase is a more suitable model of these effects than the previously used transfer to non-polar solvent model. The study of an extensive data set of model compounds determined that the values of interaction volume are positive [89]. They also concluded that the positive contribution to $\Delta V_\mathrm{u}$ is more significant for non-polar surfaces. Pressure perturbation calorimetry (PPC) results by Mitra *et al.*, showed a positive contribution from non-polar surfaces and a negative contribution from polar surfaces, which cancel each other out in the end result [96]. This was further supported by $\Delta V_\mathrm{u}$ correlation with void volume but not the change in ASA ($\Delta$ASA) [97]. Another important factor was raised to light by Lee *et al.* [98]. Some residues change p$K$a values when transitioning from native to the unfolded state. Thus ionization events happen upon unfolding. These effects have their own contribution to $\Delta V_\mathrm{u}$, which is also dependent on buffer selection.

To summarize, protein volume is composed of intrinsic, void, and solvation terms. The change in void volume is the most significant contributor to $\Delta V_\mathrm{u}$ and is always negative. The changes in solvation vol-

ume are still being debated. The prevailing schools of thought cross at the dissection of solvent interaction volume. Mostly, the calculations of protein intrinsic surface are being questioned, as different probe sizes, protein-solvent dividing surface selection, and the accuracy of rigid X-ray structures versus a more dynamic reality can shift the results [5, 89, 99].

## 4.2 Changes of protein volume in different solution compositions

Protein-ligand interaction volumetric research conducted in this work includes the use of cosolvents. Therefore, it is essential to review the known effects of solvent composition on protein volume. Solvents can affect the volume of different protein states differently, therefore affecting the observed changes in volume. For several decades, scientists have conducted extensive research on the volumes of proteins in various solvent compositions (different cosolvents, pH, buffers, salts), and the research continues to this day. However, due to the complexity of these systems and the number of variables, it is still challenging to predict the effects of various solvent compositions on protein volume.

### 4.2.1 Acids and bases

The first work on protein volume at different solutions was published by Kauzmann, where changes in ovalbumin and bovine serum albumin (BSA) volume due to the addition of acid were measured by dilatometry [100]. In this work, the authors showed that up to the point of denaturation, both proteins increase in volume by $11\,\mathrm{mL}$ per $1 \times 10^5\,\mathrm{g}$, which corresponds to the volume of protein's carboxylate group neutralization. Further, the research has shown that at pH where unfolding occurs (pH of unfolding was not known at the time), a decrease in volume due to unfolding compensates for the increase in volume due to carboxy group neutralization. Another observation revealed that the addition of KCl increases the pH required to denature BSA but does not mitigate the decrease in volume due to unfolding. Rasper *et al.* have later tested the volumes of acid-base titration for a number of proteins [101]. The study concludes that the volumes of protein side-chain titration are somewhat

similar to that of corresponding ionizable groups in organic molecules but depend highly on the environment in the protein structure. The results for BSA were later confirmed by El Kadi *et al.*. Additionally, the authors show that the compressibility increases until denaturation takes place and then decreases sharply [102]. Ruan *et al.* observed that the volume of unfolding increases (becomes more positive) at high pH [103]. Notably, upon unfolding, amino acid side chains change their pKa values, and thus the event is associated with specific changes in ionization. Ionization events inevitably involve buffer ionization as well, therefore as shown by Lee *et al.* the volume of unfolding depends highly on the buffer of choice [98].

### 4.2.2 Denaturants

Specific chaotropic agents such as urea or guanidine hydrochloride (GdmHCl) causes the native structure of a protein to unfold. Protein unfolding by denaturants (urea and GdmHCl) is believed to occur because of the preferential binding of these denaturants instead of water on the protein surface. This effect is closely related to the difference in solvent-accessible area between the native and unfolded states [104]. However, the effects unrelated to unfolding on protein volume by these molecules are not universally understood, and it is debatable how and if the presence of urea and GdmHCl affects the magnitude of $\Delta V_{\mathrm{u}}$.

Early dilatometric and densimetric studies on the volumes of specific model proteins (lysozyme, chymotrypsinogen A) have shown that the volume of these proteins increases with the addition of urea and GdmHCl at concentration ranges that do not unfold the proteins [105, 106]. If the concentration of denaturants increases further, there is a sharp decrease in protein volume at the point of chemical denaturation. After this decrease in volume, the protein expands with increased denaturant concentration even after the denaturation has occurred. The expansion of the protein was interpreted as the competitive binding of denaturant molecules instead of water molecules at the protein surface. In these studies, the increase in protein volume was linear and equal for both native and unfolded protein states indicating that the $\Delta V_{\mathrm{u}}$ value should be independent of denaturant concentration. A study by Herberhold *et al.* has examined the effects of various cosolvents on the stability, and $\Delta V_{\mathrm{u}}$ of Staphylococcal Nuclease [107]. A slight positive, but almost

within the margin of error, increase in $\Delta V_u$ (reduction of magnitude) with added urea was observed. PPC experiments were also employed to study the unfolding volumes of ribonuclease A in different cosolvent solutions [108]. The slight decrease in $\Delta V_u$ was most likely observed because of the decrease in the unfolding temperature with added denaturants, as $\Delta V_u$ is believed to become more positive with increased temperature [99]. Similarly, no significant dependence of $\Delta V_u$ values on GdmHCl concentration were observed using high pressure stop flow measurements on a all-$\beta$ protein [109]. On the other hand, there are data indicating that $\Delta V_u$ values decrease with added denaturing cosolvents [110]. On top of that, some authors argue that theoretically $\Delta V_u$ values should decrease in an infinitely dilute protein solution and that most previous results show the opposite because of unexplained protein-protein interactions [111]. Studies with less common denaturants, like ethanol, suggest that unfolding by different cosolvents can lead to a completely different $\Delta V_u$ value in sign and magnitude [112].

### 4.2.3  Stabilizing agents

Polyhydric alcohols stabilize proteins against various structure disturbances as these molecules are preferentially excluded from the protein surface. Thus the stability of conformations that reduce protein surface increases [113]. The authors observed that oppositely to denaturants, stabilizing polyhydric alcohols reduce the volume and compressibility of folded proteins [114]. This effect seems to be related to the molecular weight of the cosolvent, as shown with dextrans of various sizes [115]. In the study of various cosolvents on protein volume by Herberhold *et al.* polyhydric alcohols did not have a significant effect on protein unfolding volume except for glycerol which made the volume of unfolding more positive, when added at a high concentration of $1\,\mathrm{M}$ [107]. It was shown by PPC that trimethylamine-N-oxide (TMAO) – a non-alcohol protein stabilizer, makes the unfolding volume of lysozyme more positive [116]. Although some increase in $\Delta V_u$ could arise from the increased melting temperature, the effect was also present in experiments where both urea and TMAO were present, and the melting temperature was similar. Similar effects of TMAO were observed for RNase A stabilization by a mixture of shrimp osmolytes [117]. Several compounds that stabilize proteins, including betaine, glutamate, and sarcosine, are found in in-

creased quantities in deep-sea organisms. This brought about the theory of piezolytes – compounds that increase protein pressure stability specifically. Despite this correlation, a more recent study and review of the literature revealed that these molecules do not influence the volumetric properties of protein unfolding, and their ability to stabilize proteins is not volume related [118]. Overall a slight increase (more positive) in $\Delta V_u$ values with some protein stabilizing agents seem plausible.

### 4.2.4 Electrolytes

Various electrolytes can either stabilize or destabilize protein native conformation based on their position in the Hofmeister series. As observed in the before mentioned study by Herberhold *et al.* a stabilizing salt $K_2SO_4$ raises the melting temperature of staphylococcal nuclease by increasing the Gibbs energy of unfolding ($\Delta G_{u,0}^\circ$), but the stabilization against pressure occurs through the reduction of the negative $\Delta V_u$. It is thought that the pressure unfolded state in the presence of $K_2SO_4$ retains some secondary structure, and thus the difference between native and unfolded states is reduced. Similarly, an increase in NaCl concentration reduced the absolute value of unfolding in lysozyme and its mutants [91]. In the same study by Herberhold *et al.*, a destabilizing $CaCl_2$ salt had the opposite effect – an increase in $\Delta V_u$ absolute value [107]. Similar results were found for the unfolding of ribonuclease A [108].

### 4.2.5 Effects of molecular crowding

Macromolecular crowding has recently drawn lots of attention in the field of protein research. As high concentrations of different proteins and other macromolecules constantly surround the cells' proteins, it is questionable whether results from dilute proteins solutions reflect actuality within the cell. Wang *et al.* was perhaps first to explore the effects of molecular crowding on pressure unfolding of proteins [119]. The study showed that the addition of large quantities of dextran or polyethylene glycol and increased protein concentration raised the melting pressure of staphylococcal nuclease slightly. Fits of the unfolding curve revealed that both $\Delta G_{u,0}^\circ$ and the magnitude of $\Delta V_u$ (more negative) increases upon the addition of these polymers. Thus a large increase in magnitude of $\Delta V_u$ (from $-60.3\,\mathrm{mL\,mol^{-1}}$ up to $-112.6\,\mathrm{mL\,mol^{-1}}$) was compensated

by an increase in $\Delta G_u^\circ$. PPC technique showed that the unfolding volume of lysozyme in the presence of Ficoll was more positive [116] as well. Contrary, Erlkamp *et al.*, using Ficoll as a crowding agent, found no effects on staphylococcal nuclease unfolding volume (if adjusted for temperature)[120]. Zhai *et al.* obtained similar results of dextran effects by using high pressure FT-IR spectroscopy on ribonuclease A [121]. In 30% dextran the volume of unfolding decreased from $-45\,\mathrm{mL\,mol^{-1}}$ to $-76\,\mathrm{mL\,mol^{-1}}$, but the melting pressure increased. This effect did not persist at higher temperatures. Conversely, lysozyme in crowded solutions showed different results. Authors attribute the increase to both higher temperature of unfolding and possible retention of secondary structures in the unfolded state. On the other hand self crowding of lysozyme did not have significant effects on unfolding volume [116, 122].

### 4.2.6 Summary and considerations

In the majority of studies, the effects of denaturing cosolvent concentration on $\Delta V_u$ values are small and negligible when adjusted for external factors. On the other hand, some cases of protein unfolding volume reduction in magnitude by stabilizing agents seem plausible. Stabilization could arise from different unfolded forms of the protein in the presence of stabilizers or the reduction of protein volume in its native form. Both positive and negative effects on $\Delta V_u$ values were observed when crowded media is used. Positive effects are often attributed to retention of secondary structure in crowded environments, while negative effects could mean an interaction between native protein and crowding polymer with a positive interaction volume. Ionization also plays a role in the volume changes associated with protein unfolding; thus, secondary solutions such as buffers significantly influence protein unfolding volume. Only a few studies focused on the influence of electrolytes on unfolding volumes. These studies suggest that protein stabilizing salts, contrary to intuition, makes the volume of unfolding more negative, and destabilizing salts makes the $\Delta V_u$ value more positive.

A persisting theme in solvent influence on unfolding volume is the dependence of $\Delta V_u$ values on external effects. Many studies and reviews show that the volume of unfolding increases towards the positive with increased temperature [89, 99]. Various cosolvents can increase or decrease the melting temperatures of proteins. Therefore, this $\Delta V_u$-temperature

relationship must be accounted for when analyzing the results of techniques that measure the unfolding volume at melting temperature, e.g., PPC. On the other hand, most $\Delta V_\text{u}$ determination techniques involve tracking of protein pressure unfolding, which inherently means that the unfolding volume is determined at a specific non-ambient pressure. It is argued that pressure does not have significant effects on $\Delta V_\text{u}$ values, because pressure induced protein unfolding data is in good agree with PPC results (several kbar pressure versus several bar pressure jump) [99]. This would mean that the compressibility differences between folded and unfolded protein forms are negligible. However, some minor differences in compressibility between native and unfolded protein forms are known [123]. It is proposed that the compressibility during unfolding should decrease because of the intrinsic contribution and increase because of the thermal (solvent exposed area related) contribution [5]. Therefore this compensatory effect could lead to various overall compressibility changes for different proteins – positive, negative, and zero. Because of this phenomenon, some pressure effects on unfolding volumes might not be dismissed entirely and could explain inconsistencies between results. Overall, a multi-technique approach is required to determine volumes of unfolding in different conditions and confirm whether the unfolded state in different media is uniform.

## 4.3 Specific small ligand binding volume

Pioneering studies on specific small ligand binding volume were done by G.Weber group. The group, using high pressure fluorescence measurements showed that riboflavin binding protein binds flavin mononucleotide with a $\Delta V_\text{b}$ value of $-3.3\,\text{mL}\,\text{mol}^{-1}$ [9]. Gekko *et al.* has employed densimetry and sound velocity measurements for ligand binding volume studies. The authors have shown that the volume of lysozyme is decreased by $50\,\text{mL}\,\text{mol}^{-1}$ to $75\,\text{mL}\,\text{mol}^{-1}$ when N-acetyl-D-glucosamine and its oligomers are bound [10]. The authors also observed a decrease in compressibility. The origins of binding volume and compressibility decrease could not be separated from the data available at the time. More recently, a study on this system was done by Son *et al.*. [124]. The authors observed a similar binding volume value of $-44\,\text{mL}\,\text{mol}^{-1}$ for Tri-N-acetylglucosamine binding to lysozyme. In this work volu-

metric measurements were complimented with solvent accessible surface area calculations. The authors deduced that positive changes in intrinsic and hydration volume occure upon binding and a large negative change to thermal volume. Based on these studies it was calculated that 79 water molecules are released upon binding. Volumetric properties of dihydrofolate reductase interaction with various ligands was studied by Kamiyama *et al.* [125]. In this study, based on the ligand both positive and negative binding volumes and changes in compressibility were observed. The authors attribute these effects to changes in cavity volume. They concluded that the effects of dehydration are positive but minor compared to changes in cavities. Dubins *et al.* observed ligand binding induced volume and compressibility changes of Ribonuclease A by a combination of densimetry ultrasonic velocimetry and high pressure methods [11]. The study showed a reduction in protein intrinsic volume and compressibility when cytidine 2'-monophosphate and cytidine 3'-monophosphate is bound, but compensatory effects by a positive volume change from hydration effects lead to a small positive total volume of binding. Combining obtained data with structural information it was calculated that $210 \pm 40$ water molecules are released when the binding occurs. Finally, a correlation between reduction in intrinsic compressibility, volume and the reduction of protein configurational entropy was observed. Filfil *et al.* observed positive binding volume and compressibility in glucose – hexokinase interaction [126]. Again, it was concluded that the sum binding volume results from compensation between dehydration and protein packing effects. The authors also concluded that the process is entropy-driven, because the positive change in entropy due to water release to bulk solution prevails over the negative protein conformational entropy.

Various techniques including FPSA, densimetry and high pressure NMR were used to determine the volume of inhibitor binding to heat shock protein 90 (HSP90), which appeared to be negative [127–129]. FPSA was also used to determine binding volumes of lipid binding to human serum albumin (HSA) [130]. The values of binding volume were small and positive ($8\,\mathrm{mL\,mol^{-1}}$ to $31\,\mathrm{mL\,mol^{-1}}$. In the studies of HSP90 and HSA, it was also shown how ligand binding shifts the whole pressure-temperature phase diagram, stabilizing proteins against both pressure and temperature [128, 130].

More recently, ligand binding to calmodulin was studied, incorporating high pressure Fourier transform infrared spectroscopy, small-angle X-ray scattering, and elastic incoherent neutron scattering [131, 132]. The authors showed how high pressure leads to water penetration to the $Ca^{+2}$ saturated calmodulin core. The study also revealed that calmodulin, known to undergo structural changes upon ligand binding, is more pressure stable when peptides or a small ligand (trifluoperazine) are bound. The structure with trifluoperazine was the most packed and, therefore, stable against pressure.

Recently, changes in volume upon protein-ligand interaction in non-dilute solutions attracted much attention. Ligand binding volume was studied in environments that mimic certain aspects of the cell, like cosolvent solutions [12], two-phase systems and crowding [133, 134]. Oliva *et al.* used an aqueous two-phase system composed of dextran and polyethylene glycol to study the binding of 8-Anilinonaphthalene-1-sulfonic acid (ANS) to BSA at high pressures. The study showed that the binding is hindered in the two-phase system when compared to buffer, but the binding volume is similar in both conditions. In a similar two-phase aqueous system, the effects of high pressure on the kinetics of $\alpha$ - chymotrypsin catalyzed hydrolysis were explored. Based on the kinetic constants at different pressure, the substrate's binding volume in both water and the two-phase system was calculated to be small positive. The magnitude of binding volume was lower in the two-phase system. The effects of dimethyl sulfoxide (DMSO) on proflavin binding of chymotrypsin were studied by high pressure UV-Vis and fluorescence spectroscopy. DMSO decreased the binding constant of proflavin. The close to zero binding volume in buffer solutions increased to the positive side with added DMSO concentration.

In conclusion, the changes in volume upon ligand binding to proteins were studied for a few decades. However, most studies were done by few groups, suggesting that the study of volumetric phenomena still have not gained the traction that other aspects of protein-ligand interaction have. So far, no comprehensive correlation of binding volumes and their determinants to ligand structure was achieved. Moreover, most of the studies were done in dilute aqueous solutions and only a few pioneering studies on binding volume were done in media that more closely resembles the environment within organisms. This leaves, many knowledge

gaps that can be filled by volumetric studies of ligand binding in model systems.

# Materials and Methods

# Chapter 5

# Materials

## 5.1  Surfactants and poly(amino acid)s

Cationic surfactants—octylamine, nonylamine, decylamine, undecylamine, dodecylamine, tridecylamine—were purchased from Sigma-Aldrich and Acros Organics, either as hydrochloride salts or as amines. Anionic surfactants—1-decanesulfonic acid, dodecylsulfate, 1-dodecanesulfonic acid, 1-nonanesulfonic acid—were purchased from Sigma-Aldrich and Acros organics as sodium salts. Poly(L-glutamic acid) sodium salt, poly(L-aspartic acid) sodium salt, poly(L-arginine) hydrochloride, poly(L-lysine) hydrochloride, and poly(L-ornithine) hydrochloride were purchased from Sigma-Aldrich and Alamanda Polymers. Average polymer length was 50 to 700 residues. Poly(amino acid), surfactant and buffer solutions were stored at $4\,°\mathrm{C}$ temperature.

Poly(amino acid) salts were stored at $-20\,°\mathrm{C}$, while salts of buffers and surfactants were stored at room temperature $(20\,°\mathrm{C})$. Solutions were prepared by dissolving substances in distilled Milli-Q water. Solutions from pure amines were prepared by dissolving them in Milli-Q water and titrating with HCl until the pH value of 5 was reached and amines were visibly dissolved.

## 5.2 Buffers and salts

## 5.3 Ligands

Structures of CA inhibitor compounds used in this study are presented in Figure 5.1. Compounds **1** – 4-Aminobenzenesulfonamide (sulfanil-
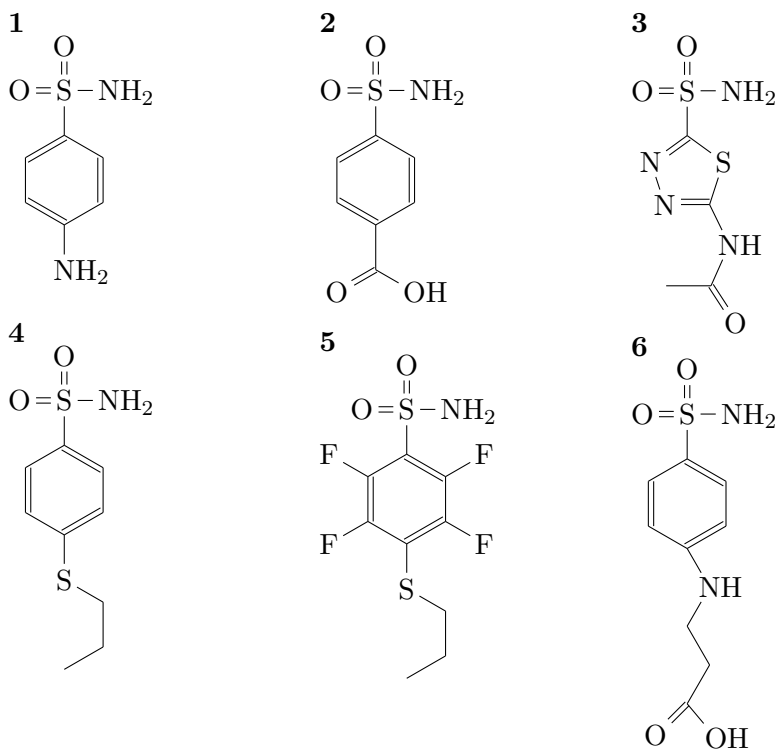


Figure 5.1: Compounds that were used to measure protein-ligand binding volume.

amide) [135], **2** – p-carboxybenzenesulfonamide (carzenide) [136], **3** – acetazolamide were purchased from Sigma-Aldrich. The synthesis of compounds **4** – 4-(propylthio)benzenesulfonamide and **5** – an analogous 2,3,5,6-tetrafluoro-4-(propylthio)benzenesulfonamide were described by Dudutienė *et al.* [137]. The synthesis of compound **6** – a 4-amino-substituted benzenesulfonamide was done by Rutkauskas *et al.* [138].

## 5.4 Proteins

Expression of $^{15}$N labeled, recombinant human CA I and CA II were performed by Zigmantas Toleikis. The proteins were expressed in *E.coli* strain BL21(DE). The overnight culture (10 mL) was grown in LB media with 0.060 mM $ZnCl_2$, then harvested by centrifugation (5 min, 4000 × G), and re-suspended in M9 minimal nutrition medium with $1 \, g \, L^{-1}$ of $^{15}$N labeled ammonium chloride (42.2 mM ($6 \, g \, L^{-1}$) $Na_2HPO_4$, 22 mM ($3 \, g \, L^{-1}$) $KH_2PO_4$, 2 mM $MgSO_4$, and a mixture of trace metals), $4 \, g \, L^{-1}$ of D-glucose, 0.060 mM $ZnCl_2$, and 0.1 g L ampicillin. The culture was grown at 37 °C, 220 rpm for approximately 6 hours until the optical density at 600 nm reached 0.6 to 0.8 and protein expression was induced with 0.20 mM isopropylthio-$\beta$-galactoside and 0.4 mM $ZnCl_2$ was added. The culture was harvested by centrifugation after 16 h of protein expression at 20 °C and 220 rpm stirring.

The expression of non-labeled proteins was done by Vaida Juozapaitienė and Aurelija Mickevičiūtė. The proteins were expressed in *E.coli* strain BL21(DE). The overnight culture (10 mL) was grown overnight in LB medium with 0.060 mM $ZnCl_2$. The culture was grown at 37 °C, 220 rpm for approximately 6 hours until the optical density at 600 nm reached 0.6 to 0.8 and protein expression was induced with 0.20 mM isopropylthio-$\beta$-galactoside and 0.4 mM $ZnCl_2$ was added. The culture was harvested by centrifugation after 16 h of protein expression at 20 °C and 220 rpm stirring.

The $^{15}$N labeled proteins CA I and CA II were purified by Vilma Michailovienė as explained in the coauthored publication [139].

Non-labeled CA I, CA II and CA XIII were also purified by Michailovienė. It was done using nickel immobilized metal affinity chromatography (chelating Sepharose Fast Flow) and ion exchange (SP-Sepharose column for CA I and CM-Sepharose for CA II and CA XIII) as previously described [140–142].

# Chapter 6

# High pressure fluorescence spectroscopy

## 6.1 Fluorescent pressure shift assay

Fluorescent pressure shift assay or PressureFluor is a method that determines protein-ligand binding volume based on the ligands ability to stabilize proteins against pressure denaturation [127–130, 143, 144]. Here I describe the experimental setup, mathematical framework and practical consideration of this technique.

### 6.1.1 Experimental conditions

FPSA experiments of compound **1** binding to CA I and compounds **4** and **5** binding to CA II were done in 20 mM HEPES buffer pH 7.5, with 1.2 M to 1.5 M GdmHCl and 2 % v/v DMSO. The concentration of CA I and CA II was 5 µM.

Experiments of compounds **2** and **3** binding to CA II were done in 10 mM Bis-Tris buffer pH 7.0, with 0.8 M GdmHCl and 2 % v/v DMSO. The concentration of CA II was 3 µM.

### 6.1.2 Experimental setup

High pressure fluorescence spectroscopy experiments were conducted with ISS PC1 photon-counting spectrofluorimeter equipped with a high-pressure cell. The simplified scheme of the experimental setup are displayed in Figure 6.1. A glass cuvette is filled with the sample and cov-
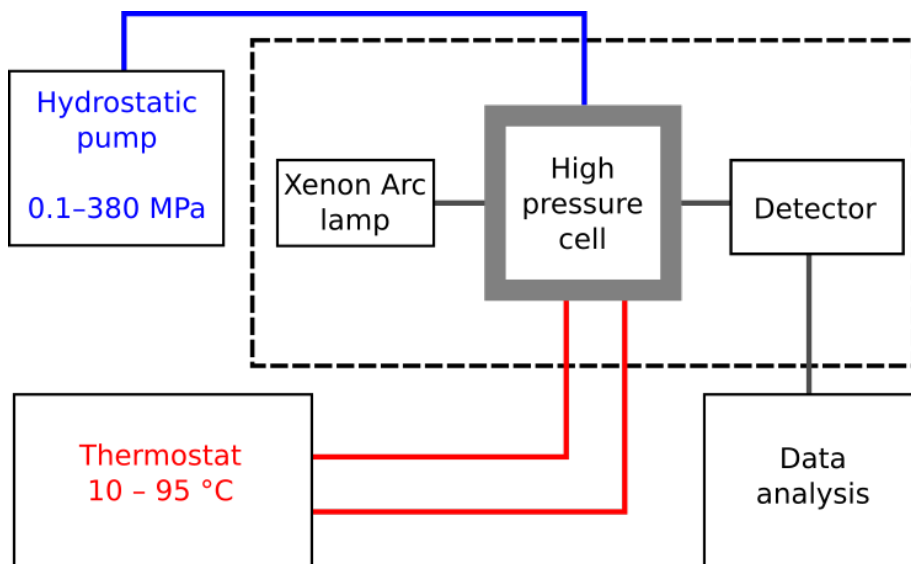
Figure 6.1: Simplified scheme of high pressure fluorescence equipment.

ered with a film. The cuvette is placed into the high pressure cell, which is filled with deionized water. The high-pressure cell has sapphire windows withstanding pressure up to $380\,\mathrm{MPa}$. A manual hydrostatic pump generates the pressure. Tubing runs throughout the pressure cell, which allows the flow of water from the thermostat to ensure the desired temperature. Xenon arc lamp provides the illumination, which passes trough monochromator and $2\,\mathrm{mm}$ wide slits. The detector collects the fluorescence data and passes it to the computer.

### 6.1.3 Protein pressure unfolding

Pressure-induced unfolding of proteins is approximated to be a reversible two state transition between native (N) and unfolded (U) states:

$$N \rightleftharpoons U \tag{6.1}$$

As described by Tanford [145], for a two state process, where both states have distinct fluorescent marks, the total fluorescence as a function of

pressure can be expressed as:

$$f(p) = f_s(p - p_0) + f_N + \frac{f_U - f_N}{1 + \exp(\Delta G_u^\circ)/RT)} \qquad (6.2)$$

Here, $f_N$ and $f_U$ are fluorescence parameters characteristic in the N and U states of the protein. The fluorescence parameters can denote fluorescence yield (intensity), the position of spectral maxima, the center of spectral mass. The selection is further discussed in the section 6.3. The parameter $f_s$ describes a linear shift in the fluorescence at increased pressures and resembles an individual property of a particular fluorophore. In equation (6.2) $R$ is the universal gas constant, $T$ is the experimental temperature, and $\Delta G_u^\circ$ is the change in standard Gibbs energy of unfolding, which can be described in terms of pressure as:

$$\Delta G_u^\circ = \Delta G_{u,0}^\circ + \Delta V_u(p - p_0) + \frac{\Delta \beta_u}{2}(p - p_0)^2 \qquad (6.3)$$

Here, $\Delta G_{u,0}^\circ$ is the change in the standard Gibbs energy of unfolding at pressure $p_0$, $\Delta V_u$ is the change in volume upon protein unfolding (unfolding volume), and $\Delta \beta_u$ is the change of compressibility upon unfolding. From this model, we can calculate the melting pressure of the protein $p_m$. Parameter $p_m$ denotes the pressure at which half of the protein is unfolded, and it can be obtained from the midpoint of the native-to-unfolded transition.

The effects of thermodynamic parameters in equations (6.3) and (6.2) on the unfolding curve can not always be understood empirically. Therefore, visualization of how each variable changes the unfolding curve may aid in the interpretation of experimental results. Figure 6.2 shows simulations of the two state unfolding model from equation 6.2. $\Delta G_{u,0}^\circ$ describes the stability of the protein in given conditions. It can be varied by changing the composition of the solution (adding cosolvents, changing the pH) or by changing external conditions such as temperature. As shown in the Panel A of Figure 6.2, differences in $\Delta G_{u,0}^\circ$ result in a linear shift of $p_m$ values. Changes in unfolding volume (Panel B) influence the steepness of the curve. Processes with high negative volume change occur in a narrow pressure range. As the volume change becomes less negative, the curve is flattened, and higher pressure is required to achieve the transition's midpoint. Changes in compressibility (Panel C) affect
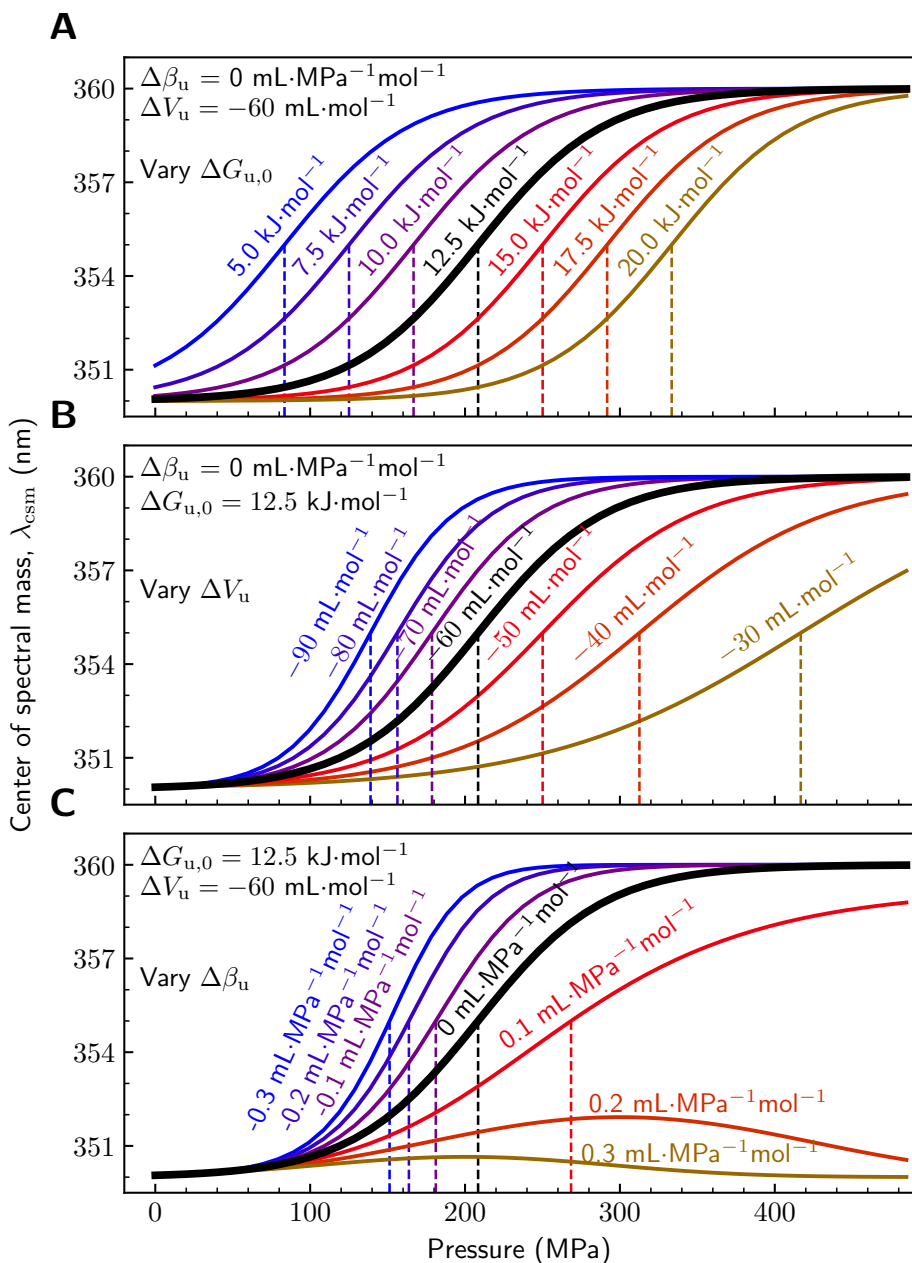
Figure 6.2: Simulations of pressure unfolding curves. A single parameter was varied in each panel: $\Delta G_{u,0}^{\circ}$ (A), $\Delta V_u$ (B), $\Delta \beta_u$ (C).

the curve similarly to those in $\Delta V_b$, but to a larger extent because the term changes non-linearly with the increase in pressure. When planing a

pressure unfolding experiment, the starting conditions should be chosen such that the transition begins in as low pressure as possible. Lower melting pressure can be achieved by reducing protein stability with denaturants, pH or temperature. Transition at low pressure is preferable because the maximal experimentally accessible pressure range available is the most limiting factor in pressure-induced unfolding experiments.

### 6.1.4 Dosing model

To calculate the change in volume upon protein-ligand binding, $\Delta V_{\mathrm{b}}$, the $p_{\mathrm{m}}$ values from pressure unfolding experiments must be related to the ligand concentration. This relationship is described by the following equation:

$$L_{\mathrm{t}} = (\exp(-\Delta G_{\mathrm{u}}^{\circ}/RT) - 1) \times \left( \frac{P_{\mathrm{t}}}{2\exp(-\Delta G_{\mathrm{u}}^{\circ}/RT)} + \frac{1}{\exp(-\Delta G_{\mathrm{b}}^{\circ}/RT)} \right), \tag{6.4}$$

where $L_{\mathrm{t}}$ is the total ligand concentration and $P_{\mathrm{t}}$ is the total protein concentration. $\Delta G_{\mathrm{b}}^{\circ}$ is the change in standard Gibbs energy of protein-ligand binding expressed as:

$$\Delta G_{\mathrm{b}}^{\circ} = \Delta G_{\mathrm{b},0}^{\circ} + \Delta V_{\mathrm{b}}(p - p_0) + \frac{\Delta \beta_{\mathrm{b}}}{2}(p - p_0)^2, \tag{6.5}$$

where $\Delta G_{\mathrm{b},0}^{\circ}$ is the change in standard Gibbs energy of binding at pressure $p_0$, $\Delta V_{\mathrm{b}}$ is the binding volume and $\Delta \beta_{\mathrm{b}}$ is the compressibility change upon binding. This model is difficult to use because it has six parameters: $\Delta G_{\mathrm{u},0}^{\circ}$, $\Delta V_{\mathrm{u}}$, $\Delta \beta_{\mathrm{b}}$, $\Delta G_{\mathrm{b},0}^{\circ}$, $\Delta V_{\mathrm{b}}$ and $\Delta \beta_{\mathrm{b}}$. Due to the practical difficulty of high pressure experiments, the number of data points is usually scarce. Therefore, it is needed to obtain some information about fitted parameters from other methods and fix them (or put some restrains) when fitting the remaining parameters of interest. Unfolding related parameters ($\Delta G_{\mathrm{u},0}^{\circ}$, $\Delta V_{\mathrm{u}}$, $\Delta \beta_{\mathrm{b}}$) can be fixed using unfolding model values from the experiments with no ligand. $\Delta G_{\mathrm{b},0}^{\circ}$ value can be obtained by several methods, e.g., ITC or thermal shift assay (TSA). The contribution of $\Delta \beta_{\mathrm{b}}$ is difficult to separate, but it could be determined by sound velocity measurements or implied from the change of $K_{\mathrm{b}}$ with pressure in similar systems. In this simulation, for simplicity, it is set to zero. After this simplification, one parameter is left, which is $\Delta V_{\mathrm{b}}$. The model is very sensitive to the values of $\Delta V_{\mathrm{b}}$ (see Figure 6.3). Changing
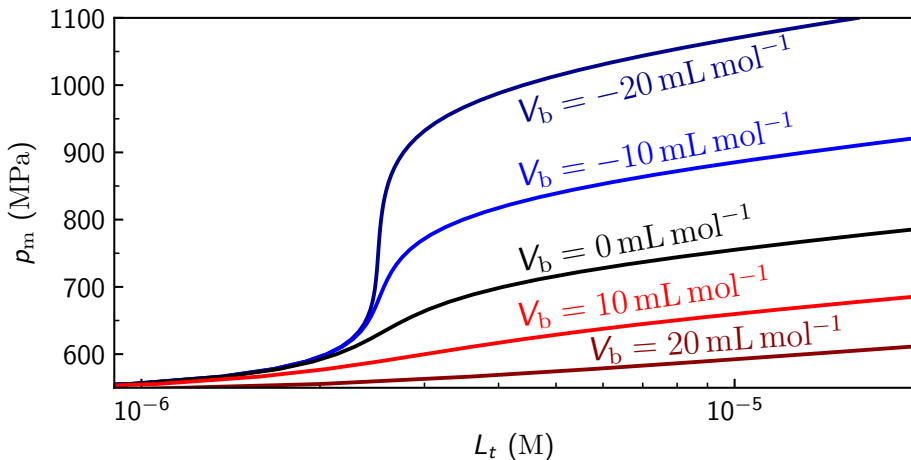
Figure 6.3: Dosing curve simulations. Fixed values were: $\Delta G^{\circ}_{u,0} = 36.6\,\text{kJ}\,\text{mol}^{-1}$, $\Delta V_u = -68\,\text{mL}\,\text{mol}^{-1}$, $\Delta \beta_u = 0$, $\Delta G^{\circ}_{b,0} = -43.5\,\text{kJ}\,\text{mol}^{-1}$, $\Delta \beta_b = 0$. $\Delta V_b$ was varied from $-20\,\text{mL}\,\text{mol}^{-1}$ to $20\,\text{mL}\,\text{mol}^{-1}$.

the $\Delta V_b$ parameter in the range of $-20\,\text{mL}\,\text{mol}^{-1}$ to $20\,\text{mL}\,\text{mol}^{-1}$ resulted in several hundred MPa differences of $p_m$ values, at higher ligand concentrations. $\Delta V_b$ values can be expected to be atleast in the range of $-140\,\text{mL}\,\text{mol}^{-1}$ to $100\,\text{mL}\,\text{mol}^{-1}$ [4, 129]. Therefore, if appropriate restrains on the parameters are made, the dosing model is sufficiently sensitive to $\Delta V_b$ values.

## 6.2 Denaturant-induced protein unfolding

### 6.2.1 Mathematical model

Proteins can be unfolded by denaturants such as urea or guanidinium hydrochloride (GdmHCl). Chemical denaturation is often thought of as a reversible two-state process. In this case, fluorescence or another relevant signal can be related to protein state populations by equation [145]:

$$f([\text{GdmHCl}]) = f_N + \frac{f_U - f_N}{1 + e^{\Delta G^{\circ}_u/RT}}. \tag{6.6}$$

Here $f_U$ and $f_N$ denote experimentally measurable signals corresponding to the unfolded and folded states of a protein, respectively. $\Delta G^{\circ}_u$ is the change in standard Gibbs energy of unfolding. Parameters $f_U$ and

$f_N$ can be related to signal from various techniques, e.g., fluorescence, optical rotation, infrared light absorbance and others. In this thesis, the center of spectral mass from tryptophan fluorescence spectra is used, as explained in detail in section 6.3. The effects of denaturants on $\Delta G_u^\circ$ is often assumed to be linear and can be expressed in terms of denaturant concentration [146]:

$$\Delta G_u^\circ = \Delta G_{u,0}^\circ + m \times [\text{GdmHCl}], \tag{6.7}$$

where $m$ (also termed $m$-value) denotes a coefficient relating denaturant concentration to the stability of a protein.

In some cases a three-state model is more appropriate. It can be expressed as:

$$f = f_N + Y_i(f_i - f_N) + Y_u(f_U - f_N), \tag{6.8}$$

where $Y_i$ and $Y_u$ are the fractions of intermediate and unfolded states, respectively [147, 148]. These states are described by equations

$$Y_i = \frac{K_1}{1 + K_1 + K_1 K_2} \tag{6.9}$$

and

$$Y_u = \frac{K_1 K_2}{1 + K_1 + K_1 K_2}, \tag{6.10}$$

where $K_1$ and $K_2$ are equilibrium constants of the native-to-intermediate (N $\to$ I) and the intermediate-to-unfolded (I $\to$ U) transitions, respectively:

$$K_1 = \exp\left(\frac{m_{N \to I} \times [\text{GdmHCl}] - \Delta G_{0,N \to I}^\circ}{RT}\right) \tag{6.11}$$

$$K_2 = \exp\left(\frac{m_{I \to U} \times [\text{GdmHCl}] - \Delta G_{0,I \to U}^\circ}{RT}\right) \tag{6.12}$$

Here $\Delta G_{0,N \to I}^\circ$ and $\Delta G_{0,I \to U}^\circ$ are changes in the Gibbs energy, and $m_{N \to I}$ and $m_{I \to U}$ are the $m$-values of the corresponding transitions, respectively.

## 6.2.2 Experimental setup

Denaturant unfolding experiments were performed with a Varian Cary Eclipse fluorescence spectrophotometer. The excitation wavelength used was $295\,\text{nm}$. Experiments were conducted in $10\,\text{mM}$ Bis-Tris buffer

pH 7.0 with 2% of volume DMSO.

## 6.3 Methods for tracking protein unfolding by intrinsic fluorescence

Several amino acid residues (Phe, Trp, Thr) that constitute protein structure can fluoresce [149]. Due to its quantum yield, extinction coefficient and sensitivity to the environment, tryptophan is the most used for protein studies of the three [150]. To separate Trp fluorescence from other residues, excitation wavelength of 295 nm or higher is used. The resulting fluorescence spectra has a wavelength maxima ($\lambda_{max}$) ranging from 305 nm to 355 nm. This value has a rough correlation to Trp solvent exposure [151]. Because tryptophan is non-polar, it is usually buried in the hydrophobic core of the protein. In this state, its fluorescence tends to be skewed to shorter wavelengths. As the protein unfolds and Trp residues are exposed to water, a red shift is expected.

In pressure unfolding experiments, we need to choose a parameter to represent $f_N$ and $f_U$ values. The main criterion for this parameter is to accurately represent the ratio between N and U forms of the protein. The simplest parameter is the fluorescence intensity at a single wavelength, representing the N or U form of the protein. For example, if in standard conditions where most of the protein is in its native form, maximal fluorescence is at $\lambda = 330$ nm. As the protein unfolds, the amount of this protein in this state reduces, and intensity diminishes. This way $f_N$ would be equal to the intensity value at the start of the experiment ($I_{330nm}$) and $f_U$ would be the intensity value at the plateau at the end of the experiment. A single intensity value is the fastest method for tracking protein unfolding and may be useful for higher throughput but it offers limited accuracy. Due to common overlap of N and U spectra, the measured intensity at a fixed wavelength is a sum of both N and U signals, which cannot be distinguished. An extension of this method is to track intensity changes at two wavelengths, for example, 330 nm representing N state and 350 nm representing U state. In this method, the ratio between two intensity values ($I_{330nm}/I_{350nm}$) would be used as $f_N$ and $f_U$ parameters. In high pressure fluorescence spectroscopy, the speed at which pressure can be raised is usually the limiting factor, not the speed at which fluorescence spectra can be recorded. Therefore, data

from the whole spectra can be used to improve accuracy even more. One way to use it is to determine the position of $\lambda_{\text{max}}$. As the ratio between the N and U forms changes with increasing pressure, the spectrum shifts, and the position of $\lambda_{\text{max}}$ accurately represents the ratio of protein states. A further modification of this method is to use the center of spectral mass instead, which for a given range of 320 nm to 420 nm is calculated with equation:

$$\lambda_{\text{csm}} = \frac{\sum_{\lambda=320}^{400} I(\lambda) \times \lambda}{\sum_{\lambda=320}^{400} I(\lambda)} \tag{6.13}$$

This value tracks the shift in the spectra and is more robust than a single wavelength maxima value because spectral noise has minor effects on $\lambda_{\text{csm}}$.

For the research in this thesis, $\lambda_{\text{csm}}$ was chosen as the best parameter to track changes in protein structure. One of the main benefits of tracking spectral shift over intensity is that values obtained from different experiments can be compared. Fluorescence intensity values are usually presented in relative units and can only be compared to measurements of the same sample if the data are not normalized. If one would try to compare intensity values from different experiments, any changes in the setup will change the absolute values of this parameter. Even if the equipment and sample filling procedure is ideally uniform small fluctuations in protein concentration (which are often inevitable in the micromolar concentrations) will cause fluctuations in intensity values. Spectral shifts, on the other hand, can be compared when obtained with different equipment. Even experiments with different protein concentrations can be compared if other effects like crowding or precipitation are not a factor. A Gaussian fit was applied to the spectra to diminish the effects of spectral noise even further. This "glosses" over minor and random abnormalities of the spectra, and the $\lambda_{\text{csm}}$ values are calculated from the Gaussian fit. Certain caution is still required, as $\lambda_{\text{csm}}$ can be impacted by fluorescence from species of non-interest. For example, sulfonamide inhibitors that were used in the study exhibit fluorescence when excited with 295 nm light (Figure 6.4). The fluorescence intensity of ligand **1** (100 µM) has a maximum of approximately 350 nm and interferes with the fluorescence intensity of a protein signal. If we would use $\lambda_{\text{max}}$, it could show us the stationary peak of the ligand instead of the protein. As the concentration of ligand **1** is increased, values of the
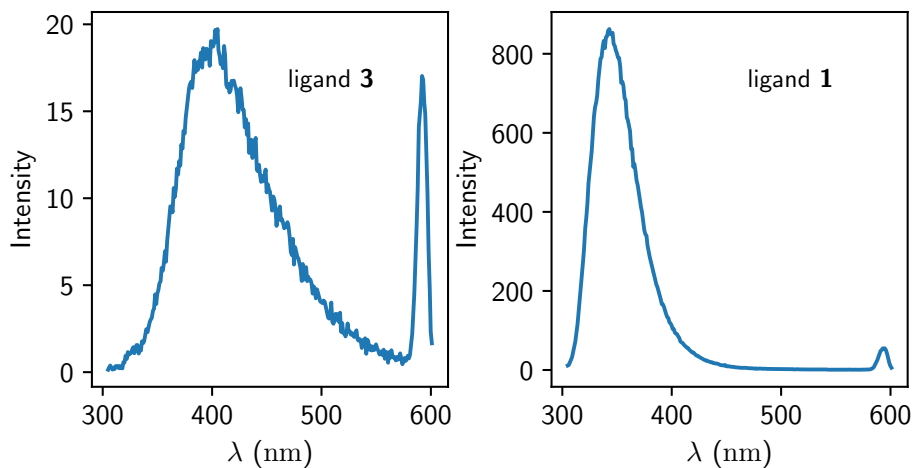
Figure 6.4: Fluorescence spectra of $100\,\mu M$ ligands **3** (left) and **1** (right) in the same buffer as pressure unfolding experiments, with no protein present. Excitation wavelength was $295\,nm$.

maxima of the spectra at extremes are closer to the center of ligand **1** fluorescence spectra (Figure 6.5), but relative ratios remain the same. The normalized results from different experiments can still be compared and used for global data analysis, as shown in Figure 6.6.
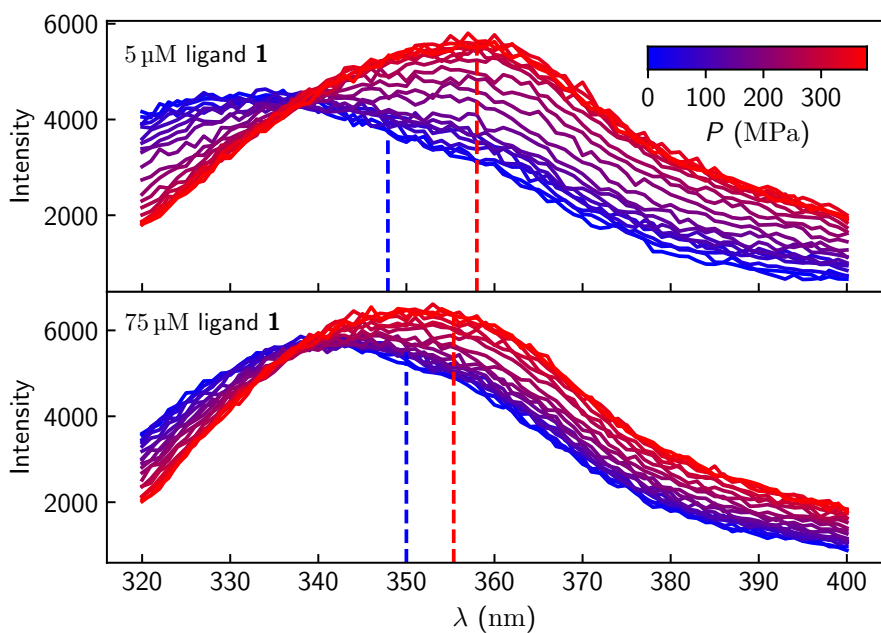
Figure 6.5: Fluorescence spectra of $5\,\mu M$ CA I with $5\,\mu M$ (top) and $75\,\mu M$ (bottom) ligand **1**. Excitation wavelength is $295\,nm$.
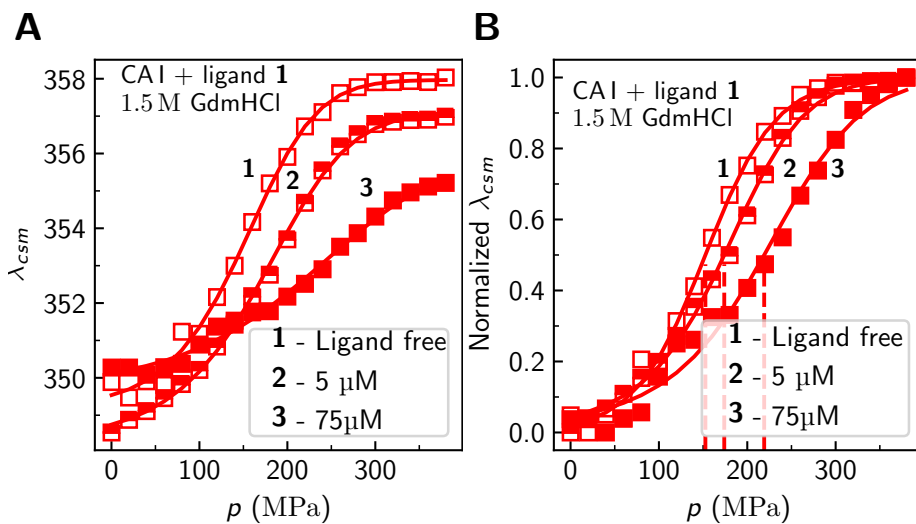
Figure 6.6: Unfolding curves of CA I with different concentrations of ligand **1** (0, 5 µM, 75 µM). Panel A represents changes in $\lambda_{csm}$ with pressure and panel B shows the same data but $\lambda_{csm}$ is normalized in respect to N (0) and U (1) states. The dashed lines in panel B represent interpolations from the midpoint of the fit towards the x-axis, from which $p_m$ values are calculated.

# Chapter 7

# Thermal shift assay

Thermal shift assay (TSA), is an effective affinity measurement technique based on protein thermal stability measurements [152]. It offers label-free detection of binders and protein-ligand affinities in the wider ranges than other techniques. The method was widely used not only for high throughput drug screening [153] and ligand affinity measurements [154], but also for protein quality characterization during purification [155] and selection of protein crystallization conditions [156, 157]. In this chapter, the basics of TSA that relate to this theses will be described.

## 7.1   Procedure and equipment

The standard operating procedure of TSA for ligand binding was recently described by Kazlauskas *et al.* [158]. In TSA experimental equipment consists of a real-time thermal cycler, which is commonly used for quantitative polymerase chain reaction (qPCR). In this work, Corbett Rotor-Gene 6000 (QIAGEN Rotor-Gene Q) instrument was used. The instrument ensures a gradual and precise increase in sample temperature while providing live fluorescence data from many samples.

A dosing series of eight samples, including the ligand-free control, were prepared for each protein-ligand pair at a single GdmHCl concentration. The samples were prepared by mixing a starting solution consisting of buffer (50 mM phosphate buffer pH 7.0 with 50 mM NaCl), GdmHCl (0.2 M to 1.2 M), DMSO (2 % of volume) and 400 µM of selected ligand. An identical solution for dilution was prepared with only

the ligand omitted. Samples 2-7 were prepared by performing a series of two-fold dilutions (1.5 fold for ligand **2**). A sample was mixed in a 1:1 ratio with the dilution liquid. The resulting solution was used for the subsequent sample. At this point, eight samples (including the starting and dilution solutions) with ligand concentrations from 0 µM to 400 µM are obtained. 10 µL of each solution was placed into 0.2 mL tubes. A separate solution was prepared consisting of the same buffer and additives, but with 20 µM of CA II and 200 µM of 8-Anilinonaphthalene-1-sulfonic acid (ANS). 10 µL of protein solution was added to the samples in the 0.2 mL tubes resulting in 8 samples each with 0 µM to 200 µM of ligand and 10 µM of protein. The samples were placed in the instrument and heated from 25 °C to 99 °C at a rate of 1 °C min$^{-1}$. Fluorescence in each sample was excited by $(365 \pm 15)$ nm wavelength light, the detection wavelength was $(460 \pm 15)$ nm.

## 7.2 Data analysis

The data analysis of TSA consists of two parts: first, the melting temperatures ($T_\mathrm{m}$) of each sample must be calculated, then the $T_\mathrm{m}$ values must be plotted against ligand concentration and the dose dependence is evaluated. The process has been described many times in the literature [152, 159, 160]. ANS – the fluorescent probe used in this work is quenched mostly by water. Therefore its fluorescence changes with protein conformation [161]. Fluorescence yield as a function of temperature-dependent protein state can be expressed as:

$$f = f_{\mathrm{N},T} + \frac{f_{\mathrm{U},T} - f_{\mathrm{N},T}}{1 + \frac{1}{K_\mathrm{u}}}, \tag{7.1}$$

where $f_{\mathrm{N},T}$ and $f_{\mathrm{U},T}$ are the temperature-dependent fluorescence yields and $K_\mathrm{u}$ is the unfolding constant of the protein (N $\xrightleftharpoons{K_\mathrm{u}}$ U). $f_{\mathrm{N},T}$ and $f_{\mathrm{U},T}$ are approximated as linear equations:

$$f_{\mathrm{N},T} = f_{\mathrm{N},T_\mathrm{m}} + m_\mathrm{N}(T - T_\mathrm{m}), \tag{7.2}$$

$$f_{\mathrm{U},T} = f_{\mathrm{U},T_\mathrm{m}} + m_\mathrm{U}(T - T_\mathrm{m}), \tag{7.3}$$

where $m_\mathrm{N}$ and $m_\mathrm{U}$ are the slopes of the pre and post-transitional regions in the fluorescence versus temperature plot, shown in Figure 7.1. The
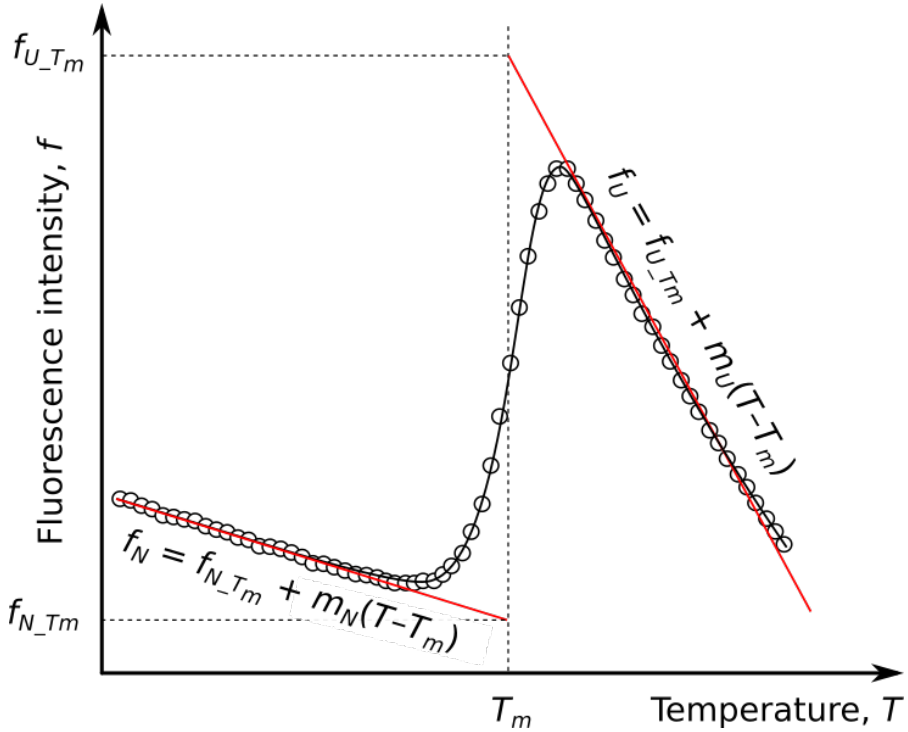
Figure 7.1: An example of a protein thermal unfolding curve used in a TSA experiment. Adapted from [160].

final expression is obtained by inserting expressions in equations (7.2) and (7.2) into equation (7.1):

$$f = f_{N,T_m} + m_N(T - T_m) + \frac{f_{U,T_m} - f_{N,T_m} + (m_U - m_N)(T - T_m)}{1 + \frac{1}{K_u}} \quad (7.4)$$

The midpoint in temperature, $T_m$, where the amount of folded and unfolded protein is equal, is the midpoint of the transition (Figure 7.1). TSA data can be automatically fitted, and $T_m$ values can be calculated by using Thermott software[162]. Raw TSA data of this work was processed with Thermott software.

After the $T_m$ values are obtained, the relation between ligand dosage and the shift in $T_m$ values must be established. A lengthy derivation of the mathematical basis for the dosing curve is described in [160]. From equilibrium and mass conservation relationships three equations are derived:

$$
\begin{cases}
L_\mathrm{t} = (K_\mathrm{u} - 1)\left(\dfrac{1}{K_\mathrm{b}} + \dfrac{P_\mathrm{t}}{2K_\mathrm{u}}\right), & \text{(7.5)}\\[2em]
K_\mathrm{u} = e^{\displaystyle -\frac{\Delta H^\circ_{\mathrm{u},T_r} + \Delta C^\circ_{p,\mathrm{u}}(T_\mathrm{m} - T_r) - T_\mathrm{m}\left(\Delta S^\circ_{\mathrm{u},T_r} + \Delta C^\circ_{p,\mathrm{u}} \ln \frac{T_\mathrm{m}}{T_r}\right)}{RT_\mathrm{m}}}, \\[2em]
K_\mathrm{b} = e^{\displaystyle -\frac{\Delta H^\circ_{\mathrm{b},T_0} + \Delta C^\circ_{p,\mathrm{b}}(T_\mathrm{m} - T_0) - T_m\left(\Delta S^\circ_{\mathrm{b},T_0} + \Delta C^\circ_{p,\mathrm{b}} \ln \frac{T_\mathrm{m}}{T_0}\right)}{RT_\mathrm{m}}}.
\end{cases}
$$

Here the $\Delta H^\circ_{\mathrm{u},T_r}$ and $\Delta H^\circ_{\mathrm{b},T_0}$ are enthalpy changes of unfolding and ligand binding, $\Delta S^\circ_{\mathrm{u},T_r}$ and $\Delta S^\circ_{\mathrm{b},T_0}$ are entropy changes of unfolding and ligand binding, $\Delta C^\circ_{p,\mathrm{u}}$ and $\Delta C^\circ_{p,\mathrm{b}}$ are changes in constant pressure heat capacity upon protein unfolding and binding. $T_0$ is the temperature of ligand-free protein unfolding, and $T_r$ is the reference temperature for which the binding parameters are calculated ($25\,^\circ\mathrm{C}$ was used in this thesis). The dosing curves in this theses were fit globally as explained in the results section using the author's fitting script made with python and the "lmfit" package [163].

# Chapter 8

# High pressure NMR

## 8.1 The usage of $^1$H$-^{15}$N HSQC NMR usage in protein-ligand binding experiments

High pressure NMR is a powerful tool for tracking fluctuations in protein states. Numerous variations of NMR techniques are relevant to proteins and there are many applications from protein structure determination to catalytic kinetics. However, this thesis is limited to $^1$H$-^{15}$N heteronuclear single quantum coherence ($^1$H$-^{15}$N HSQC) spectroscopy, and specifically, its use for protein-ligand binding research. $^1$H$-^{15}$N HSQC NMR spectroscopy requires the protein to be labelled with $^{15}$N isotope. Labelling can be done by expressing the protein in a culture grown in $^{15}$N labelled media. $^1$H$-^{15}$N HSQC links covalently bonded nitrogen, and hydrogen atom spins by magnetization transfer via J-coupling. This linkage means that peaks in the 2D spectra represent a single amide residue. Therefore each peak represents either an amide group of a specific amino acid in the protein background or an amide group in the Gln/Asn side chain. Sidechain signals can be identified and separated by a double peak on the N chemical shift axis since two hydrogen atoms are linked to the same nitrogen atom. After this separation, a 2D spectrum that is a unique fingerprint of the protein is left.

Peak position and shape in the spectra contain information on protein structure and dynamics. The uniqueness and diversity of protein structure create environmental differences for each atom. In turn, environmental differences around the observed atoms cause diversity in chemical shifts. Proton shifts are most noticeably caused by ring cur-

rents, magnetic anisotropy and electric fields. Ring currents can cause large shifts in proton peaks and are mostly induced by the proton's proximity to an aromatic ring. Magnetic anisotropy effects are the cause of non-uniform magnetic fields induced by $\pi$ systems. The most noticeable are magnetic field disturbances by carbonyl and amide groups. Electric field effects are caused by full or partial charges on neighbouring atoms. This effect usually is minor due to the charge effects from individual atoms being cancelled out due to the distribution of opposites. Origins of nitrogen shifts are harder to separate because of the number of effects that influence them. Amino acid identity, side-chain conformation and hydrogen bonding all have strong effects on nitrogen shifts. Hydrogen bonding to carbonyl group next to the amide nitrogen produces a larger shift than a bond to the nitrogen itself, suggesting not fully understood effects [164].

The chemical exchange of an atom between two or more states different in magnetic environment produces a shift in peak position and/or broadening of the peak. Chemical exchange can be separated into three different classes based on how its rate compares with the difference in resonance frequency between the two states – fast, intermediate and slow. For example, consider an exchange between two similarly populated states, A and B. In a slow regime, the exchange rate between the states is much slower than the time it takes to record the spectra. In this situation, molecules stay in either of the states throughout the whole recording; this produces two sharp peaks representing each state. On the other extreme, if the exchange rate is much faster than the time of recording and an atom undergoes multiple transitions between the two states, spending its time in each, proportionally to the population ratio of the given states. A fast exchange will produce a peak with a position that is between the peaks of two separate states, with the exact position proportional to the fractions of each state. In an intermediate exchange regime, the exchange range is in a similar timescale as the NMR spectra recoding. The peaks become broadened between the two separate positions and may even become so broad that the peak becomes indistinguishable from the spectral noise.

### 8.1.1 Mathematical models

Both fast and slow exchange can be used to study protein-ligand binding thermodynamics. For an simple protein-ligand binding event:

$$[\text{P}] + [\text{L}] \underset{k_{\text{off}}}{\overset{k_{\text{on}}}{\rightleftharpoons}} [\text{PL}], \tag{8.1}$$

the ratio of reaction rate constants $k_{\text{on}}$ and $k_{\text{off}}$ is related to the dissociation constant $K_d$:

$$K_d = \frac{k_{\text{off}}}{k_{\text{on}}}. \tag{8.2}$$

The forward rate constant $k_{\text{on}}$ is similar for most open binding site events and is approximately equal to $10^9 \, \text{M}^{-1}\text{s}^{-1}$. Therefore, $K_d$ is directly proportional to $k_{\text{off}}$, which means weak ligands participate in a fast exchange regime. In fast exchange, the exact shift of a peak can be expressed by equation:

$$\delta = (1 - \theta)\delta_{\text{f}} + \theta\delta_{\text{b}}, \tag{8.3}$$

where $\theta$ is the fraction of ligand-bound protein state and $\delta_{\text{f}}$, $\delta_{\text{b}}$ are the respective chemical shifts of free and bound state. We can rearrange this relationship to express bound fraction as:

$$\theta = \frac{\delta_{\text{f}} - \delta}{\delta_{\text{f}} - \delta_{\text{b}}}. \tag{8.4}$$

If a titration of protein with the ligand is performed, it is possible to obtain $\delta_{\text{f}}$ and $\delta_{\text{b}}$ values from experiments with no ligand and those where the protein is saturated with the ligand. Generally, changes in shift due to protein-ligand binding ($\Delta\delta$) is used. This way $\delta_{\text{f}}$ is zero and $\delta_{\text{f}}$ is equal to the maximum change in chemical shift in the experiment ($\Delta\delta_{\text{max}}$). Using balance equations to relate saturation with $K_{\text{d}}$ the observed change in shift then can be expressed as:

$$\Delta\delta = \Delta\delta_{\text{max}} \left( \frac{(P_{\text{t}} + L_{\text{t}} + K_{\text{d}}) - \sqrt{(P_{\text{t}} + L_{\text{t}} + K_{\text{d}})^2 - 4P_{\text{t}}L_{\text{t}}}}{2P_{\text{t}}} \right) \tag{8.5}$$

$\Delta\delta$ from raw peak shifts for a 1D spectrum is simply the absolute value of the difference in shifts. For a 2D $^1\text{H}-^{15}\text{N}$ HSQC spectrum it can be calculated from Pythagorean theorem, with the additional normalization

of gyromagnetic ratios:

$$\Delta\delta = \sqrt{(\delta_{\mathrm{b}}^{1\mathrm{H}} - \delta_{\mathrm{f}}^{1\mathrm{H}})^2 + \left(\frac{\gamma^{15\mathrm{N}}}{\gamma^{1\mathrm{H}}}\right)^2 (\delta_{\mathrm{b}}^{15\mathrm{N}} - \delta_{\mathrm{f}}^{15\mathrm{N}})^2}. \qquad (8.6)$$

Here, $\delta_{\mathrm{b}}^{1\mathrm{H}}$, $\delta_{\mathrm{f}}^{1\mathrm{H}}$ and $\delta_{\mathrm{b}}^{15\mathrm{N}}$, $\delta_{\mathrm{f}}^{15\mathrm{N}}$ are proton and nitrogen shifts for the respective protein states and $\gamma^{15\mathrm{N}}$, $\gamma^{1\mathrm{H}}$ are gyromagnetic ratios for $^{1}$H and $^{15}$N atoms. Equation (8.5) can be simultaneously fitted to results for multiple peaks that are related to the same binding event. Fitting multiple peaks can greatly improve the accuracy of the fitted parameters. It is also worth noting that fitting of this equation is most accurate when the protein concentration is close to $K_d$ values [165]. This requirement can often be a limiting factor for stronger ligands since high protein concentrations are required for NMR experiments are quite high.

In a slow exchange regime, the determination of binding constants is more difficult. First, the slow exchange is usually accompanied by low $K_{\mathrm{d}}$ values. Accurate measurement of a low $K_{\mathrm{d}}$ value using titration is difficult due to the steepness of the titration curve. In other words, all of the added ligand binds to the protein, which means no detectable amounts of ligand-free protein remains after the added ligand concentration reaches the stoichiometric ratio. Determination of such large binding constants can be done using competitive titration techniques or by secondary effects like protein stabilization against unfolding like in the FPSA technique. Despite that, some ligands fall in the "golden range" of binding strength and kinetics. These are conditions where two detectable, slow exchange peaks exist even when ligand added exceeds the stoichiometric point. In this case, the fraction of bound ligand can be calculated using the intensity ratio of the two peaks. For better accuracy, the peak area or peak volume (for 2D spectra) can be used in calculations. In Figure 8.1, a sketch of hypothetical $^{1}$H$-^{15}$N HSQC NMR spectra is shown. In this case the fraction of ligand-bound protein is equal to the intensity of ligand bound peak, adjusted by the total intensity produced by both ligand-bound ($I_{\mathrm{PL}}$) and ligand-free ($I_{\mathrm{P}}$) peaks of the residue:

$$\theta = \frac{I_{\mathrm{PL}}}{I_{\mathrm{PL}} + I_{\mathrm{P}}}. \qquad (8.7)$$

When $\theta$ is obtained, the ligand-free protein concentration can be calculated from mass balance equations by subtracting the concentration of
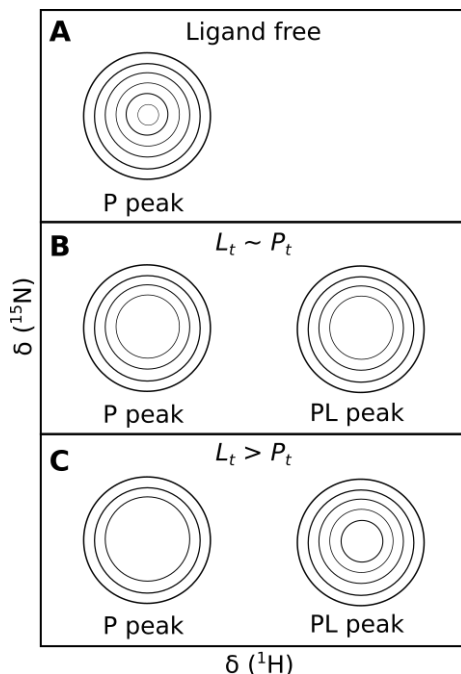
Figure 8.1: Representation of a hypothetical $^1H-^{15}N$ HSQC NMR peak of a protein residue involved in ligand binding. Panel A represents a single ligand-free peak of a residue. In panel B, a doubling of the peak is seen. Each represents the residue of the protein that is ligand-free (P) and ligand-bound (PL). In panel C, the increased ligand concentration result in a lower population of ligand-free protein and lower intensity of P peak. The population of protein-ligand complex increases, and the intensity of the PL peak increases accordingly.

the complex ($[PL]$) from total ligand concentration ($L_t$):

$$[L] = L_t - [PL] = L_t - P_t \times \theta. \tag{8.8}$$

Here $P_t$ is the total protein concentration. $K_d$ then can be related to saturation in respect to ligand concentrations with the Hill-Langmuir equation:

$$\theta = \frac{[L]}{[L] + K_d}. \tag{8.9}$$

Alternatively this relationship, by using mass balance equations, can be

expressed in terms of $L_t$ similarly to equation (8.5):

$$\theta = \frac{(P_t + L_t + K_d) - \sqrt{(P_t + L_t + K_d)^2 - 4P_tL_t}}{2P_t} \qquad (8.10)$$

Finally, $K_d$ can be calculated by fitting equation (8.9) or equation (8.10) to titration data. For better accuracy data from multiple relevant peaks can be fitted simultaneously.

### 8.1.2 Experimental setup

The NMR spectroscopy raw data were obtained at the Centre de Biochimie Structurale, University of Montpellier, by Zigmantas Toleikis and Christian Roumestand, the coauthors of the recent publication [139]. Protein samples of 0.52 mM or 0.43 mM CA I and 0.34 mM CA II were prepared in buffer (10 mM Bis-Tris, 50 mM NaCl, 10 % $D_2O$, 4 % DMSO, pH 6.2 for CA I and pH 6.4 for CA II) with different concentration of compound **1** or **6**, which were prepared in pure DMSO. High-pressure NMR spectroscopy was used to record 2D $^1H-^{15}N$ HSQC spectra of CA I and CA II at various pressures. The protein solution of 0.33 ml was added into a a ceramic tube (5 mm outer and 3 mm inner diameter) from Daedelus Innovations (Aston, PA, USA). Hydrostatic pressure was applied to the sample directly within the magnet through an inox-line filled with low-density paraffin oil (Sigma) using the Xtreme Syringe Pump from Daedelus Innovations. 2D $^1H-^{15}N$ HSQC spectra were recorded at 25 °C and eight different pressures ranging from 5 MPa to 210 MPa on a Bruker AVANCE III 600 MHz equipped with a 5 mm Z-gradient TXI probe head. Water suppression was achieved using the WATERGATE method [166]. $^1H$ chemical shifts were directly referenced to the water resonance (4.7 ppm), while $^{15}N$ chemical shifts were referenced indirectly to the $^{15}N/^1H$ absolute frequency ratios. Water resonance was used as a reference because the most commonly used referencing compound DSS (Sodium trimethylsilylpropanesulfonate) might inhibit CA I and CA II. All NMR experiments were processed with TOPSPIN software (Bruker), and the spectra were analyzed with CcpNmr Analysis V2 software[167]. A full set of spectra for one sample throughout the pressure range were recorded in approximately 20 hours with CA I, and 30 hours with CA II protein samples.

The resonance assignment of human CA I was determined from pre-

vious studies [55] and taken from Biological Magnetic Resonance Data Bank (entry number: 4022, doi:10.13018/BMR4022). The assignment of CA II was kindly shared by Ronald A. Venter from Duke University NMR center[168].

# Chapter 9

# Isothermal titration calorimetry

## 9.1 General principles of ITC

Isothermal titration calorimetry is one of the most popular techniques in molecular biophysics. ITC earned its role in biophysics because it offers an in-depth characterization of interaction alongside the simplicity of use and accuracy [169].

In general, an isothermal titration calorimeter is composed of two cells – a reference cell and a sample cell. In a typical protein-ligand binding experiment by ITC, the reference cell is filled with a buffer solution, while the sample cell contains one of the molecules to be tested, typically the macromolecule. A syringe filled with the second molecule is inserted into the sample cell. During the experiments, the contents of the syringe are gradually and accurately injected into the sample cell. The calorimeter maintains an equal temperature between the two cells. As the interaction in the sample cell takes place, heat is released if the process is exothermic or taken up if the process is endothermic. Power required to maintain the temperature of the cells is being constantly recorded; therefore, the heat released or taken up with each injection ($\delta H$) can be calculated by calculating the area of each peak. This data then is plotted against the molar ratio of tested molecules during each injection as shown in Figure 9.1. The enthalpy of interaction ($\Delta H_{\mathrm{b}}^{\circ}$) in ITC is determined directly. It can be done by calculating the area under the isotherm. Alternately the height of the isotherm can be used
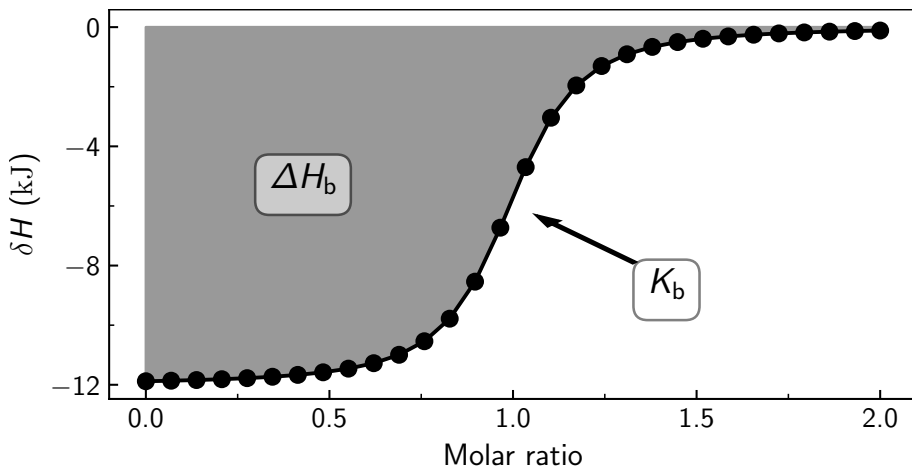
Figure 9.1: Simulation of an ITC isotherm.

to approximate the $\Delta H_b^\circ$ value. The binding constant can be calculating by fitting a mathematical model to the data expressed by equation [16]:

$$\delta H = \Delta H \left( \frac{1}{2} + \frac{1 - (1+r)/2 - y/2}{\sqrt{y^2 - 2y(1-r)(1+r)^2}} \right). \qquad (9.1)$$

Here $y$ is the molar ratio at the give injection ($y = [L_t][M_t]$) and r is the inverse Wisemann factor: $1/r = c = [M_t]K_b$. The Gibbs energy of binding can be then calculated from equation (1.4). Knowing $\Delta G_b^\circ$ and $\Delta H_b^\circ$ the entropy change of binding can be calculated from equation (1.1). For events where binding stoichiometry is not clear, the stoichiometry parameter is often used. In those cases the $[M_t]$ in (9.1) is replaced by the number of binding sites described as the product of stoichiometry and protein concentration: $n \times [M_t]$.

ITC has limitations on the range of $K_b$ values that can be calculated. The limit is related to the Wiseman factor, which also means that it is related to the total concentration of macromolecule used ($[M_t]$). It is commonly stated that the limits for acceptable $c$ values are 1 to 500. The limitation arises because large $c$ values produce very steep isotherms with no points in the transition region and very low $c$value values produce straight lines; both cannot be used for accurate determination of $K_b$. In consequence $\Delta S_b^\circ$ is also determined incorrectly as it is calculated from $\Delta H_b^\circ$ and $K_b$ values.

## 9.2 ITC setup and data analysis for charged polymer-surfactant interactions

### 9.2.1 ITC experiments

In the ITC experiments, the poly(amino acid) concentration was expressed per amino acid monomer. Concentrations of the poly(amino acid)s were determined as described previously [8]. Most experiments were performed with TA Instruments Nano ITC calorimeter with the cell and the syringe volumes of 1.00 mL and 250 µL, respectively. The calorimeter cell was usually loaded with a 0.5 mM to 2 mM solution of charged poly(amino acid) and the syringe – with a 3.25 mM to 20 mM solution of oppositely charged surfactant of various aliphatic chain length. Here and further, the concentration of polymers is expressed for the number of monomers in the solution. The usual titration at constant temperature was carried out in 25 injections of 10 µL at time intervals of at least 3 min and with a syringe stirring speed of 200 rpm. At least 3 min of data was collected before the first injection to ensure the stability of the baseline. Before the experiment, the calorimeter cell was washed with Milli-Q water and pre-rinsed with the prepared solution for the cell. The experimental temperature range was from 13 ℃ to 61 ℃. The experiments were repeated 2 to 10 times.

### 9.2.2 Data analysis

Raw data were processed with NITPIC software [170], with which an isotherm was obtained from noise filtered and baseline adjusted peak integrations. A two-species association model ($A + B \rightleftharpoons AB$) described previously was fitted to isotherm using SEDPHAT software [171]. Parameters of repeated experiments were fit globally. Polymer-surfactant interaction is a sum of several phenomena happening simultaneously. Therefore the typical two species association model does not describe the system perfectly. Furthermore, due to the low association enthalpy, the lowest concentration of the polymer residues in the cell was 0.5 mM. The limitation means that for stronger interactions, the $K_b$ value could not be determined accurately due to the $c$ being too high. Because of these complications, the model was only used to determine the $K_b$ of weaker interactions, and for stronger interactions, a minimal $K_b$ value

was determined instead. Enthalpy values for all experiments were determined by integration of the area under the curve using a numerical "trapz" function from the SciPy package for Python 3 [172].

# Results and Discussion

# Chapter 10

# Determination of Volume Change upon Protein-ligand Interaction by FPSA

The FPSA technique is limited by experimental pressure. FPSA requires the protein to be fully unfolded by pressure. The pressure required for full protein unfolding in most cases exceeds the capabilities of the equipment. Therefore, FPSA experiments require protein-destabilizing agents. Ideally, the changes in the solvent reduce the $\Delta G_{u,0}^{\circ}$ of the protein without changing other pressure unfolding parameters in equation (6.3). As explained in the methods section, a reduction of $\Delta G_{u,0}^{\circ}$ results in a linear shift of $p_{m}$ values, and a complete protein unfolding can be obtained using lower pressure. In addition to pressure, proteins can be destabilized and unfolded by high or low temperatures, and cosolvents [173, 174]. Since it is known that temperature and unfolding volume are highly related [175], thus cosolvents are a choice for protein destabilization for the use in FPSA. Popular denaturing agents like urea and GdmHCl, are often thought to linearly decrease the Gibbs energy of unfolding with the coefficient known as the $m$-value [146]. However, in some cases the effects of cosolvents, especially GdmHCl are not always linear [176] and there are some indications that cosolvents can affect binding volume [12]. Therefore, this section explores the pathways of
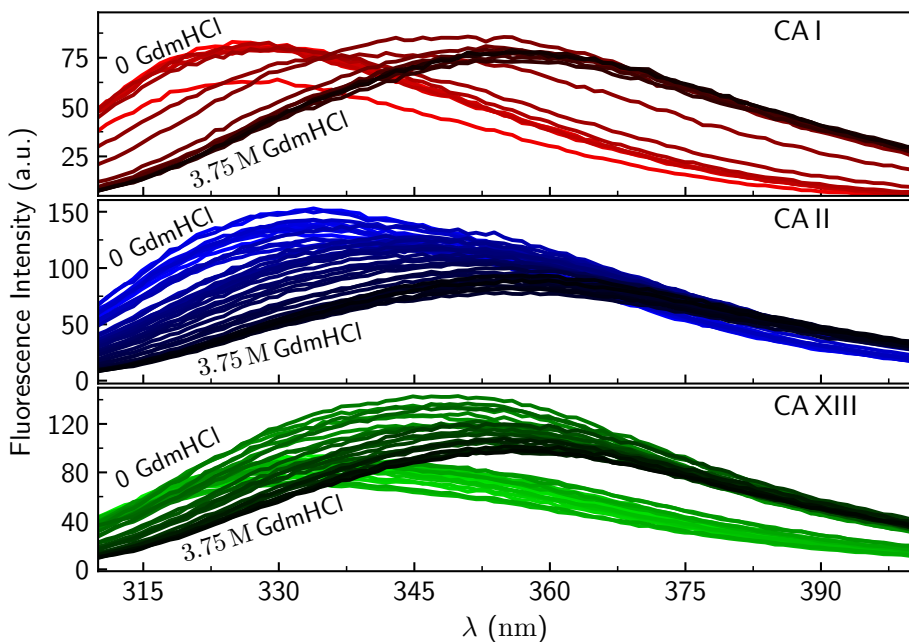
Figure 10.1: Fluorescence spectra of $5\,\mu M$ CA I (Top), CA II (Middle), CA XIII (Bottom) with $0\,M$ to $3.75\,M$ of added GdmHCl. Darker lines signify a larger GdmHCl concentration. Excitation wavelength was $295\,nm$.

CA unfolding with GdmHCl, and GdmHCl effects CA stability in high pressure.

## 10.1 Carbonic anhydrase stability against GdmHCl and pressure

Destabilization by GdmHCl deviates from the linear model and exhibits nonuniform unfolding pathways for different proteins, but despite that, it is often used as a destabilizing agent.

Fluorescence spectra of solutions containing CA isoforms I (CA I), II (CA II) and XIII (CA XIII) were recorded with up to $3.75\,M$ of added GdmHCl (Figure 10.1, bottom panel). Increase in concentrations of GdmHCl resulted in a red shift in fluorescence spectra of all three CA isoforms. $\lambda_{\mathrm{csm}}$ values were calculated for the wavelength range of $320\,nm$ to $400\,nm$. This range was narrowed to make the $\lambda_{\mathrm{csm}}$ values compara-

Table 10.1: Parameters of the models obtained by fitting the results shown in Figure 10.2

| Parameter | CA I | CA II | CA XIII |
|---|---|---|---|
| $\Delta G^{\circ}_{u,0}$ (kJ mol$^{-1}$) | 22.3 | | |
| $\Delta G^{\circ}_{0,N\rightarrow I}$ (kJ mol$^{-1}$) | | 26.8 | 43.8 |
| $\Delta G^{\circ}_{0,I\rightarrow U}$ (kJ mol$^{-1}$) | | 20.9 | 18.8 |
| $m$ (kJ/mol/M$_{[\text{GdmHCl}]}$) | 12.8 | | |
| $m_{N\rightarrow I}$ (kJ/mol/M$_{[\text{GdmHCl}]}$) | | 26.4 | 30.7 |
| $m_{I\rightarrow U}$ (kJ/mol/M$_{[\text{GdmHCl}]}$) | | 9.6 | 8.4 |
| $f_N$ (nm) | 345 | 350 | 351 |
| $f_i$ (nm) | | 354 | 354 |
| $f_U$ (nm) | 359 | 359 | 359 |

ble with those obtained by another spectrofluorimeter. Unfolding curves were obtained by plotting $\lambda_{\text{csm}}$ values against GdmHCl concentrations (Figure 10.2). CA I unfolding with GdmHCl was best described by the
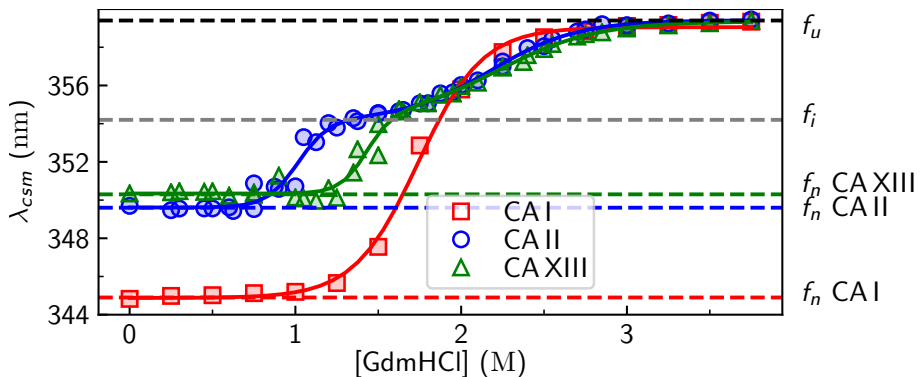


Figure 10.2: Unfolding of 5 µM CA I (red squares), CA II (blue circles) and CA XIII (green triangles) by GdmHCl. $\lambda_{\text{csm}}$ values were calculated from spectra in Figure 10.1 for the wavelength range 320 nm to 400 nm. Solid lines depict fits to equations (6.6) (CA I) or (6.8) (CA II, CA XIII). Dashed lines depict $\lambda_{\text{csm}}$ values for the distinct protein states: native ($f_N$), intermediate ($f_i$), unfolded ($f_U$).

two-state model (6.6), while CA II and CA XIII followed the three state model with a stable intermediate state (6.8). Respective models were fitted, and the results are shown in table 10.1. Several authors previously reported a three-state unfolding pathway of human and bovine CA II isoform [177–179]. Although intermediate states have been detected with

circular dichroism spectroscopy for bovine and human CA I [180–182], these states seem to be populated in a relatively narrow range and are not detectable from our fluorescence data. To my knowledge, there are no published studies on GdmHCl unfolding pathways of CA XIII. Little is known about the origins and attributes of the stable intermediates. CA II unfolding in urea undergoes a two-step transition but Borén *et al.* showed that increasing ionic strength of the solution populates the intermediate state in a wider range of urea as well [178]. This difference suggests that the stabilizing effects by the ionic nature of GdmHCl counteract its denaturant properties, allowing a partially unfolded state to be stable at a certain GdmHCl concentration range. In the results of this thesis, the intermediate state has a signature $\lambda_{csm}$ value of 354.2 nm for both CA I and CA XIII. The parameters of transition from intermediate to fully unfolded states ($\Delta G^\circ_{0,I \to U}$, $m_{I \to U}$) are also similar for the two isoforms, which suggests that the intermediate state is not as specific and structure related as the native form. CA II looses esterase and $CO_2$ hydration activity in GdmHCl concentrations greater than 0.9 M [180, 183], this coincides with the transition from native to intermediate state.

These results confirm that even structurally related proteins have different stability against GdmHCl-induced protein unfolding and have different unfolding pathways. Early results suggest that GdmHCl concentrations in which native population starts to diminish should not be used in ligand binding studies. However, these results leave the following questions open: "How CA stability in GdmHCl solutions is related to pressure-induced unfolding?" and "What effect do sulfonamide inhibitors have on CA structure perturbation by GdmHCl and pressure?".

## 10.2 Unfolding of CA by pressure in solutions with GdmHCl

Pressure-induced unfolding of CA I, CA II and CA XIII were done in GdmHCl solutions of various concentrations. Figure 10.3 shows the unfolding curves of CA II in the presence of 0.5 M, 0.8 M, 1.0 M, and 1.1 M GdmHCl. GdmHCl concentrations up to 0.8 M shifts the unfolding curve towards lower pressure without changing the $f_N$ and $f_U$ parameters of the curves or the shape of the curve. Although there is a systematic 2 nm difference between $\lambda_{csm}$ values obtained with the fluo-
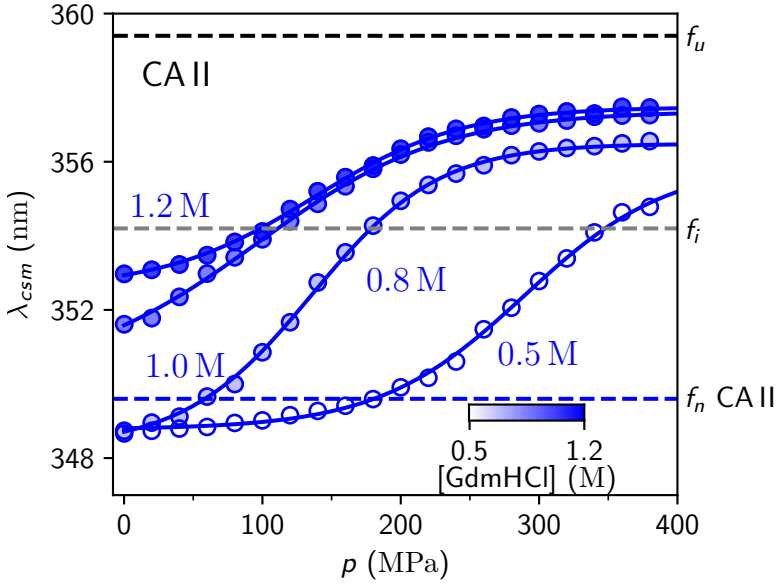
Figure 10.3: Pressure-induced unfolding curves of CA II in solutions with 0.5 M, 0.8 M, 1.0 M, 1.2 M of GdmHCl. Solid lines represent fits to the pressure unfolding model in equation (6.2). Dashed lines represent the $\lambda_{\text{csm}}$ values for native, intermediate and unfolded forms determined in Figure 10.2.

rimeter used for GdmHCl unfolding experiments and the high pressure fluorimeter, the unfolding curves start at a similar $f_{\text{N}}$ values if GdmHCl concentration is low. At 1 M GdmHCl the unfolding curve loses its sigmoidal shape at the beginning and starts at a higher $\lambda_{\text{csm}}$ value. These characteristics, alongside GdmHCl-induced unfolding results, indicate that at these conditions, no population is dominant and rather, native and intermediate states co-exist. GdmHCl-induced unfolding data at 1.2 M GdmHCl show that the intermediate state dominates. A stable intermediate state seems to be confirmed by pressure-induced unfolding results as well, since, in these conditions, the unfolding curve regains its sigmoidal shape and starts at a $\lambda_{\text{csm}}$ value similar to that of $f_{\text{i}}$ in the GdmHCl-induced unfolding experiment. In all tested GdmHCl concentrations, pressure-induced unfolding of CA II exhibited a two-state transition. The $\lambda_{\text{csm}}$ values at the end of all pressure-induced unfolding experiments were significantly higher than the intermediate state in GdmHCl-induced unfolding. It can be concluded that the stable intermediate is a particularity onset by high GdmHCl concentrations and

not a rule for all methods of structure disturbance. The $f_U$ values for all unfolding curves are significantly lower than those obtained by unfolding with GdmHCl. These values might indicate that state of CA II unfolded by pressure is not identical to the state unfolded by GdmHCl. Another possibility is that this is an effect caused by high concentration of GdmHCl at high pressure and it is independent of protein state. There was a general tendency for $f_U$ values obtained by pressure-induced unfolding (e.g., Figure 10.3) to increase with added GdmHCl. Therefore, I will assume further that $f_U$ values, obtained by unfolding with pressure, depend on GdmHCl and should not be a global parameter when comparing pressure unfolding data in different conditions.

For a clearer view of how CA stability against pressure and GdmHCl relate to each other, $p_m$ values of the three CA isoforms were plotted against GdmHCl concentration in Figure 10.4. Melting pressure values,
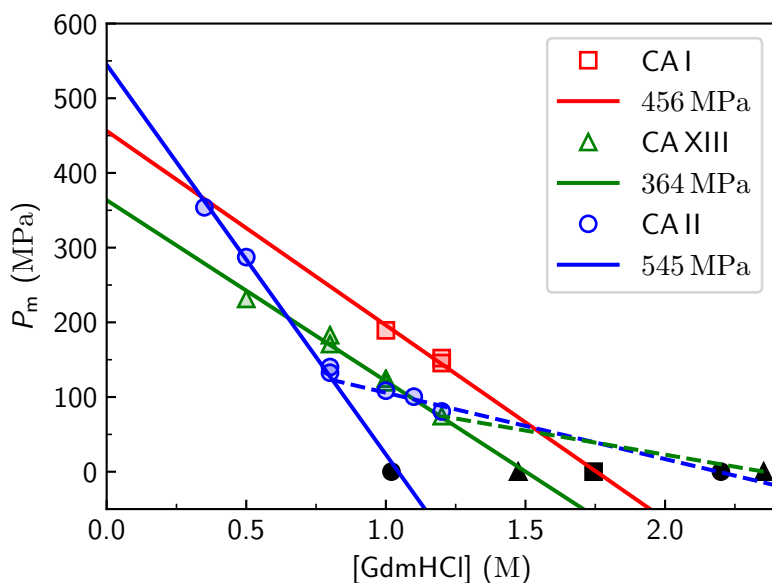


Figure 10.4: Melting pressures of CA I (red squares), CA II (blue circles) and CA XIII (green triangles) in solutions with different GdmHCl concentrations. Solid lines represent linear fits with extrapolations towards GdmHCl-free solution. Black markers represent midpoints of GdmHCl-induced unfolding at ambient pressure in Figure 10.2. Both first and second transition mid points are represented for CA II and CA XIII. Dashed lines represents linear fits for points beyond the first transition in GdmHCl unfolding as determined in Figure 10.2.

plotted in Figure 10.4, were obtained from the midpoints of unfolding curve models. The results of model parameters are given in table 10.2.

Table 10.2: Parameters of CA I, CA II, CA XIII pressure-induced unfolding curve models in solutions of different GdmHCl concentrations.

| CA I | | | | |
|---|---|---|---|---|
| | $\Delta G^{\circ}_{u,0}$ (kJ mol$^{-1}$) | $\Delta V_u$ (mL mol$^{-1}$) | $f_N$ (nm) | $f_U$ (nm) |
| Global | No | No | Yes | No |
| 0.35 M GdmHCl | 8.0 | -42 | 347 | 358 |
| 1.2 M GdmHCl | 13.5 | -93 | 347.2 | 358 |
| 1.2 M GdmHCl | 9.5 | -62 | 347 | 358 |
| CA II first transition | | | | |
| | $\Delta G^{\circ}_{u,0}$ (kJ mol$^{-1}$) | $\Delta V_u$ (mL mol$^{-1}$) | $f_N$ (nm) | $f_U$ (nm) |
| Global | No | No | Yes | No |
| 0.35 M GdmHCl | 21.3 | -54 | 349 | 356 |
| 0.5 M GdmHCl | 17.1 | -58 | 349 | 354 |
| 0.8 M GdmHCl | 8.8 | -66 | 349 | 355 |
| 0.8 M GdmHCl | 10.6 | -79 | 349 | 355 |
| CA II second transition | | | | |
| | $\Delta G^{\circ}_{u,0}$ (kJ mol$^{-1}$) | $\Delta V_u$ (mL mol$^{-1}$) | $f_N$ (nm) | $f_U$ (nm) |
| Global | No | No | No | No |
| 1 M GdmHCl | 6.9 | -56 | 352 | 356 |
| 1.1 M GdmHCl | 4.7 | -40 | 352 | 356 |
| 1.2 M GdmHCl | 3.7 | -40 | 352 | 356 |
| CA XIII | | | | |
| | $\Delta G^{\circ}_{u,0}$ (kJ mol$^{-1}$) | $\Delta V_u$ (mL mol$^{-1}$) | $f_N$ (nm) | $f_U$ (nm) |
| Global | No | No | Yes | No |
| 0.5 M GdmHCl | 13.2 | -57 | 349 | 354 |
| 0.8 M GdmHCl | 14.4 | -79 | 349 | 356 |
| 0.8 M GdmHCl | 13.1 | -77 | 349 | 355 |
| 1 M GdmHCl | 10.1 | -84 | 349 | 357 |
| 1 M GdmHCl | 9.9 | -79 | 349 | 357 |

| 1.2 M GdmHCl | 5.5 | -73 | 349 | 357 |

Four global fits were done for different ensembles of data: CA I, CA II, CA II intermediate and CA XIII first transition. $\Delta G_{u,0}^{\circ}$ and $\Delta V_u$ parameters were left local as $\Delta G_{u,0}^{\circ}$ is expected to decrease with GdmHCl concentration and GdmHCl effects on $\Delta V_u$ aren't well known. For simplicity $\Delta \beta_u$ parameter was set to 0 for all fits. Variation of the $\Delta \beta_u$ parameter did not change the $p_m$ values of the models but changed the $\Delta V_u$ values. As explained in section 2.2 and visualized in Figure 6.2, at a certain value range $\Delta V_u$ and $\Delta \beta_u$ parameters can compensate each other. This compensation means that several combinations of $\Delta V_u$ and $\Delta \beta_u$ can produce very similar unfolding curves. In these cases, unrealistically precise and abundant data would be required to separate the contribution of each parameter. Ideally, other methods, such as sound velocity measurements, could help to verify the results. Moreover, the difference in compressibility between folded and unfolded states is insignificant due to the good agreement between PPC and pressure-induced unfolding experiments [99]. Therefore, in this thesis, changes in the unfolding curve "flatness" are attributed to $\Delta V_u$, while $\Delta \beta_u$ is set to 0. Although this assumption has limitation, it enables studies of protein-ligand binding at elevated pressures. Parameter $f_N$ was global for all ensembles except that of CA II intermediate state. This difference in $f_N$ appears because both native and intermediate forms exist in the beginning of those experiments. Parameter $f_U$ was varied for each experiment separately. As explained earlier, there was a general tendency for $\lambda_{csm}$ values to have different plateaus at high pressure, dependent on GdmHCl concentration. Parameter $f_s$ was set to $0.0042 \, \mathrm{nm \, MPa^{-1}}$ for CA II, based on the experiments without GdmHCl, for other ensembles it was set to zero.

In Figure 10.4 the $p_m$ values decrease linearly with GdmHCl concentration up to 0.8 M for CA II and 1.2 M for CA I and CA XIII. In this experiment, the $p_m$ values are in line with midpoints of GdmHCl-induced unfolding at ambient pressure (black marks). This confirms the linear relationship model (equation (6.7)) in this range. The linear fits could be extrapolated to GdmHCl-free solution, this way, $p_m$ values in water ($p_m(\mathrm{H_2O})$) were calculated. The $p_m$ values for experiments with CA II, in GdmHCl concentrations greater than the mid-

point of the first transition (1.0 M), are in line with the midpoint of the second transition. The linear fit for these points has a smaller slope ($-89\,\text{MPa/M}_{[\text{GdmHCl}]}$) compared to the linear fit of points in low GdmHCl concentration ($-522\,\text{MPa/M}_{[\text{GdmHCl}]}$). The slopes to linear fits are directly proportional to the denaturant $m$-value. The magnitude of $m$-value is related to the changes in solvent accessible surface area upon unfolding ($\Delta$ASA) [104]. This relationship means that the intermediate state has a greater surface area accessible to the solvent than the native form. This result is in agreement with the molten globule model, which is a common representation of intermediates in protein unfolding. CA unfolding volume values from fits in table 10.2 had a negative correlation with GdmHCl concentration. At higher GdmHCl concentrations, $\Delta V_u$ was increasingly more negative. A similar tendency was observed by Sasahara *et al.*; where the authors showed that the slopes of $\Delta G_{u,0}^\circ$ versus pressure plots were increasing with GdmHCl at low temperatures [184]. This tendency suggests using the linear extrapolation method with caution, but as the tendency was most pronounced in temperatures of 10 °C to 15 °C, assuming linearity for our results done at 20 °C is a reasonable simplification.

## 10.3 Ligand binding in GdmHCl solutions measured by TSA

To test how GdmHCl affects the binding parameters of CA inhibitors, TSA experiments were conducted in protein solutions with different amounts of GdmHCl. CA II isoform and three compounds—**2**, **3**, **5**—of different binding affinity were tested at GdmHCl concentrations up to 1.2 M. TSA is based on protein thermal denaturation and stabilization against it by ligands. Addition of GdmHCl lowered melting temperature ($T_m$) values of temperature-induced CA II unfolding. The unfolding transitions of CA II could not be observed in GdmHCl concentrations greater than 1 M GdmHCl; at those conditions the $T_m$ values too low to observe, indicating that CA II is largely unfolded at room temperature with that amount of GdmHCl. Figure 10.5 shows examples of CA II unfolding curves in the presence and absence of ligand **5**. A mathematical model given in equation (7.4) was fitted to the data. If the concentration of ligand **5** is less than the stoichiometric ratio, two thermal unfolding
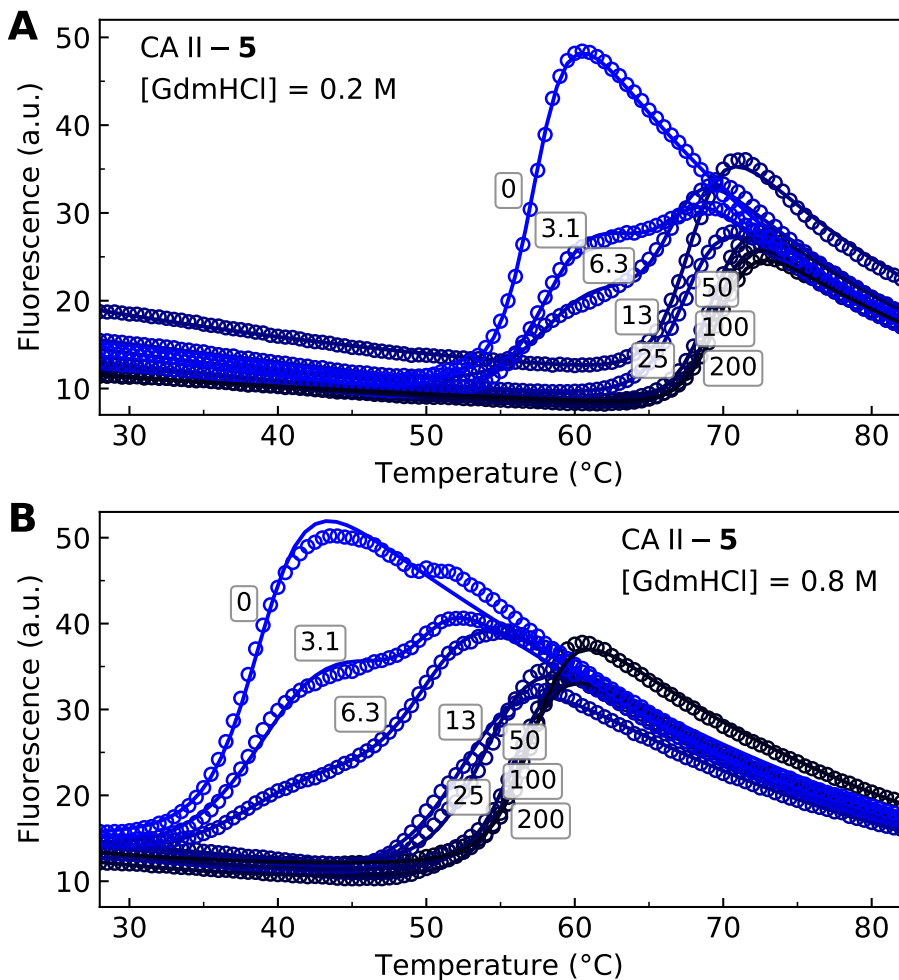
Figure 10.5: Thermal denaturation curves of $10\,\mu\mathrm{M}$ CA II in the presence of $0\,\mu\mathrm{M}$ to $200\,\mu\mathrm{M}$ **5**. Measurements were taken in a solution with $0.2\,\mathrm{M}$ (panel A) and $0.8\,\mathrm{M}$ (panel B) of GdmHCl. The lines represent model fits.

peaks are visible. The second peak appears because very tightly bound protein-ligand complexes denature separately from the ligand-free protein [154]. In this case, the mathematical model described in [154] was fitted instead.

Dosing curves at $0.2\,\mathrm{M}$ and $0.8\,\mathrm{M}$ GdmHCl are shown in Figure 10.6. The dosing data were fitted globally for a set of experiments in the same GdmHCl concentration, only ligand-dependent variables ($K_\mathrm{b}$,
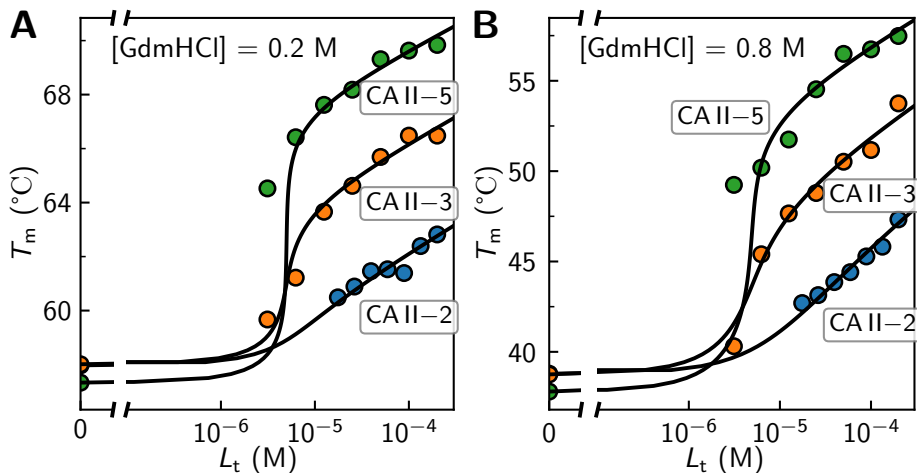
Figure 10.6: TSA dosing curves of CA II with three ligands – **2** (blue), **3** (orange), and **5**(green). The data shown were acquired in solutions with 0.2 M (panel A) and 0.8 M (panel B) GdmHCl.

$\Delta H_b^\circ$, $_bC_p$) were local. Results of all fits are given in table 10.3. Results

Table 10.3: The fitted parameters of CA II interaction with compounds **2**, **3**, and **5** obtained by the non-linear regression analysis of the TSA dosing curves.

| [GdmHCl] (M) | $\Delta H_u^\circ$ kJ mol$^{-1}$ | $K_b$ **2** | $K_b$ **3** | $K_b$ **5** |
|---|---|---|---|---|
| 0.0 | 672 | $8.4 \times 10^4$ | $4.6 \times 10^6$ | $3.1 \times 10^8$ |
| 0.2 | 840 | $7.1 \times 10^5$ | $7.0 \times 10^7$ | $9.8 \times 10^9$ |
| 0.4 | 360 | $1.4 \times 10^5$ | $2.7 \times 10^7$ | $2.5 \times 10^9$ |
| 0.6 | 350 | $1.7 \times 10^5$ | $6.7 \times 10^7$ | $3.8 \times 10^9$ |
| 0.8 | 220 | $1.5 \times 10^5$ | $5.8 \times 10^6$ | $3.2 \times 10^8$ |
| 1.0 | 200 | $2.0 \times 10^5$ | $4.9 \times 10^6$ | $1.2 \times 10^9$ |

show that the enthalpies of unfolding were reduced proportionally to the added GdmHCl concentration. This reduction is the result of lower $T_m$ values because the change in heat capacity of unfolding is positive [185]. Despite that, protein-ligand binding constants, $K_b$, for tested compounds, remained the same within the margin of error expected, which is $\pm$ two-fold of $K_b$ in TSA [186]. The results confirm that CA II binding of sulfonamides is not significantly changed at concentrations of GdmHCl up to 1 M, the results are in line with the activity measure-

ments [180, 183].

## 10.4 Protein stabilization against GdmHCl and pressure denaturation by ligands

When small molecule ligands bind to a protein, it can remain folded at high pressure, which otherwise would unfold the protein [129, 143]. Therefore it would be relevant to study whether ligands stabilize protein structure against GdmHCl and high pressure similarly. Experiments of pressure-induced CA II unfolding were done in 1.2 M GdmHCl solution with ligands **5** and **4** that have different binding affinity towards CA II. The resulting unfolding curves are shown in Figure 10.7. At 1.2 M
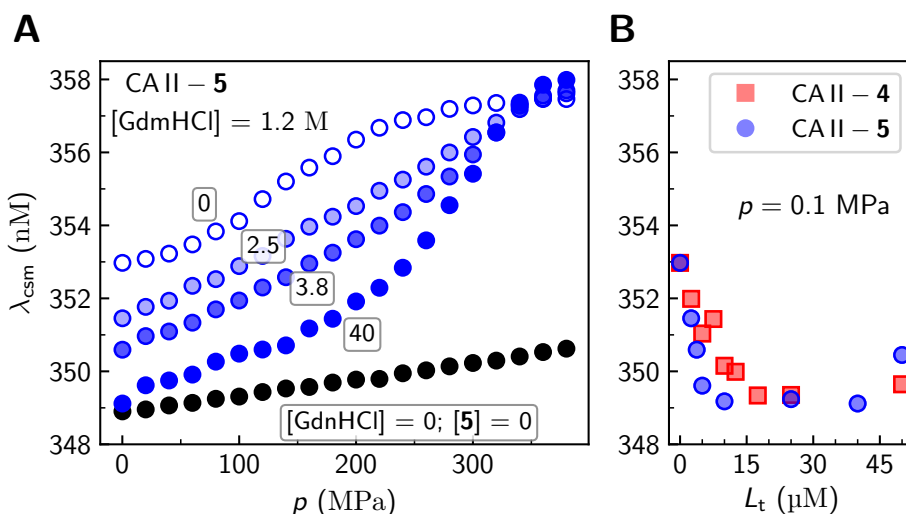


Figure 10.7: Panel A: Pressure unfolding curves of $5\,\mu M$ CA II in a solution with $1.2\,M$ GdmHCl and $0\,\mu M$ to $40\,\mu M$ of ligand **5**. Black circles represent $\lambda_{csm}$ values of CA II in GdmHCl-free buffer. Panel B: $\lambda_{csm}$ values of CA II in $1.2\,M$ GdmHCl solution at ambient pressure, plotted against the concentration of ligands **5** and **4**.

GdmHCl concentration, the intermediate state of CA II is dominant. With no ligand added, a two-state transition between intermediate and fully unfolded forms is observed. As the ligand is added the unfolding curves in Figure 10.7 A start at lower $\lambda_{csm}$ values until it reaches the $\lambda_{csm}$ value of native CA II. At high ligand concentrations, a two-state

pressure unfolding from native to fully unfolded is observed. This observation is interesting because no prolonged intermediate state is seen even at this GdmHCl concentration when the protein is unfolded by pressure. In Figure 10.7 B $\lambda_{\text{csm}}$ values of CA II at ambient pressure and 1.2 M GdmHCl are plotted against ligand concentrations. The values of $\lambda_{\text{csm}}$ values decrease until it reaches the $\lambda_{\text{csm}}$ value of the native CA II. The plateau is reached, when the protein is saturated with the ligand. Ligand **5** binds to CA II more tightly at these conditions then ligand **4** and therefore, the $\lambda_{\text{csm}}$ values reach the plateau at lower concentrations of **5** than that of **4**. From these experiments, it can be concluded that tight binding ligands can stabilize the native structure of CA II at high GdmHCl concentrations, where it would be partially unfolded otherwise.

GdmHCl-induced unfolding experiments were done at different concentrations of ligand **3**. The unfolding curves are displayed in Figure 10.8. The results of model (6.8) fitting are given in table 10.4. Higher
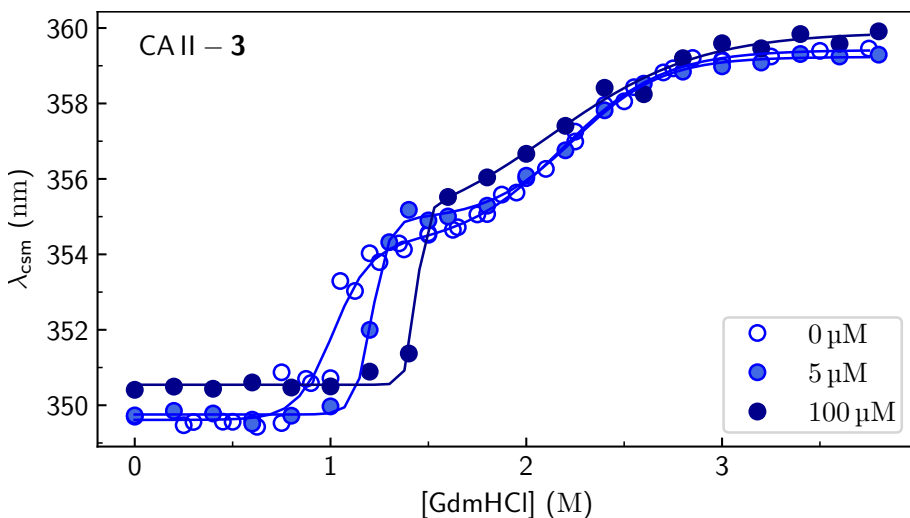


Figure 10.8: GdmHCl-induced unfolding of CA II (5 μM) with 0, 5 μM, 100 μM of compound **3**. Lines represent fits to model equation (6.8).

concentrations of ligand **3** stabilized CA II against GdmHCl unfolding in a concentration related manner, which was also manifested by an increase in $\Delta G^{\circ}_{0,\text{N}\rightarrow\text{I}}$ parameter. The difference in $\Delta G^{\circ}_{0,\text{N}\rightarrow\text{I}}$ values of ligand-free CA II and CA II-ligand **3** complex is comparable to the Gibbs energy of binding ($-43.5$ kJ/M). Therefore, it can be deduced, that be-

Table 10.4: Fitting results of model equation (6.8) for gnd-induced unfolding of CA II with added ligand **3**.

| | 0 µM **3** | 5 µM **3** | 10 µM **3** | 100 µM **3** |
|---|---|---|---|---|
| $\Delta G^{\circ}_{0,N \to I}$ (kJ mol$^{-1}$) | 27 | 70 | 52 | 140 |
| $\Delta G^{\circ}_{0,I \to U}$ (kJ mol$^{-1}$) | 21 | 25 | 23 | 14 |
| $f_i$ (nm) | 354 | 355 | 355 | 354.4 |
| $f_N$ (nm) | 350 | 350 | 350 | 350.5 |
| $f_U$ (nm) | 359 | 359 | 359 | 359.9 |
| $m_{N \to I}$ (kJ/mol/M$_{[GdmHCl]}$) | 26 | 58 | 38 | 97 |
| $m_{I \to U}$ (kJ/mol/M$_{[GdmHCl]}$) | 10 | 11 | 10 | 7.0 |

cause only the native form of the protein binds the ligand, additional energy is required to break the bonds between the protein and the ligand to disturb the native structure. In addition, added ligand has increased the $m_{N \to I}$ parameter, steepening the transition from native to intermediate states. The $m$-value parameter is usually associated with $\Delta$ASA upon unfolding. An increased $m$-value can indicate that ligand binding decreases the solvent-exposed surface area of the protein. The parameters associated with the transition from intermediate to fully unfolded states remain without significant changes when the ligand is added. This confirms that ligand **3** does not bind to the intermediate state of CA II. These findings confirm that ligands stabilize against both pressure and GdmHCl unfolding, therefore pressure unfolding experiments protein-ligand complexes can be conducted at such concentrations of GdmHCl that would unfold the ligand free protein.

## 10.5   Binding volume measurements at a single GdmHCl concentration

FPSA technique requires a complete unfolding; thus the CA isoforms must be additionaly destabilized. Although previous results have raised some indications that GdmHCl changes the volumetric parameters of the system, FPSA data at a certain GdmHCl concentration can be useful if the goal is to compare binding properties of ligands to each other [127, 129, 130]. To test if this method is applicable for CA and sulfonamide inhibitor pairs, two experiments with different protein-ligand pairs were done. FPSA results of CA I binding to compound **1** are presented in

Figure 10.9. The addition of ligand **1** shifted the midpoints of curves
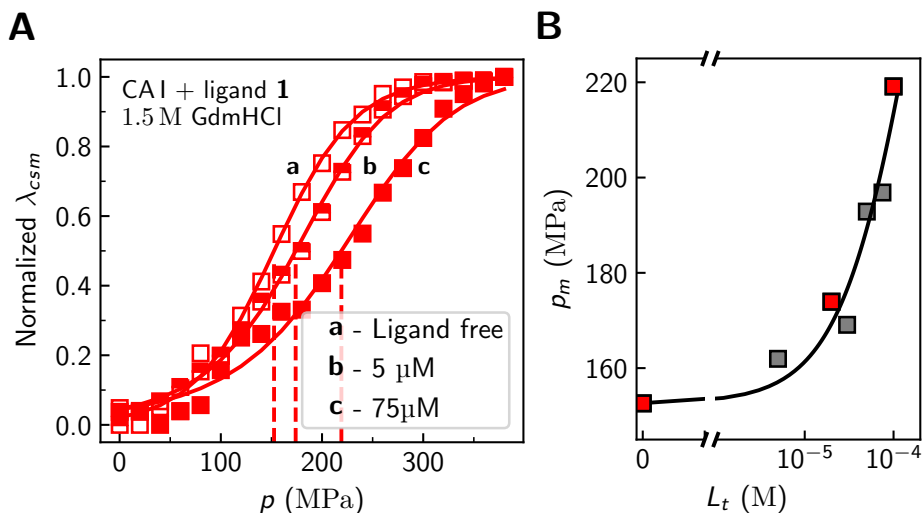


Figure 10.9: FPSA experiment of ligand **1** binding to CA I, performed at 1.5 M GdmHCl. The unfolding curves of CA I, in the absence and presence of, 5 µM and 75 µM ligand **1** are shown in panel A. The Protein concentration was 5 µM. Lines in panel A are model fits. The dosing curve obtained from the midpoints of the unfolding curves is shown in panel B. The solid black line represents a fit of the dosing model.

towards higher pressures. This effect was small enough to obtain unfolding curves in a wide ligand concentration range. The dosing curve was fitted with $\Delta G_b^\circ = 20 \, \text{kJ} \, \text{mol}^{-1}$ and $\Delta V_b = -27 \, \text{mL} \, \text{mol}^{-1}$. The $\Delta G_b^\circ$ value is comparable to that in the literature [187]. The binding volume determined by FPSA is similar to that determined by NMR [139], which is $(-23 \pm 3) \, \text{mL} \, \text{mol}^{-1}$. There are two main reasons for this discrepancy. First, unlike FPSA, the NMR experiments were done in GdmHCl-free environment. This thesis later shows that GdmHCl can alter binding volume. Second, similarly to unfolding fits, the dosing fit can also be subject to compensation between volume and compressibility parameters. In this experiment, the $\Delta \beta_b$ parameter was set to 0, but an identically good fit could be obtained with a variable $\Delta \beta_b$. This yields $\Delta V_b$ value of $-8 \, \text{mL} \, \text{mol}^{-1}$ and $\Delta \beta_b$ value of $-0.1 \, \text{mL} \, \text{mol}^{-1} \, \text{MPa}^{-1}$. Therefore, the fit can not separate contributions from these two parameters. The same system of CA I-ligand **1**, showed a linear shift in $\Delta G_b^\circ$ with pressure, as described in section 2.2 and the publication based on this
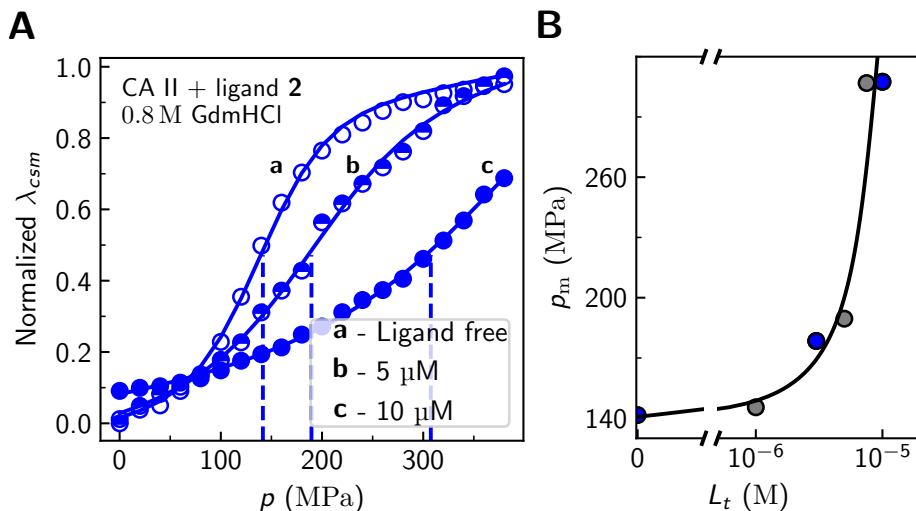
Figure 10.10: FPSA experiment of ligand **2** binding to CA II, performed at $0.8\,\mathrm{M}$ GdmHCl. The unfolding curves of CA I, in the absence and presence of, $5\,\mu\mathrm{M}$ and $10\,\mu\mathrm{M}$ ligand **2**, are shown in panel A. The protein concentration was $3\,\mu\mathrm{M}$. Lines in panel A are model fits. The dosing curve, obtained from the midpoints of the unfolding curves, is shown in panel B. The solid black line represents a fit of the dosing model.

thesis [139]. This indicates a negligible $\Delta\beta_{\mathrm{b}}$, therefore the $\Delta V_{\mathrm{b}}$ value of $-27\,\mathrm{mL\,mol^{-1}}$ and $\Delta\beta_{\mathrm{b}}$ of 0 is a more reasonable result.

Ligand **2** binding to CA II was tested at $0.8\,\mathrm{M}$ GdmHCl (Figure 10.10). In this case, full unfolding curves could not be obtained at the same GdmHCl concentration in a wide enough ligand concentration range. The addition of ligand **2** shifted the $p_{\mathrm{m}}$ values substantially towards higher pressure. Ligand concentration as low as $10\,\mu\mathrm{M}$ (three times that of the protein) was enough to shift the unfolding to experimentally unreachable pressure range. Compound **2** is a relatively weak binding ligand with a $K_{\mathrm{d}}$ of $4\,\mu\mathrm{M}$. Weak binding and a large shift in $p_{\mathrm{m}}$ signifies a large negative $\Delta V_{\mathrm{b}}$ value. The fit yielded $\Delta V_{\mathrm{b}} = -48\,\mathrm{mL\,mol^{-1}}$ and $\Delta G_{\mathrm{b}}^{\circ} = -25\,\mathrm{kJ\,mol^{-1}}$. Both increased binding strength and negative binding volume lead to the protein's stabilization against pressure. Knowing that ligand **2** is a relatively weak CA II inhibitor and that changes in volume due to protein-ligand binding can be even more negative, it can be concluded that the pressure range is not enough to conduct FPSA experiments for this system. Therefore, a

different approach is needed to test $\Delta V_\mathrm{b}$ values of a larger set of CA II ligands.

## 10.6 Obtaining $\Delta V_\mathrm{b}$ from experiments in different GdmHCl solutions

Thermodynamic parameters determined so far were only observed in particular GdmHCl concentrations. This raises two concerns. First, would the results be different in GdmHCl-free environment? Furthermore, it is not always possible to achieve protein unfolding at the same GdmHCl concentration if the ligand is a very strong binder or binds with a large negative $\Delta V_\mathrm{b}$. Both concerns can be addressed with a new approach relying on data at several GdmHCl concentrations.

As determined previously, $p_\mathrm{m}$ values of CA unfolding depend linearly on GdmHCl concentration, at a specific range. Thus $p_\mathrm{m}$ values can be extrapolated towards GdmHCl-free conditions to obtain $p_\mathrm{m}$ values in GdmHCl-free buffer ($p_\mathrm{m}(\mathrm{H_2O})$). CA II unfolding experiments were done with ligand **3** at GdmHCl concentrations ranging from 0.35 M to 1.20 M. The resulting $p_\mathrm{m}$ values are plotted in Figure 10.11. The unfolding curves were fit using the same constrains and reasoning as the fitting of the first CA II transition in section 1.2. The results of the unfolding curves are given in table 10.5.

Table 10.5: Fit results of CA II pressure-induced unfolding with various amounts of GdmHCl and ligand **3**.

| Ligand-free CA II | | | | |
|---|---|---|---|---|
| Parameter: | $\Delta G^{\circ}_{\mathrm{u},0}$ $(\mathrm{kJ\,mol^{-1}})$ | $\Delta V_\mathrm{u}$ $(\mathrm{mL\,mol^{-1}})$ | $f_\mathrm{N}$ (nm) | $f_\mathrm{U}$ (nm) |
| Global: | No | No | Yes | No |
| 0.35 M GdmHCl | 21.3 | -54 | 349 | 356 |
| 0.5 M GdmHCl | 17.1 | -58 | 349 | 354 |
| 0.8 M GdmHCl | 8.8 | -66 | 349 | 355 |
| 0.8 M GdmHCl | 10.6 | -79 | 349 | 355 |
| CA II + 10 µM **3** | | | | |
| Global: | No | No | Yes | No |
| 0.9 M GdmHCl | 14.4 | -48 | 350 | 357 |

| | | | | |
|---|---|---|---|---|
| 1.0 M GdmHCl | 12.1 | -47 | 350 | 357 |
| 1.1 M GdmHCl | 5.7 | -44 | 350 | 357 |
| 1.2 M GdmHCl | 4.0 | -47 | 350 | 357 |
| CA II + 20 μM **3** | | | | |
| Global: | No | No | Yes | Yes |
| 1.0 M GdmHCl | 15.8 | -60 | 350 | 357 |
| 1.1 M GdmHCl | 6.1 | -46 | 350 | 357 |
| 1.2 M GdmHCl | 4.2 | -57 | 350 | 357 |
| 1.2 M GdmHCl | 7.0 | -58 | 350 | 357 |
| CA II + 50 μM **3** | | | | |
| Global: | No | No | Yes | Yes |
| 1.0 M GdmHCl | 10.1 | -52 | 350 | 357 |
| 1.1 M GdmHCl | 6.2 | -53 | 350 | 357 |
| 1.2 M GdmHCl | 4.2 | -53 | 350 | 357 |
| CA II + 100 μM **3** | | | | |
| Global: | No | No | Yes | Yes |
| 1.0 M GdmHCl | 9.9 | -51 | 350 | 358 |
| 1.1 M GdmHCl | 6.1 | -52 | 350 | 358 |
| 1.2 M GdmHCl | 3.4 | -61 | 350 | 358 |
| 1.2 M GdmHCl | 3.6 | -70 | 350 | 358 |

Depending on GdmHCl concentration, $p_{\mathrm{m}}$ values shifted linearly in the presence of the ligand and $p_{\mathrm{m}}(\mathrm{H_2O})$ values could be calculated. Interestingly, the presence of a ligand shifted the $m$-value, observable from the slope of the linear model. This shift agrees with previously obtained results from CA II-**3** complex unfolding with GdmHCl. Dosing curve was obtained from calculated $p_{\mathrm{m}}(\mathrm{H_2O})$ values and is given in Figure 10.11 B. The fit of the dosing model yielded $\Delta V_{\mathrm{b}} = -8\,\mathrm{mL\,mol^{-1}}$. A negative $\Delta V_{\mathrm{b}}$ value is also indicated by $\Delta V_{\mathrm{u}}$ values of the fits in table 10.5. $\Delta V_{\mathrm{u}}$ values for CA II-**3** complex trended lower than ligand-free CA II.

The trend lines in Figure 10.11 A, show that the protein-ligand complex is more stable against pressure, but at the same time, its stability is more susceptible to changes in GdmHCl concentration. Based on the dosing model, it can be concluded that stabilization occurs from two main effects: first, the negative $\Delta V_{\mathrm{b}}$, which makes the complex more
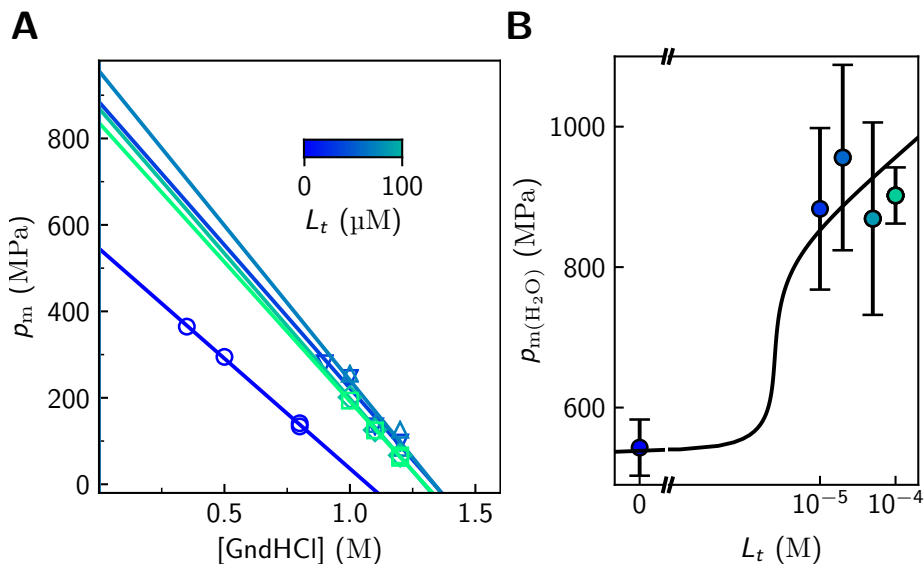
Figure 10.11: Panel A: $p_m$ values of CA II ($5\,\mu\mathrm{M}$) in solutions with $0.35\,\mathrm{M}$ to $1.20\,\mathrm{M}$ GdmHCl and $0\,\mu\mathrm{M}$ to $100\,\mu\mathrm{M}$ of ligand **3**. The lines are linear fits extrapolated to conditions with no added GdmHCl. Panel B: dosing curve from $p_m(\mathrm{H_2O})$ values obtained by extrapolations in panel A. The line is a fit to the dosing model in equation (14.4).

resistant to pressure; and second, an increased $\Delta G^{\circ}_{\mathrm{u},0}$ of the complex, which makes it more stable to a variety of perturbations since bonds between the protein and the ligand must be broken to unfold the complex. The change in $m$-value upon ligand binding can be interpreted as a reduction of $\Delta\mathrm{ASA}$. Generally, sulfonamide inhibitors bind to a specific pocket of CA. Therefore, most likely the complementary structure of the ligand shields a portion of this cavity's surface from water, reducing the surface exposed to the solvent. Since the unfolded form does not bind the ligand, it follows that the difference between folded and unfolded forms is greater for the complex than ligand-free CA II.

Overall the results show that FPSA from extrapolated $p_m(\mathrm{H_2O})$ values can be used to calculate the change in volume due to protein-ligand binding. This approach is valuable, if the unfolding of ligand-free and ligand-bound protein is impossible at the same conditions, such as the case of CA II-**3** complex. Furthermore, the difference in $m$-values of the protein and protein-ligand complex means that the difference in stability

between the forms depends on GdmHCl concentration. This dependence leads to the conclusion that $\Delta V_b$ values determined at a specific GdmHCl concentration is only true in those particular conditions and should be considered cautiously.

# Chapter 11

# Investigation of carbonic anhydrase and suflonamide interaction using high pressure NMR

## 11.1  Spectra of ligand bound and ligand free CA II $^1$H $-$ $^{15}$N HSQC NMR

NMR Spectroscopy was used to study the interaction of three protein-ligand pairs: CA I-**1**, CA I-**6** and CA II-**1**. $^1$H $-$ $^{15}$N HSQC NMR spectra (Figure 11.1) showed that the rate of interaction for all binding pairs was found to be slow (the exchange rate significantly lower than the difference in resonance frequencies). Two signals of a single amino acid, one of the ligand-free form and one of the ligand-bound form, could be observed in a single spectrum, e.g., the signal of Tyr 194 (Figure 11.2). Increasing ligand concentrations (left panels in Figure 11.2) enhanced the intensity of the peak corresponding to ligand-bound CA I. The increase in ligand concentration did not change the position of the peaks. The right panels in Figure 11.2 show the behavior of the Tyr 194 peak at different pressures and a fixed concentration of the ligand. As the pressure increases, the intensity of the ligand-bound state peak increases and both peaks propagate along $\delta(^1$H$)$ and $\delta(^{15}$N$)$ axes in the $^1$H $-$ $^{15}$N HSQC spectra. Based on the Le Chatelier's principle, at elevated pressures, the
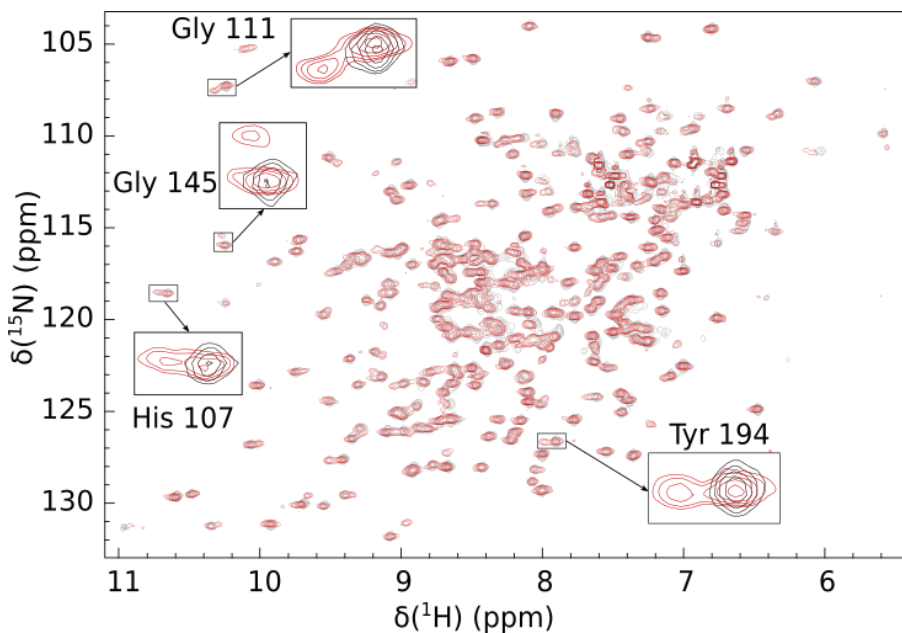
Figure 11.1: $^1\text{H}-^{15}\text{N}$ HSQC spectra of $0.5\,\text{mM}$ CA I with $0.7\,\text{mM}$ ligand **1** (red) and ligand-free (blue). Both ligand-bound and ligand-free states of the protein are detected at this concentration ratio as depicted in the enlarged peaks of amino acid residues.

protein-ligand system tries to occupy a lower volume. Thus, if increasing pressure enhances the peak intensity of the protein-ligand complex, the state of the protein-ligand system, where the ligand is bound to the protein is lower than the volume of the system where the ligand is unbound from the protein.

## 11.2  Calculation of the change in volume due to CA I-ligand 1 binding

The change in volume is defined as the partial derivative of the Gibbs energy with respect to pressure (equation (1.5)); thus, if compressibility is negligible the change in volume upon protein–ligand binding at a constant temperature, $T$, is

$$\Delta V_\text{b} = \left( \frac{\Delta G_\text{b}^{\circ}}{p} \right)_T \tag{11.1}$$

103
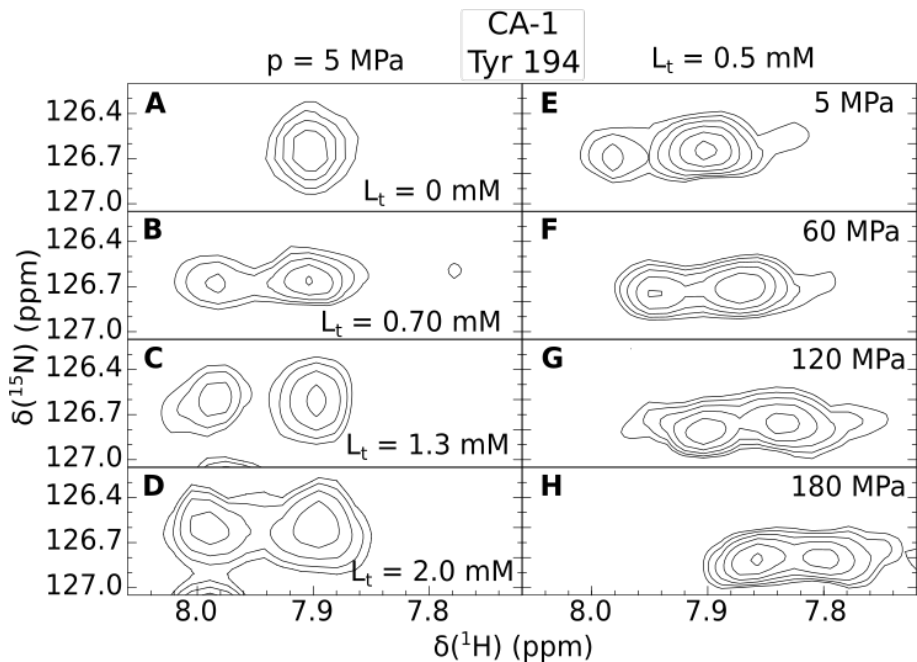
Figure 11.2: Ligand- and pressure-induced shifts of the Tyr 194 residue peak position in the $^{1}H-^{15}N$ HSQC spectra. The concentrations of compound **1** ranged from 0 mM to 2.0 mM (left panels) and pressure values ranged from 5 MPa to 180 MPa (right panels)

where $p$ denotes the pressure, and $\Delta G_b^\circ$ is the change in the standard Gibbs energy of binding (the standard state is defined as 1 mol L concentrations of the participating substances at 1 bar pressure and the activity coefficients are equal to 1). This equation shows that in order to obtain $\Delta V_b$, we need to determine $\Delta G_b^\circ$ values at different pressures. $\Delta G_b^\circ$ values can be calculated from the dissociation constant ($K_d$) values, with equation $\Delta G_b^\circ = RT \ln K_d$.

Despite the slow rate of interaction, the binding constants known in the literature for both ligands are fairly low, if compared to commercially available primary sulfonamides [187]. $K_d$ values at pH 7.0 and ambient pressure for the protein-ligand pairs are as follows: CA I-**1** $K_d = 85\,\mu M$, CA II-**1** $K_d = 13\,\mu M$, CA I-**6** $K_d = 43\,\mu M$, CA II-**6** $K_d = 13\,\mu M$. These $K_d$ values are similar to the protein concentrations required for NMR experiments; therefore, fractions of ligand-bound protein ($\theta$) are possible to obtain from peak volume values. $\theta$ values were calculated from the

amide cross peak volumes of the ligand-bound and ligand-free forms using equation (8.7).

As mentioned in section 8.1, multiple amino acid peaks can be used in analysis for better accuracy. An ensemble of amino acids, peaks of which split into two peaks when the ligand is added, was constructed for each pair based on visual inspection of the spectra. Only residues that produced clear, non-overlapping peaks throughout the pressure range were selected for further analysis. For CA I-**1** these residues were: Ile 59, Gly 104, Gly 111, Leu 131, Tyr 194, Gly 196, Thr 208, Ile 211, and His 243. For CA I-**6** the residues were: Gly 104, Gly 107, Gly 111, Ser 136, Gly 145, Tyr 194, Gly 196, Tyr 204, Thr 208. For CA II-**1**: Ile 33, Gly 82, Phe 93, Trp 97, His 107, Ala 116, Val 142, Trp 208. The positions of amino acids used for analysis in the protein 3D structures are shown in Figure 11.3 Most selected amino acids are close to the ligand binding pocket of CA isoforms. However, most probably due to remote rearrangements of the three-dimensional (3D) structure of the protein upon ligand binding, some more distant residues also showed a ligand-bound protein peak in the $^1\text{H}-^{15}\text{N}$ HSQC spectrum. The $\theta$ values of these ensembles of amino acids were averaged into a single value:

$$\theta = \frac{1}{n} \sum_i^n \theta(i). \tag{11.2}$$

Here, $\theta(i)$ is the $\theta$ value calculated from the peaks of the $i$-th amino acid. These average saturation values, calculated by equation 14.8 were used for all further analysis.

The averaged protein saturation values were plotted against total ligand concentration ($L_\text{t}$), depicted in Figure 11.4. $K_\text{d}$ values were calculated at different pressures up to 180 MPa, by non-linear regression analysis of the data using model equation (8.10). These $K_\text{d}$ values were transformed into $\Delta G_\text{b}^\circ$ values with equation (1.4) and plotted against pressure in Figure 11.4 B. The $\Delta G_\text{b}^\circ$ values decreased linearly with pressure (implying a negligible compressibility contribution), therefore $\Delta V_\text{b}$ values could be calculated from the linear slope of the fit to equation (14.7). $\Delta V_\text{b}$ value of $(-23 \pm 3)\,\text{mL}\,\text{mol}^{-1}$ was calculated.
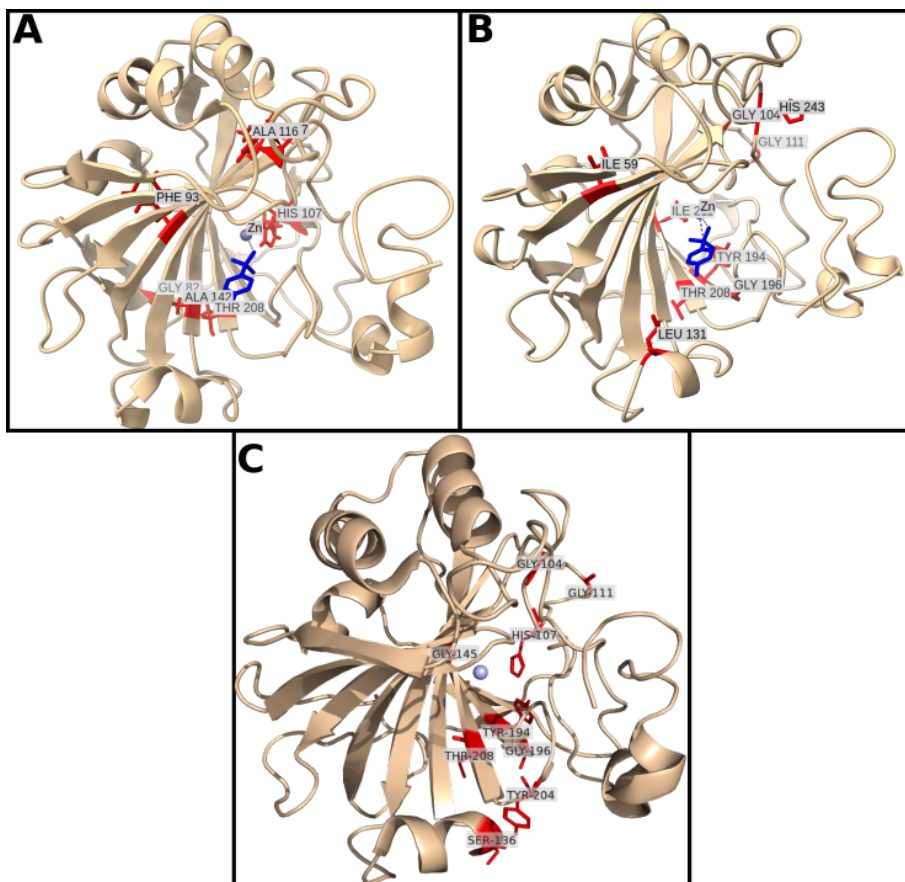
Figure 11.3: Crystal structures of the carbonic anhydrase-ligand systems used in this research. A – CA I-ligand **1** complex (PDB ID: 1CZM), B – CA II-ligand **1** complex (PDB ID: 6RL9). No CA crystal structure is available with ligand **6** so the ligand-free structure of CA I is shown in panel C (PDB ID: 2CAB). Molecules of compound **1** are shown as blue sticks. Residues that were mostly affected by protein-ligand complex formation (CA I-**1** – A, CA II-**1** – B, CA I-**6** – C) and used as ensembles for binding volume analysis are colored red and labeled.

## 11.3 $\Delta V_{\mathrm{b}}$ calculations from a single $^{1}\mathrm{H}-{}^{15}\mathrm{N}$ HSQC NMR spectrum at different pressures

NMR experiments are very expensive and require high amounts of protein. Titration experiments, as described previously, require multiple spectra with different ligand concentrations, which is not always possi-
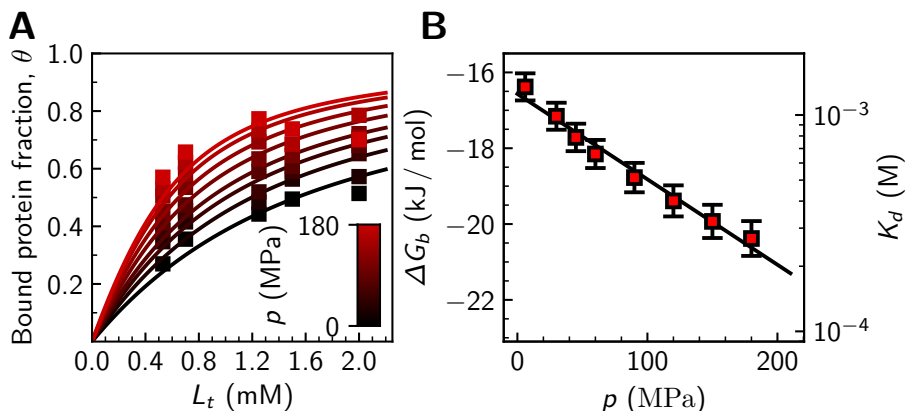
Figure 11.4: Panel A: CA I saturation with compound **1** at different pressures, calculated from the ratio of peak volumes corresponding to ligand-bound and ligand-free protein residues. Lines are fits to the model in equation (8.10). Panel B: $K_d$ and $\Delta G_b^\circ$ values from the fits plotted against pressure. The error bars depict the standard error of the fits. The line is a fit to equation (1.5).

ble. The slow exchange regime between the ligand-free states carbonic anhydrases CA I, CA II and ligand-bound state of these proteins with ligands **1** and **6** allowed an alternate method of obtaining $K_d$ values using a single concentration of the protein and the ligand. $K_d$ from single spectrum can be calculated by expressing $K_d = \frac{[P][L]}{[PL]}$ in terms of ligand-bound and ligand-free protein ratio. This can be done by rearranging the mass balance equations:

$$P_t = [P] + [PL], \tag{11.3}$$
$$L_t = [L] + [PL].$$

The resulting expression is:

$$K_d = \frac{[P]}{[PL]}\left(L_t - \frac{P_t}{1 + \frac{[P]}{[PL]}}\right). \tag{11.4}$$

In this equation the ratio of ligand-free and ligand-bound protein, $\frac{[P]}{[PL]}$, can be substituted by the ratio of intensity (volume) of the corresponding peaks and this leads to equation used to calculate the $K_d$ from the NMR

spectrum obtained at a single concentration of protein and ligand:

$$K_{\mathrm{d}} = \frac{I_{\mathrm{P}}}{I_{\mathrm{PL}}} \left( L_{\mathrm{t}} - \frac{P_{\mathrm{t}}}{1 + \frac{I_{\mathrm{P}}}{I_{\mathrm{PL}}}} \right). \tag{11.5}$$

Calculation of thermodynamic parameters from less data inherently compromises the accuracy. To evaluate the inaccuracies in the calculation of $K_d$ from a single $^1\mathrm{H}-^{15}\mathrm{N}$ HSQC spectrum, $K_{\mathrm{d}}$ values from several experiments with different ligand concentrations were calculated from spectra at different pressures using equation (14.12) (Table 11.1) and compared to $K_{\mathrm{d}}$ values from titration fits (Figure 11.5). The most ac-
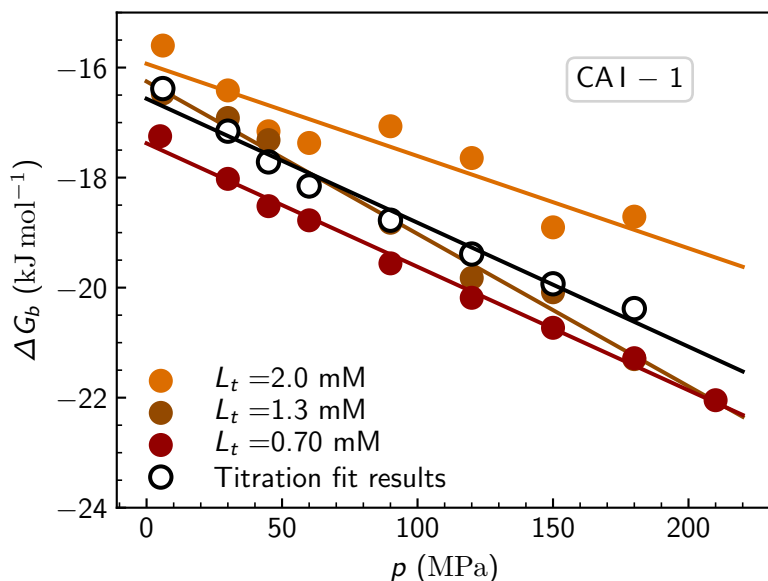


Figure 11.5: Comparison of $K_{\mathrm{d}}$ values calculated from titration fits (empty circles) and results from single spectra calculations with 0.70 mM, 1.3 mM and 2.0 mM of ligand **1** (colored circles).

curate results were calculated from the spectra with 0.70 mM of ligand. This is because, in these conditions, the amount of ligand-bound and ligand-free protein states is similar. When the amount of both states is similar, the intensities of both peaks are large enough for accurate identification and analysis of the peaks. As more ligand is added, the amount of unbound protein diminishes, and the corresponding peak becomes less distinguished, compromising the accuracy. In the same manner, ligand concentration that is too low diminishes the peaks of ligand-bound

Table 11.1: Comparison of $\Delta V_\mathrm{b}$ values calculated from a single spectrum pressure-series with different ligand concentrations.

| $L_\mathrm{t}$ (mM) | $\Delta V_\mathrm{b}$ (mL mol$^{-1}$) | Difference from $\Delta V_\mathrm{b}$ by titration (mL mol$^{-1}$) |
|---|---|---|
| 0.53 | -26 | 3.1 |
| 0.70 | -22 | 0.1 |
| 1.25 | -28 | 5.2 |
| 1.50 | -19 | 3.6 |
| 2.00 | -17 | 5.7 |

protein. In conclusion the approach of obtaining $K_\mathrm{d}$ values using a single ligand and protein concentration is accurate and can be used for a more efficient determination of binding volume, if the amount of both ligand-bound and ligand-free protein states remains similar to each other throughout the pressure range.

## 11.4   Comparison of $\Delta V_\mathrm{b}$ values from NMR

Based on the calculation method described in the previous section. Binding volumes were calculated for CA I-**6** and CA II-**1** binding pairs. The corresponding results are given in Figure 11.6. Linear fits of the data in Figure 11.6 yielded the $\Delta V_b$ equal to $(-22 \pm 4)$ ml/mol for CA I–**1**, $(-26 \pm 4)$ ml/mol for CA I–**6**, and $(-28 \pm 4)$ ml/mol for CA II–**1**. The uncertainty given next to the $\Delta V_b$ values shows the standard deviation, which was evaluated comparing $\Delta V_b$ values at different concentrations of added ligand. The binding strength values of the protein-ligand pairs line up in the same order as expected from the literature [187]. The $\Delta V_\mathrm{b}$ value for CA I-**1** is within the margin of error from the one determined by FPSA with 1.5 M GdmHCl (section 1.5). There are currently no other data on $\Delta V_\mathrm{b}$ of CA I-**6** or CA II-**1**, but the order of binding volume values for these pairs is in line with the previously observed correlation between binding strength and binding volume [129].
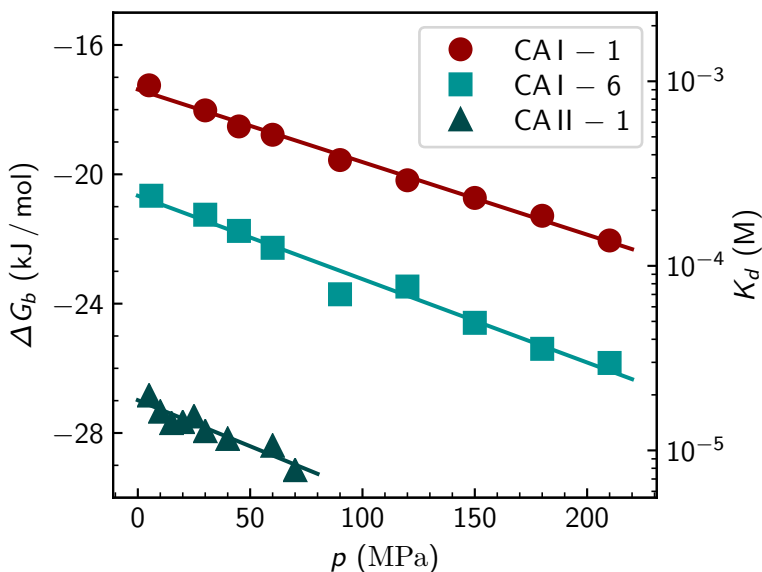
Figure 11.6: $K_d$ and $\Delta G_b^\circ$ values of binding pairs CA I-**1**, CA I-**6**, CA II-**1** at different pressures. Linear fits were used to calculate the $\Delta V_b$ values.

## 11.5 Different response to pressure by protein and protein-ligand complex

Although based on previously presented fluorescence data, the pressure range used in NMR experiments is not enough to cause significant unfolding of the protein, minor changes in protein state populations can be observed by NMR [188]. In the publication based on this thesis [139], we categorized the pressure response of CA I residues into three major categories. Select residue $^1$H and $^{15}$N chemical shifts are presented in Figure 11.7.

Some residues, such as Ile 59 and Tyr 204, showed distinct linear responses to pressure in ligand-bound and ligand-free protein states. These peaks generally had a greater chemical shift change with pressure than the average of all residues. Ligand-free state peaks of these residues underwent a higher change in the chemical shift in the $^{15}$N dimension at 210 MPa than the ligand-bound state peaks. The $\Delta\delta$ ($^{15}$N) was approximately ten times lower for the CA I-**1**-bound state of Ile 59 and up to 3 times lower for the CA I-**1**-bound state of the Tyr 204 residue, compared to that of the ligand-free state of CA I. Similar behaviour was observed
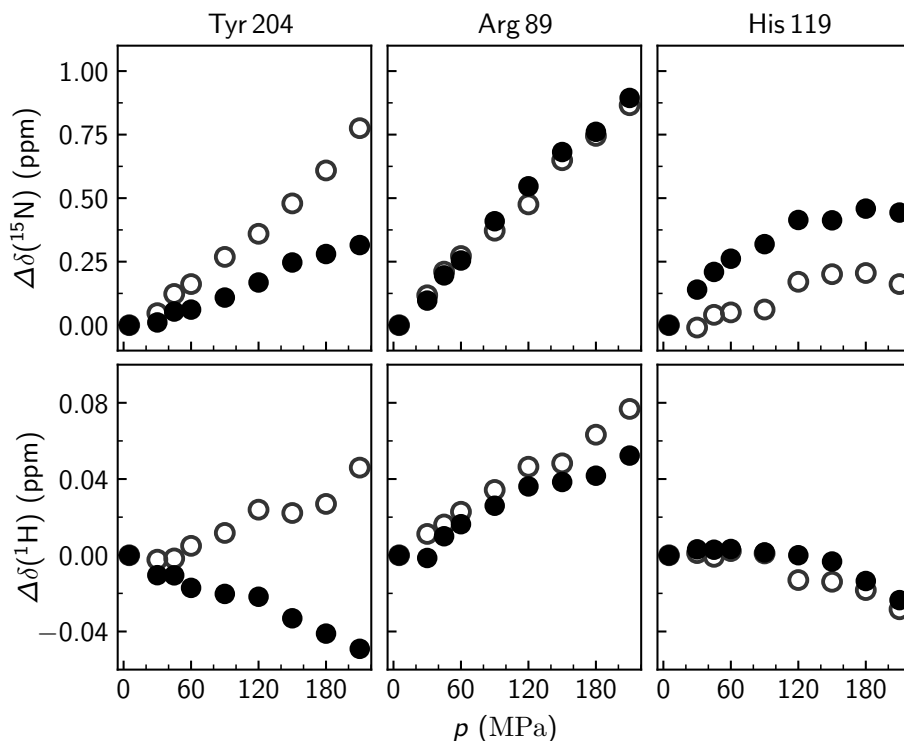
Figure 11.7: Response of CA I (0.52 mM) residues to the applied pressure in the absence (open circles) and presence (solid circles) of compound **1** (0.70 mM)

for CA II amino acid residues Ile 33 and Phe 93. Linear chemical shift variations are due to structural fluctuations within the basic folded state of the protein. Amide chemical shifts are essentially related to H-bond compressibility [188]. This difference might indicate that compound **1** reduces the volume fluctuations of Ile 59 and Tyr 204 residues in CA I. This effect could be either due to the direct ligand interaction with these amino acid residues or the change in protein conformation upon binding compound **1**. The reduced volume fluctuations have been reported in several studies of the protein-ligand interaction [189–192].

Arg 89 in Figure 11.7 is an example of second type of response. Arg 89, Val 62, Leu 147 displayed the highest linear $\Delta\delta$, but their responses to pressure were similar for both the ligand-bound and ligand-free CA I states. These trends suggest that these regions undergo fluctuations at high pressure but are not constrained by compound **1** binding

to CA I. In particular, The chemical shift change of Val 62 is nonlinear up to 210 MPa pressure. Non-linearity is often a signature of conformational change and possibly an increase in the population of low-lying excited states of this amino acid residue at high pressure. Nonlinear chemical shift variations are known to be related to structural fluctuations involving low-lying excited states that differ from the basic folded states [188].

His 94 and His 119 are of particular importance in this system. These residues together with His 96 coordinate the zinc ion in the active sites of CA I and CA II. These residues showed the third type of response to high pressures. The amide nitrogen $\Delta\delta$ values for His 94 in CA I-**6** complex and His 119 in the CA I-**1** complex were slightly greater at high pressures, when compared with the ligand-free protein state. This increase indicates that the change in dihedral angles of the peptide bond could be larger for the ligand-bound state. Although an increase was not a clear case for His 94 in the CA I-**1** complex. The chemical shift changes of these residues were close to the average ($\Delta\delta$ ($^{15}$N = 0.4 ppm at 210 MPa), therefore the residues did not display particular liability to pressure. An interesting phenomenon was observed in the proton chemical shifts of His 94 and Tyr 204. Ligand-bound state shifts moved upfield, opposite of ligand-free states of CA I with increasing pressure. This behaviour could indicate that the hydrogen bonds of these amide groups lengthen with pressure in the ligand-bound state and shorten in the ligand-free state [193].

# Chapter 12

# Polymer-surfactant interaction

In this chapter, ITC experiments of charged poly(amino acid) and oppositely charged surfactant interaction are discussed. It is a model system aimed to "purify" the contributions of charge interaction to ligand binding thermodynamics. The polymer-surfactant pairs, investigated in this chapter, can be divided into two main groups:

A  Positively charged polymer with negatively charged surfactant. These pairs were composed of positively charged amino acid homopolymers (polyarginine [poly(Arg$^+$)], polylysine [poly(Lys$^+$)], polyornithine [poly(Orn$^+$)] and negatively charged surfactants – alkyl sulfates and alkyl sulfonates of different length (sodium octyl sulfate, decyl sulfate, undecyl sulfate, dodecyl sulfate, octyl sulfonate, nonyl sulfonate, and decyl sulfonate).

B  Negatively charged polymer with positively charged surfactant. These pairs were composed of negatively charged amino acid homopolymers (polyaspartate [poly(Asp$^-$)], polyglutamate [poly(Glu$^-$)]) and positively charged surfactants – alkyl ammonium chlorides of different length (decylammonium, undecylammonium, dodecylammonium, and tridecylammonium).

The tested systems are presented in Figure 12.1 This chapter describes the measurements of thermodynamic parameters in various systems of charged polymers and surfactants. The effects of ionic strength, tem-
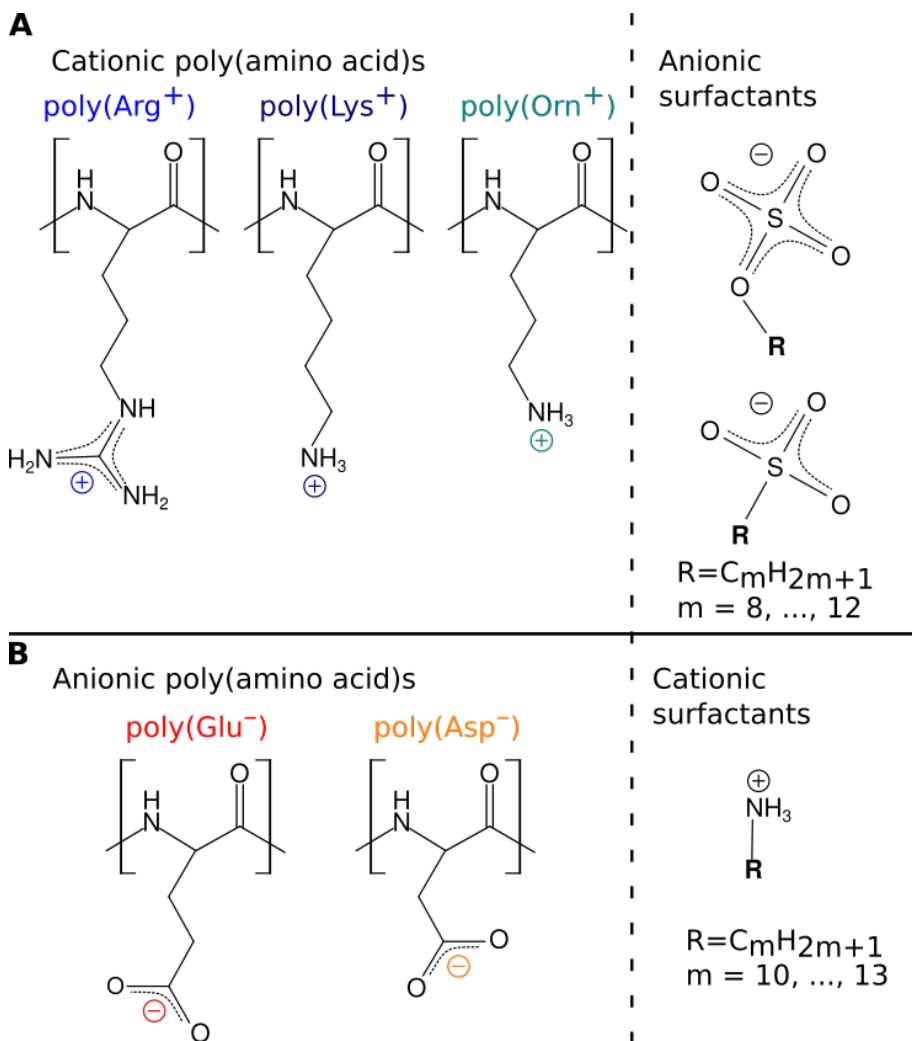
Figure 12.1: Surfactant and poly(amino acid) systems used in this work. Panel **A**: positively charged polymers with negatively charged surfactants; panel **B**: negatively charged polymers with positively charged surfactants.

perature and chemical structure on the thermodynamic properties of interacting ion pairs are also described in this chapter.

## 12.1 Reaction stoichiometry and effects of ionic strength.



**A**

Power ($\mu$J s$^{-1}$)

140

100

60

$C_{12}H_{25}SO_4^-$
poly(Arg$^+$)

**B**

$\delta H$ (kJ mol$^{-1}$)

0

−9

−18

$C_{12}H_{25}SO_4^-$
poly(Arg$^+$)

$[C_{12}H_{25}SO_4^-]/[\text{-Arg}^+\text{-}]$

**C**

Power ($\mu$J s$^{-1}$)

150

140

$C_{12}H_{25}NH_3^+$
poly(Glu$^-$)

0    1500    3000    4500

Time (s)

**D**

$\delta H$ (kJ mol$^{-1}$)

4

2

0

$C_{12}H_{25}NH_3^+$
poly(Glu$^-$)

0    1    2

$[C_{12}H_{25}NH_3^+]/[\text{-Glu}^-\text{-}]$
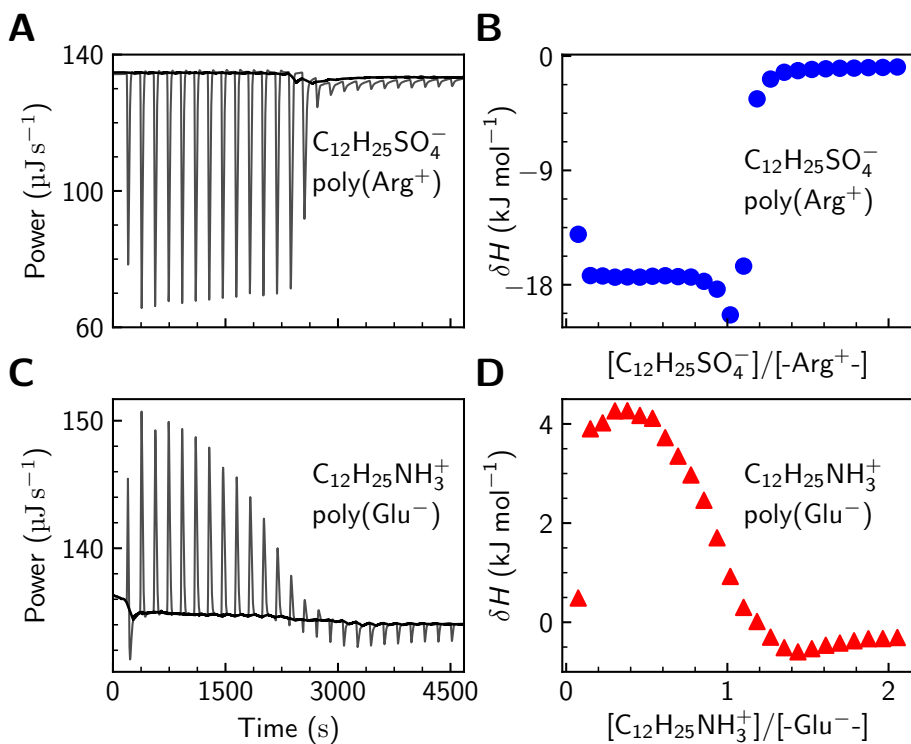
Figure 12.2: Raw ITC data and isotherms of SDS binding to poly(Arg$^+$) (panels **A** and **B**) and dodecylammonium binding to poly(Glu$^-$) (panels **C** and **D**) at neutral pH. The syringe contained 5 mM surfactant solution that was titrated into 0.5 mM (expressed per amino acid) solution of poly(amino acid) at 25 °C.

Figure 12.2 shows the raw ITC data (panels **A, C**) and isotherms (panels **B, D**) of SDS binding to poly(Arg$^+$) (**A, B**) and dodecylammonium binding to poly(Glu$^-$) (**C, D**) at $T = 25$ °C. At this temperature, alkyl sulfate binding to poly(Arg$^+$) is exothermic, while dodecylammonium binding to poly(Glu$^-$) is endothermic. The first injection data points in panels **B** and **D** are of lower accuracy because of the time needed for thermal equilibration and partial diffusion of the surfactant from the syringe to the cell prior to the first injection and are commonly removed from the analysis. The isotherm of poly(Arg$^+$) binding

to SDS contains a distinct dip in the enthalpy at the charge neutralization point (where the amount of surfactant molecules in the cell is equal to the amount of amino acid residues in the polymer). Similar isotherm shapes are observed for SDS titration into polyethyleneimines by Wang *et al.* [62].

The experiments shown in Figure 12.2 had the stoichiometry parameter $n$ approximately equal to 1. This was the case for all experiments done in water. The interaction between surfactant and poly(amino acid) displayed an absorption or release of heat until the charge neutralization point was reached. Further titration produces only dilution heat. The reactions between surfactants and poly(amino acid)s were investigated at various ionic strengths by changing NaCl concentration. The data in Figure 12.3 show that addition of $50\,\mathrm{mM}$ and $200\,\mathrm{mM}$ sodium chloride increasingly reduced the binding stoichiometry parameter $n$. NaCl concentrations of $1\,\mathrm{M}$ and higher completely halted the binding of SDS to poly($\mathrm{Arg}^+$).

## 12.2 Binding enthalpy as a function of aliphatic chain length

A series of experiments with various aliphatic chain lengths of surfactants were conducted to address the role of aliphatic chain length in the binding process. The results are visually summarized in Figure 12.4, and in tables 12.2, 12.3, 12.4 and 12.5. The binding enthalpy was mostly endothermic for alkyl sulfate binding to positively charged poly(amino acid), except for $\mathrm{C_8H_{17}SO_4}^-$ binding to poly($\mathrm{Lys}^+$) and poly($\mathrm{Orn}^+$). The opposite system of alkyl amine binding to poly($\mathrm{Asp}^-$) and poly($\mathrm{Glu}^-$) exhibited mostly positive interaction enthalpies. The common trait for all binding pairs was the binding enthalpy dependence on the alkyl chain length of the surfactant. Panels A and B of Figure 12.4, show the measured $\Delta H^\circ$ values of surfactant–poly(amino acid) interaction dependence on the total number of carbon atoms in the aliphatic chain, $m$. The addition of a $\mathrm{CH_2}$ group to the hydrophobic chain of a surfactant had a negative contribution to the interaction enthalpy. These dependences were linear, the enthalpic contribution of the $\mathrm{CH_2}$ group for various surfactant–poly(amino acid) systems at $25\,^\circ\mathrm{C}$ are given in table 12.1. Isotherm shapes of all experiments suggest a high de-
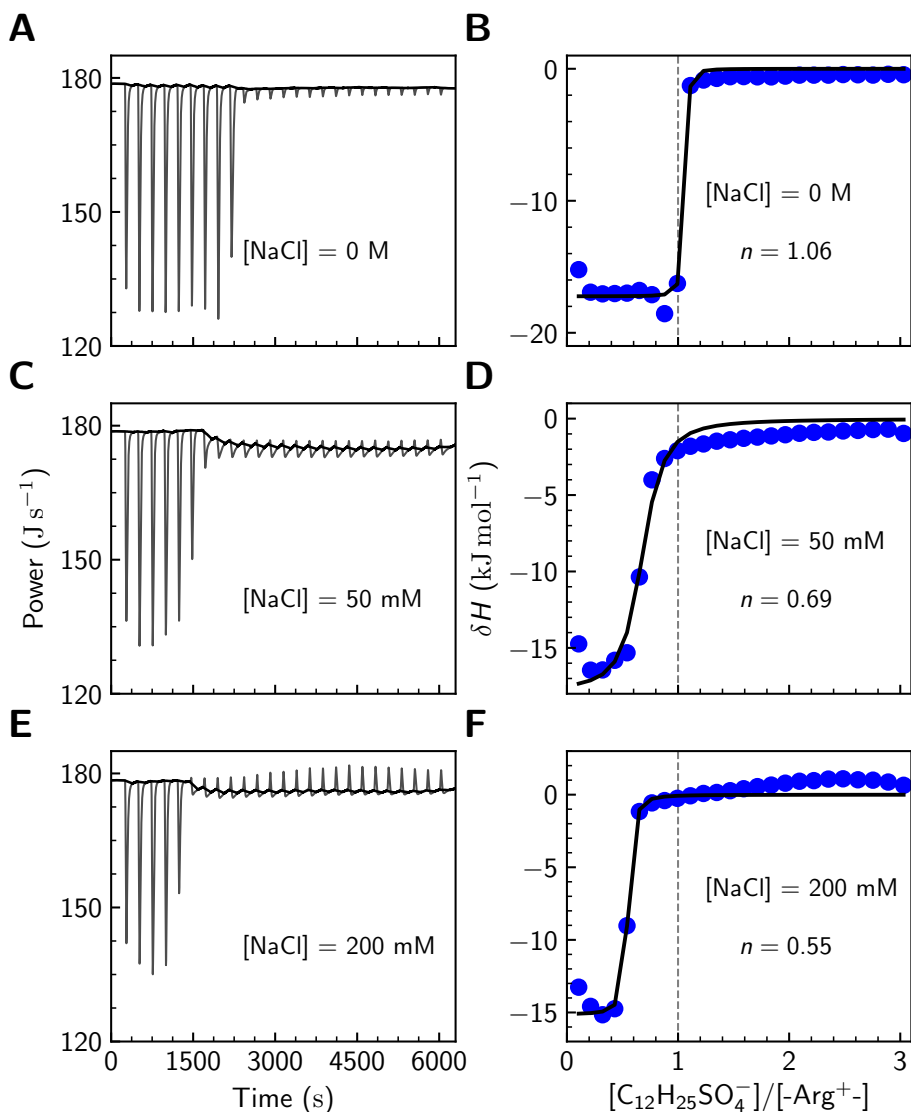
Figure 12.3: Raw ITC data and isotherms of SDS binding to poly(Arg$^+$) at various concentrations of added NaCl: (**A**, **B**) 0 mM, (**C**, **D**) 50 mM, and (**E**, **F**) 200 mM. Curves in panels **B**, **D**, and **F** were obtained by using two species binding model (equation (9.1)) that yielded stoichiometry parameter, $n$.

gree of cooperativity. In most cases, the reaction became more exothermic as the titration neared the charge neutralization point. Although this was not observed for endothermic interactions, e.g., $C_{10}H_{21}NH_3^+$
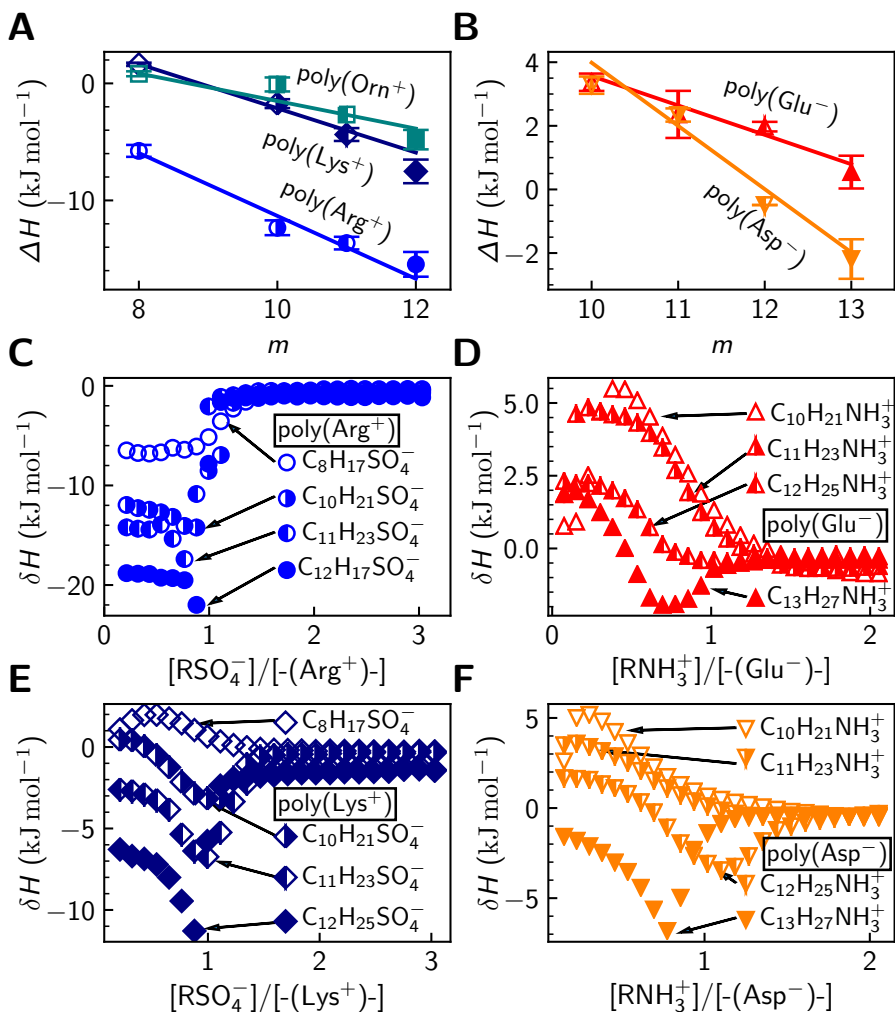
Figure 12.4: ITC experiment results of different length surfactant interaction with poly(amino acid)s at $T = 25\,^{\circ}\mathrm{C}$. Enthalpies of linear alkyl sulfate binding to positively charged poly(amino acid)s and alkylamine binding to negatively charged poly(amino acid)s are plotted against chain length in panels **A** and **B**, respectively. Panels **C** and **E** show isotherms of $\mathrm{RSO_4}^-$ binding to poly($\mathrm{Arg^+}$) and poly($\mathrm{Lys^+}$), panels **D** and **F** – $\mathrm{RNH_3}^+$ binding to poly($\mathrm{Glu^-}$) and poly($\mathrm{Asp^-}$), respectively.

binding to poly($\mathrm{Asp^-}$) and poly($\mathrm{Glu^-}$), the reaction turned more endothermic towards neutralization point. The cooperativity was less pronounced in experiments of alkyl sulfate binding to poly($\mathrm{Arg^+}$) than other pairs. In addition, poly($\mathrm{Arg^+}$) binding of alkyl sulfates displayed a sig-

Table 12.1: The change in enthalpy of a charged polymer-surfactant interaction upon the addition of one $CH_2$ group in the aliphatic chain at $25\,°C$.

| System | $CH_2$ group contribution to $\Delta H°$ (kJ/mol/$CH_2$) |
|---|---|
| poly($Arg^+$)-alkyl sulfate | $-2.7 \pm 0.30$ |
| poly($Lys^+$)-alkyl sulfate | $-1.9 \pm 0.51$ |
| poly($Orn^+$)-alkyl sulfate | $-1.2 \pm 0.53$ |
| poly($Asp^-$)-alkylamine | $-2.0 \pm 0.51$ |
| poly($Glu^-$)-alkylamine | $-0.92 \pm 0.28$ |

nificantly higher $\Delta H°$ and a steeper binding isotherm than all other interactions. These differences suggest that in poly($Arg^+$)-$RSO_4{}^-$ interactions, the head group attraction plays a more important role resulting in a different titration course.

Table 12.2: Changes in enthalpy and constant-pressure heat capacity of alkyl sulfate and alkane sulfonate binding to poly($Arg^+$), measured by ITC.

| | poly($Arg^+$) | | |
|---|---|---|---|
| Surfactant | $T$ | $\Delta H°$ | $\Delta C_p°$ |
| | (°C) | (kJ mol$^{-1}$) | (kJ mol$^{-1}$ K$^{-1}$) |
| | 13 | $-10.2 \pm 0.2$ | |
| | 25 | $-15.4 \pm 1.1$ | |
| $C_{12}H_{25}SO_4{}^-$ | 37 | $-21.0 \pm 0.8$ | $-0.41 \pm 0.01$ |
| | 49 | $-26.8 \pm 0.9$ | |
| | 61 | $-28.7 \pm 0.5$ | |
| | 13 | $-8.8 \pm 0.2$ | |
| | 25 | $-13.6 \pm 1.1$ | |
| $C_{11}H_{23}SO_4{}^-$ | 37 | $-19.9$ | $-0.43 \pm 0.01$ |
| | 49 | $-24.1 \pm 2.0$ | |
| | 61 | $-28.5 \pm 2.4$ | |
| | 13 | $-7.0 \pm 0.4$ | |
| | 25 | $-12.3 \pm 0.6$ | |
| $C_{10}H_{21}SO_4{}^-$ | 37 | $-17.0 \pm 2.1$ | $-0.40 \pm 0.01$ |
| | 49 | $-21.6 \pm 1.6$ | |

| | | | |
|---|---|---|---|
| | 61 | $-25.2 \pm 2.4$ | |
| | 13 | $-2.9 \pm 0.1$ | |
| | 25 | $-5.8 \pm 0.5$ | |
| $C_8H_{17}SO_4{}^-$ | 37 | $-7.0 \pm 0.9$ | $-0.18 \pm 0.04$ |
| | 49 | $-9.3 \pm 0.4$ | |
| | 61 | $-11.6 \pm 0.1$ | |
| $C_{10}H_{21}SO_3{}^-$ | 25 | $-8.6 \pm 0.6$ | |
| $C_9H_{19}SO_3{}^-$ | 25 | $-4.2 \pm 1.0$ | |
| $C_8H_{17}SO_3{}^-$ | 25 | $-3.0 \pm 1.2$ | |

Table 12.3: Changes in enthalpy of alkyl sulfate and alkane sulfonate binding to poly(Lys$^+$) and poly(Orn$^+$), measured by ITC.

| | poly(Lys$^+$) | | poly(Orn$^+$) | |
|---|---|---|---|---|
| Surfactant | $T$ | $\Delta H^\circ$ | $T$ | $\Delta H^\circ$ |
| | ($^\circ$C) | (kJ mol$^{-1}$) | ($^\circ$C) | (kJ mol$^{-1}$) |
| $C_{12}H_{25}SO_4{}^-$ | 25 | $-6.9 \pm 1.0$ | 25 | $-4.2 \pm 0.8$ |
| $C_{11}H_{23}SO_4{}^-$ | 25 | $-4.4 \pm 0.6$ | 25 | $-2.7 \pm 0.1$ |
| $C_{10}H_{21}SO_4{}^-$ | 25 | $-1.7 \pm 0.4$ | 25 | $-0.2 \pm 0.6$ |
| $C_8H_{17}SO_4{}^-$ | 25 | $1.6 \pm 0.1$ | 25 | $-0.8 \pm 0.2$ |
| $C_{10}H_{21}SO_3{}^-$ | 25 | $2.9 \pm 0.3$ | 25 | $2.2 \pm 0.2$ |
| $C_9H_{19}SO_3{}^-$ | 25 | $2.4 \pm 0.1$ | 25 | $3.0 \pm 0.5$ |
| $C_8H_{17}SO_3{}^-$ | 25 | $2.1 \pm 0.3$ | 25 | $2.0 \pm 0.2$ |

Table 12.4: Changes in enthalpy and constant-pressure heat capacity upon alkyl ammonium binding to poly(Glu$^-$), measured by ITC.

| | poly(Glu$^-$) | | |
|---|---|---|---|
| | $T$ | $\Delta H^\circ$ | $\Delta C_p^\circ$ |
| | ($^\circ$C) | (kJ mol$^{-1}$) | (kJ mol$^{-1}$ K$^{-1}$) |
| | 25 | $-2.2 \pm 0.6$ | |
| $C_{13}H_{27}NH_3{}^+$ | 37 | $-5.7 \pm 0.4$ | $-0.15 \pm 0.05$ |
| | 49 | $-10.3 \pm 1.0$ | |

| | T | $\Delta H°$ | $\Delta C_p°$ |
|---|---|---|---|
| | 60 | $-16.3 \pm 0.8$ | |
| C$_{12}$H$_{25}$NH$_3{}^+$ | 25 | $-0.5$ | |
| | 37 | $-3.7 \pm 0.3$ | $-0.20 \pm 0.04$ |
| | 49 | $-8.1 \pm 0.9$ | |
| | 60 | $-8.9 \pm 1.3$ | |
| C$_{11}$H$_{23}$NH$_3{}^+$ | 25 | $-2.3 \pm 0.2$ | |
| | 37 | $-2.1 \pm 1.1$ | $-0.26 \pm 0.03$ |
| | 49 | $-3.1 \pm 0.1$ | |
| | 60 | $-5.9 \pm 0.9$ | |
| C$_{10}$H$_{21}$NH$_3{}^+$ | 25 | $3.3 \pm 0.3$ | |
| | 37 | $0.9 \pm 0.2$ | $-0.39 \pm 0.05$ |
| | 49 | $-1.4 \pm 0.4$ | |
| | 60 | $-1.9 \pm 0.5$ | |

Table 12.5: Changes in enthalpy and constant-pressure heat capacity upon alkyl ammonium binding to poly(Asp$^-$), measured by ITC.

| poly(Asp$^-$) | | | |
|---|---|---|---|
| | $T$ | $\Delta H°$ | $\Delta C_p°$ |
| | | (°C) | (kJ mol$^{-1}$) |
| C$_{13}$H$_{27}$NH$_3{}^+$ | 25 | $0.55 \pm 0.50$ | |
| | 37 | $-5.1 \pm 0.6$ | $-0.12 \pm 0.02$ |
| | 49 | $-9.9 \pm 1.3$ | |
| | 60 | $-12.7 \pm 1.7$ | |
| C$_{12}$H$_{25}$NH$_3{}^+$ | 25 | $2.0 \pm 0.2$ | |
| | 37 | $-2.3 \pm 0.2$ | $-0.20 \pm 0.12$ |
| | 49 | $-6.2 \pm 1.1$ | |
| | 60 | $-9.7 \pm 0.3$ | |
| C$_{11}$H$_{23}$NH$_3{}^+$ | 25 | $2.4 \pm 0.7$ | |
| | 37 | $0.2 \pm 0.1$ | $-0.23 \pm 0.02$ |
| | 49 | $-3.0 \pm 0.5$ | |
| | 60 | $-4.5 \pm 0.1$ | |
| C$_{10}$H$_{21}$NH$_3{}^+$ | 25 | $3.4 \pm 0.3$ | |
| | 37 | $1.44$ | $-0.43 \pm 0.03$ |
| | 49 | $0.0 \pm 0.1$ | |

| | |
|---|---|
| 60 | $-1.3 \pm 0.1$ |

## 12.3 Temperature dependence of interaction enthalpy

ITC experiments with different poly(amino acid)-surfactant binding pairs were done in a wide range of temperatures. Charged surfactant binding to the poly(amino acid) of an opposite charge was increasingly more exothermic at higher temperatures. The increase of interaction enthalpy was observed in all of the tested systems (see Figures 12.5, 12.6, and 12.7). The data show that even the endothermic interactions and endothermic peaks at the beginning of the titration turn exothermic at higher temperatures. For example, in a $RNH_3^+$–poly($Glu^-$) system at $37\,°C$, the endothermic reaction profiles were observed only for aliphatic chains of 10 and 11 carbon atoms, while in $RNH_3^+$–poly($Asp^-$) system at $37\,°C$ – only for decylammonium. The reactions were fully exothermic in all of the tested systems at $49\,°C$.

The plots of enthalpy as a function of temperature were used to calculate the change in constant pressure heat capacity of the reaction ($\Delta C_p^\circ$) by applying linear fits and assuming that the heat capacity is temperature-independent in the investigated temperature range. In the poly($Glu^-$) and poly($Asp^-$) systems, the $\Delta C_p^\circ$ values were increasingly negative for the alkylamines of longer aliphatic chains (Tables 12.4,12.5). Slightly different tendencies were observed in $RSO_4^-$–poly($Arg^+$) system. $\Delta C_p^\circ$ value of $(-0.18\pm0.04)\,kJ/mol/K$ for $C_8H_{17}SO_4^-$–poly($Arg^+$) was determined. The increased chain length increased the absolute value of $\Delta C_p^\circ$ and, within an error range, it remained similar for other long-chain alkyl sulfate series (Table 12.2).

## 12.4 Sulfonate and sulfonic acid binding to poly(amino acid)s

The enthalpies of alkyl sulfate binding to poly($Arg^+$) were more negative than that of sulfonic acid bearing aliphatic chains of the same length. The data show that interaction enthalpy between poly($Arg^+$) and alkyl

Figure 12.5: ITC results of of poly(Glu$^-$) interaction with alkyl ammonium surfactants at different temperatures. Panel **A** shows the effect of temperature on the binding enthalpy. The lines are linear fits used to obtain $\Delta C_p^\circ$ values. Panel **B** shows the same data plotted as enthalpy versus the length of surfactant aliphatic chain at different temperatures, the linear fits yield methyl group contribution to the interaction enthalpy. Panels **C**–**F** show integrated ITC curves for various alkylammonium surfactant binding at different temperatures.

sulfonic acid containing $m$ carbon atoms in the aliphatic chain is approximately equal to the interaction enthalpy between poly(Arg$^+$) and alkyl sulfate containing one less carbon atom (Figure 12.8). This result sug-
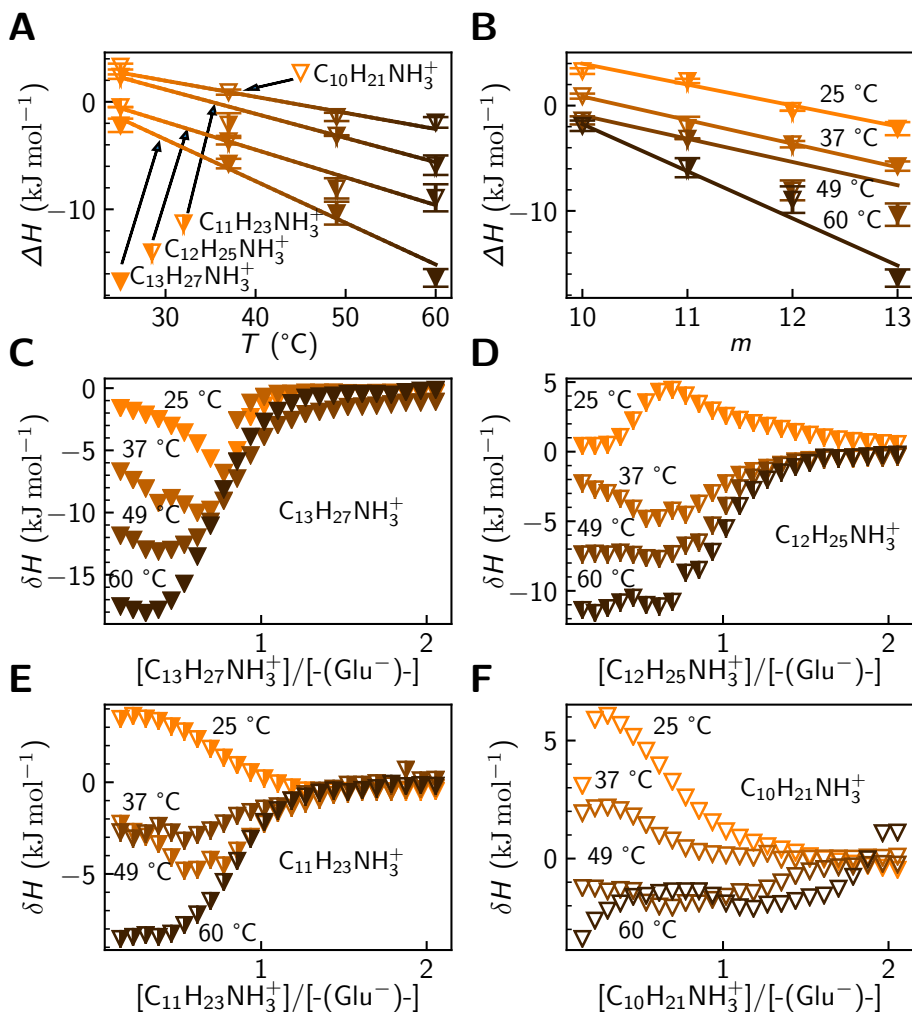
Figure 12.6: ITC results of of poly(Asp$^-$) interaction with alkyl ammonium surfactants at different temperatures. Panel **A** shows the effect of temperature on the binding enthalpy. The lines are linear fits used to obtain $\Delta C_p^\circ$ values. Panel **B** shows the same data plotted as enthalpy versus the length of surfactant aliphatic chain at different temperatures, the linear fits yield methyl group contribution to the interaction enthalpy. Panels **C**–**F** show integrated ITC curves for various alkylammonium surfactant binding at different temperatures.

gests that the surfactant chain lengthening via oxygen between the sulfur and carbon atoms of the sulfate plays a similar role as an additional CH$_2$ group in the aliphatic chain. The slope was not confirmed in exper-
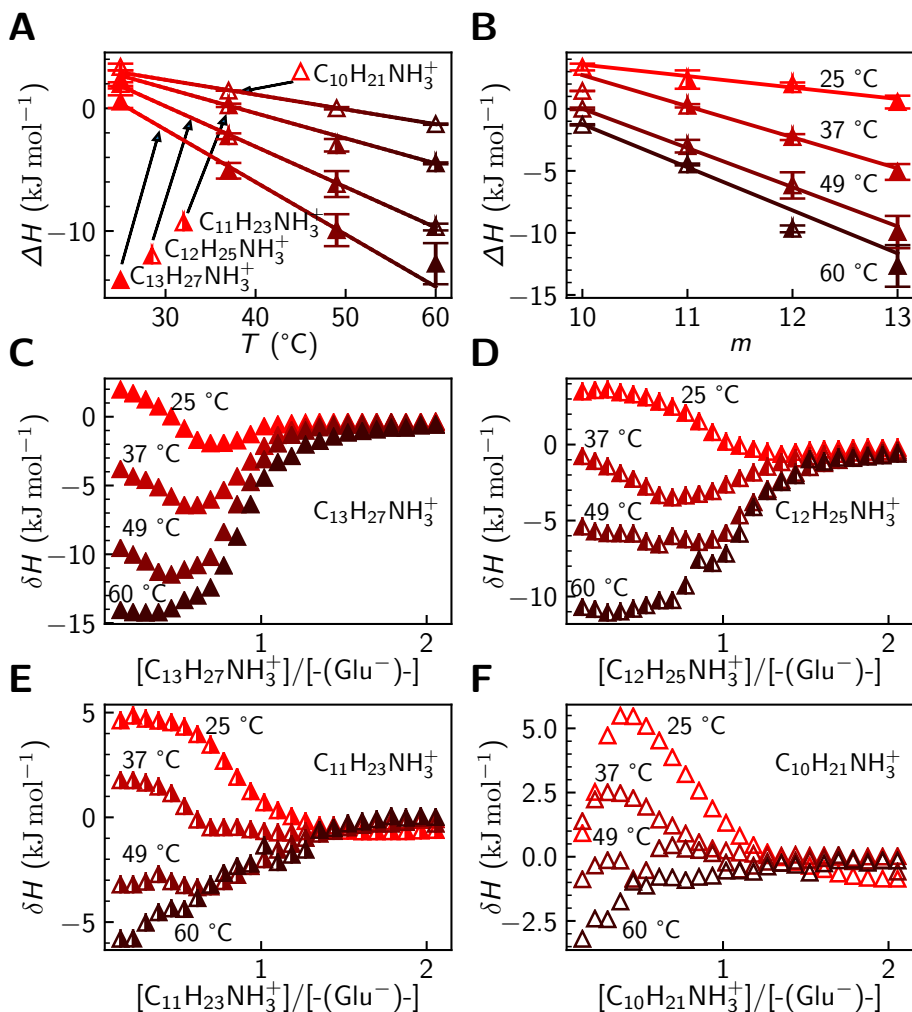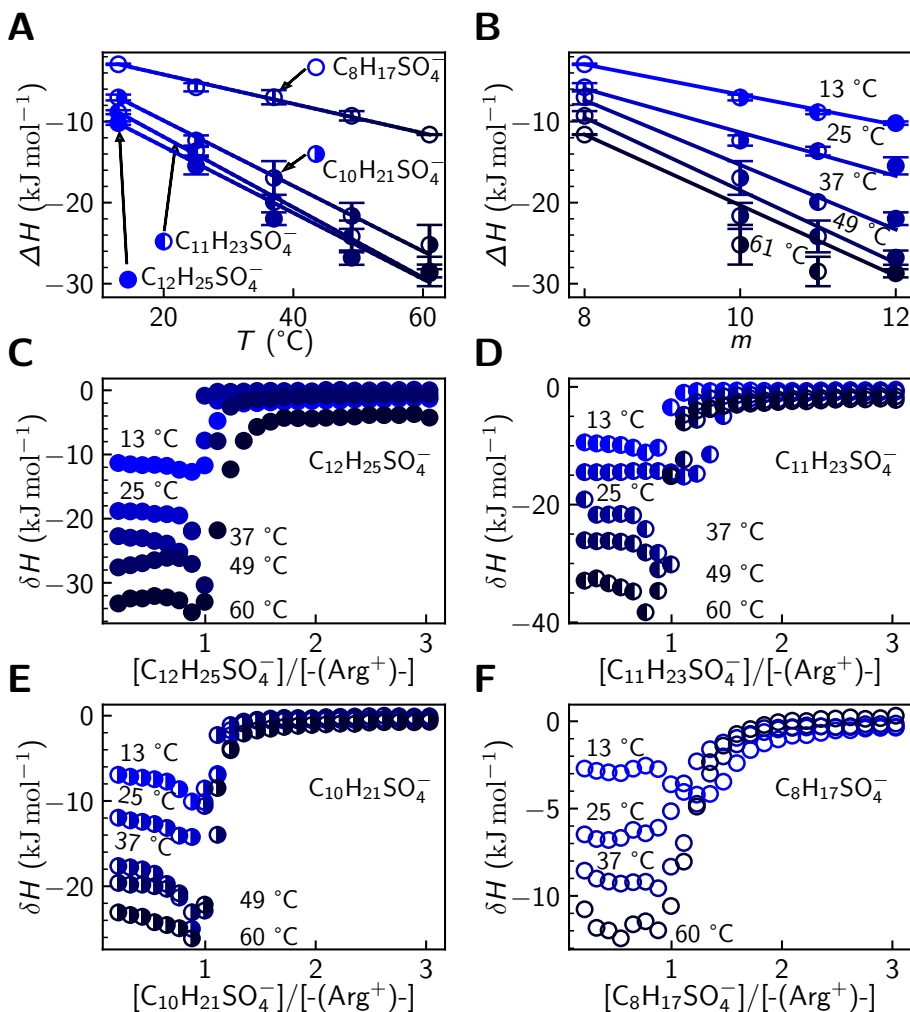
Figure 12.7: ITC results of of poly(Arg$^+$) interaction with alkyl sulfate surfactants at different temperatures. Panel **A** shows the effect of temperature on the binding enthalpy. The lines are linear fits used to obtain $\Delta C_p^\circ$ values. Panel **B** shows the same data plotted as enthalpy versus the length of surfactant aliphatic chain at different temperatures, the linear fits yield methyl group contribution to the interaction enthalpy. Panels **C**–**F** show integrated ITC curves for various length alkyl sulfate binding at different temperatures.

iments of sulfonate binding to other cationic poly(amino acid)s, where the enthalpies of binding to either poly(Lys$^+$) or poly(Orn$^+$) seemed to increase with longer alkyl chains, contrary to all of the other systems
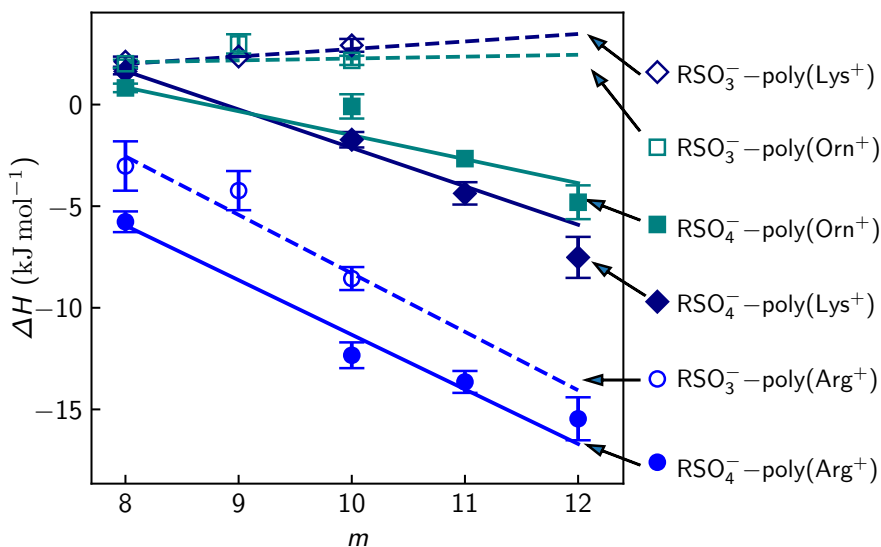
Figure 12.8: A comparison between enthalpies of alkyl sulfate (filled symbols, continuous lines) and alkane sulfonate (open symbols, dashed lines) binding to poly(Arg$^+$), poly(Lys$^+$) and poly(Orn$^+$). The enthalpy as a function of chain length plots yielded the CH$_2$ group contribution to the interaction enthalpy.

studied here. It appears that the slopes may still be similar if longer chain surfactants could be investigated. In these experiments, enthalpies were close to zero, which makes them difficult to analyze accurately using ITC; thus, it is not clear whether this is a phenomenon or experimental error.

## 12.5 The change in heat capacity of surfactant binding to poly(amino acid)s

The temperature dependencies of $\Delta H^\circ$ allowed the estimation of the constant-pressure heat capacities ($\Delta C_p^\circ$) of such binding reactions. Figure 12.9 shows the heat capacities obtained by applying linear fits to the enthalpy dependency on temperature. Heat capacity appears to be independent of temperature within the studied 13 °C to 61 °C tem-

perature range. All measured changes in heat capacity were negative and increased in absolute value upon increasing the surfactant chain length. With a possible exception of poly(Arg$^+$), the dependencies of $\Delta C_p^\circ$ on chain length were linear. Fits were applied to $\Delta C_p^\circ$-chain length dependency yielding the contribution of an additional $CH_2$ to group to $\Delta C_p^\circ$ value, which were in the range of $-0.10\,\text{kJ}\,\text{mol}^{-1}\,\text{K}^{-1}$ to $-0.061\,\text{kJ}\,\text{mol}^{-1}\,\text{K}^{-1}$ (Figure 12.9). The values seem to be within the margin of error from one another and an average value of $(-0.092\pm 0.018)\,\text{kJ}\,\text{mol}^{-1}\,\text{K}^{-1}$ can be accepted.
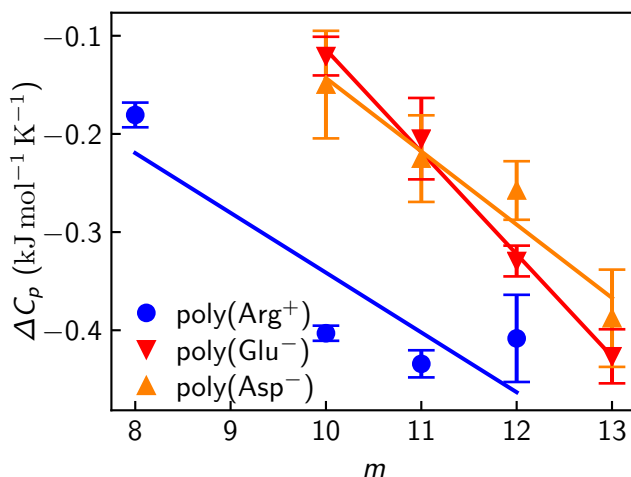


Figure 12.9: The $\Delta C_p^\circ$ values of varied length alkyl sulfate surfactant binding to poly(Arg$^+$) and alkylammonium surfactant binding to poly(Asp$^-$) and poly(Glu$^-$). The dependencies on alkyl chain length were approximated as linear yielding the values of the $\Delta C_p^\circ$ of the $CH_2$ group equal to $(-0.061\pm 0.018)\,\text{kJ}\,\text{mol}^{-1}\,\text{K}^{-1}$ for poly(Arg$^+$), $(-0.075\pm 0.021)\,\text{kJ}\,\text{mol}^{-1}\,\text{K}^{-1}$ for poly(Asp$^-$), and $(-0.100\pm 0.008)\,\text{kJ}\,\text{mol}^{-1}\,\text{K}^{-1}$ for poly(Glu$^-$). The average was $(-0.092\pm 0.018)\,\text{kJ}\,\text{mol}^{-1}\,\text{K}^{-1}$.

An alternative way of viewing the data and obtaining the changes in heat capacity is shown in Figure 12.10. By plotting the temperature dependencies for the enthalpies of $CH_2$ group contribution to the binding to poly(amino acid), contributions to $\Delta C_p^\circ$ can be obtained. The obtained average value of the $\Delta C_p^\circ$ of the $CH_2$ group was similar to the average value from Figure 12.9 and was equal to $(-0.064\pm 0.006)\,\text{kJ}\,\text{mol}^{-1}\,\text{K}^{-1}$.
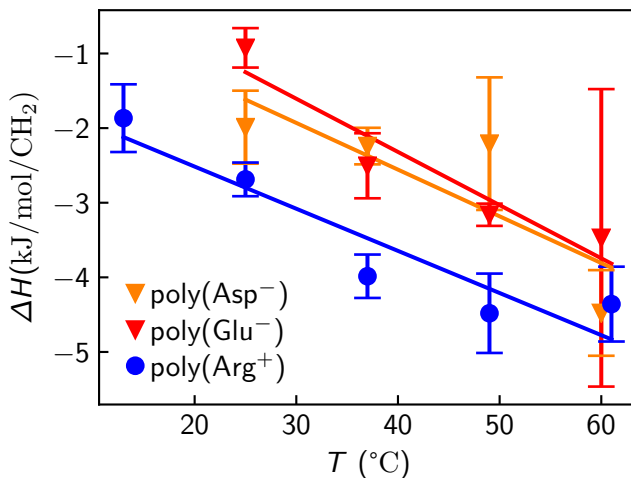
Figure 12.10: Enthalpy contributions of the $CH_2$ group for alkyl sulfate surfactant binding to poly($Arg^+$) and alkylammonium binding to poly($Asp^-$) and poly($Glu^-$), at different temperatures. The values were obtained from the slopes of linear fits shown in panels **B** of figures 12.5, 12.6 and 12.7. The slopes yielded approximate $\Delta C_p^\circ$ values for the $CH_2$ group equal to $-0.056\,\mathrm{kJ/mol/K}$ for poly($Arg^+$), $-0.062\,\mathrm{kJ/mol/K}$ for poly($Asp^-$), and $-0.071\,\mathrm{kJ/mol/K}$ for poly($Glu^-$). The average was $(-0.064 \pm 0.006)\,\mathrm{kJ/mol/K}$.

# Discussion and Conclusions

# Chapter 13

# Interpretation of volume change upon binding of primary sulfonamides to carbonic anhydrases.

## 13.1 Origins of volume changes upon protein-ligand binding

Volumes of sulfonamide inhibitor binding to carbonic anhydrases determined in this thesis are small and negative, and vary in the range of $-8\,\mathrm{mL\,mol^{-1}}$ to $-48\,\mathrm{mL\,mol^{-1}}$. Binding volume values in a similar range were determined by multiple techniques for various systems, the literature data are summarized in figure 13.1. Although very few, the cases in the literature, where $\Delta V_\mathrm{b}$ values for the same protein-ligand system are obtained by different methods are in good agreement with each other. Therefore, the currently available data raises no concerns about systemic discrepancies between values obtained by different methods. However, the amount of data obtained over five decades is exceptionally low. Due to this scarcity and the complexity of protein-ligand binding phenomena, the implications of the binding volume magnitude towards the whole picture of ligand binding remain unclear.

Binding volume is difficult to predict due to the number of possible contributions. Although protein and small molecular ligand binding

might seem like a relatively simple process, it is composed of numerous fundamental effects (hydrogen bonds, hydrophobic interaction, ionic interaction, ionization of chemical groups, changes in protein structure), most of which can contribute to $\Delta V_{\mathrm{b}}$. Due to the main variable, pressure, being difficult to operate, data on binding volume in the literature is scarce compared to data on other parameters, e.g., enthalpy. Due to these reasons, it is difficult to explain protein-ligand binding volume values in terms of molecular processes. Therefore, I will discuss possible origins of binding volume.
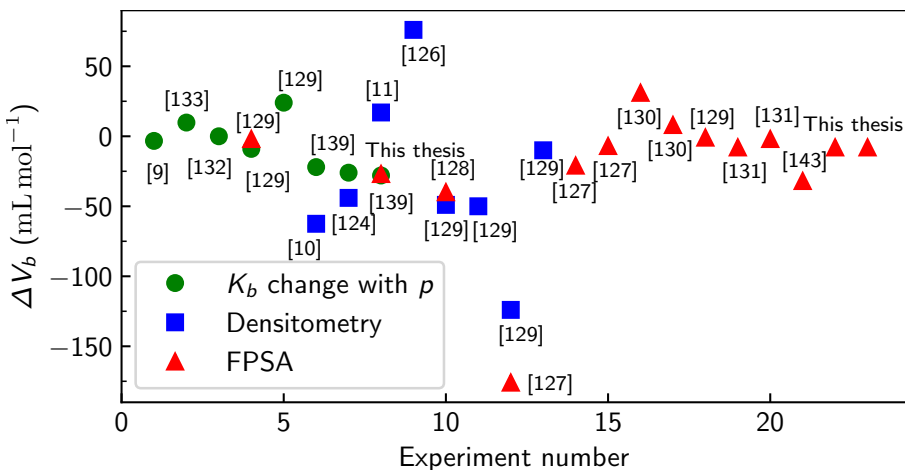


Figure 13.1: Summary of $\Delta V_{\mathrm{b}}$ values from the literature reviewed in section 4.3 (references [9–11, 124–131, 133, 139, 143]) and also this thesis. The experiment numbers on the abcissa axis represent $\Delta V_{\mathrm{b}}$ measurements of different protein-ligand pairs. The experiments are grouped into three categories by experiment type. Green circles represent experiments where $\Delta V_{\mathrm{b}}$ is determined by tracking changes to binding at defferent pressures; blue squares represent data from densimetry measurements; red squares represent values obtained by tracking protein stabilization against pressure by ligands.

### 13.1.1   Changes in protein void volume

The volume that protein takes up in a solution can be decomposed into solvent excluded volume and changes in solvent volume due to interactions with the protein [88]. The first term can be separated into van der Waals volume of the protein ($V_{\mathrm{vdW}}$) and void volume ($V_{\mathrm{void}}$). $V_{\mathrm{vdW}}$ is

131

the minimal volume that the protein molecule can occupy in a solution and is constant. Fluctuations of protein solvent excluded volume, e.g., during unfolding, come from changes in void volume [194]. It is known that ligand binding can change the conformations of proteins. Conformation fluctuations are especially prominent during allosteric regulation and cooperative binding events [195, 196]. These conformation changes could lead to a change in protein void volume. For example, it has been shown that binding of biotin to streptavidin results in increased packing of the protein [197]. Conformational "tightening" and reduction of flexibility was observed in BSA when binding ANS or its derivatives [161, 198]. It is also known that even non-allosteric ligands can induce conformational changes in proteins [199, 200]. Kamiyama *et al.* showed that dihydrofolate reductase interaction with specific ligands comes with a positive binding volume [125]. Analysis of crystal structures showed that the positive binding volume came from the increase in the internal void volume. From these examples, it can be concluded that positive or negative changes in protein void volume can be observed upon ligand binding.

### 13.1.2   Changes in solvation volume

Changes in solvation accompany ligand binding to proteins. In a typical case, water molecules that hydrate exposed groups of the ligand and protein are released into the bulk water upon binding, as these previously solvated groups form contacts with each other. Contributions of solvation are subject to controversy in the literature. Generally, it is thought that exposing polar and non-polar groups to water results in a decrease in volume [92–95]. A decrease in volume means that if water molecules are shed from the ligand and protein interface upon binding, fewer chemical groups are solvated, and the system's volume should increase. The difference in volume between a water molecule in bulk solvent and a water molecule that is a part of the hydration shell of a solute ($V_0 - V_\mathrm{h}$) is approximately $-1.8\,\mathrm{mL/M}$ for polar and charged surfaces, and $-0.6\,\mathrm{mL/M}$ for non-polar surfaces [5].

Changes in solvation were determined to be a significant contributor to binding volume in several early studies, where changes in volume upon protein-ligand binding volume were determined along with dissection of their origins. In the work of Kamiyama and Gekko, volume changes of

dihydrofolate reductase in the presence of various ligands were dissected into two major contributions [125]. Volume change upon protein-ligand binding was mostly attributed to changes in cavity volume, but a small positive contribution from dehydration was determined. Dubins *et al.* was the first to perform a study of binding volume using a combinatorial approach using several methods, including densimetry and spectroscopy at high pressure [11]. This study showed that ribonuclease A binds cytidine 2'-monophosphate and cytidine 3'-monophosphate with a small increase in volume. The resulting increase in volume was a product of compensation between contributions of dehydration and changes in internal volume. By comparing obtained values with literature knowledge on volume of hydration, the authors calulated the number of water molecules released upon binding. Chen and Makhatadze argue that historical treatment of changes in protein hydration as a transfer from polar to non-polar solvent is "an inadequate to model thermodynamics of hydration" [89, 201]. This group proposed that transfer from solution to gas phase is a more appropriate way to model hydration. By comparing partial molar volumes of various model compounds to their geometric volume, the researchers concluded that the hydration volume for both polar and non-polar groups is always positive. Further, an algorithm for the calculation of changes in volume upon protein unfolding was constructed. This approach was counter-criticized in a publication by Chalikian, and McGregor [5]. The authors emphasized the importance of separating thermal volume ($V_{\mathrm{T}}$). Thermal volume represents the space between the solute and the solvent. The authors stated that if van der Waals surface of the solute is taken as the dividing surface, the density of hydration shell water can be underestimated, leading to the apparent increase in volume due to hydration. The authors stated that the compensatory effects between thermal and hydration volume change are the cause of apparent positive volumes of protein hydration. As the exact contribution of hydration awaits scientific consensus, there is no doubt that hydration changes come with a significant volume change.

### 13.1.3   Changes in volume due to ionization

Ligand binding is often associated with ionization effects of the buffer and the binding species. The contribution of buffer ionization to the whole protein-ligand binding system often causes large discrepancies

between observed and intrinsic thermodynamic parameters of binding [202–204]. It is also possible that in this kind of ligand binding event, $\Delta V$ of buffer ionization also contributes to the observed ligand binding volume. It is known for that different ionization events have distinct $pK_a$ dependencies in relation to pressure, henceforth different $\Delta V$ of ionization [205–208]. The values of ionization volumes in magnitude are comparable to those of protein structure fluctuations during unfolding and binding. Ionization reactions of protein side chains are also associated with a volume change of a similar magnitude as summarized by Rasper, and Kauzmann [209]. Ionization events associated with proteins are also inevitably associated with the ionization of buffering agents. Using pressure perturbation calorimetry (PPC), Lee *et al.* determined that apparent protein transition volumes differ based on the buffer species. The structural transition of protein was linked to ionization, and the differences in $\Delta V$ of transition correlated with volumes of buffer ionization [98]. Since volumes of ionization are comparable in magnitude to volume changes during protein transitions, it can be concluded that ionization volumes have a possible contribution to the apparent volumes of binding.

## 13.2   Relevance to CA-sulfonamide interaction

All three of the discussed origins of binding volume have relevance towards carbonic anhydrases and their inhibitors. Carbonic anhydrases do not undergo significant changes in the protein structure upon ligand binding. These enzymes are often deemed as a textbook example of a rigid target [48, 210]. Therefore, changes in void volume could be insignificant contributors to ligand binding volume. However, this school of thought was based mostly on X-Ray structures. Recent NMR data suggests a degree of dynamics in the active site when the ligand is not present [211]. When the protein is ligand-free, it appears that some populations of the protein have the open loop next to the binding pocket; when the ligand is bound, the loop is in a closed position. Although this movement does not appear to affect voids throughout the protein structure, a total change in the void volume can not be neglected. Rigid structures obtained from X-ray crystallography might not fully reflect small fluctuations and less populated states of the protein.

As reviewed earlier, sulfonamide inhibitors bind to the zinc atom replacing a water molecule and through hydrogen bonding with specific residues. On top of that, both hydrophilic and hydrophobic sides of the binding pockets interact with various sulfonamide inhibitors [46]. These events mean that previously hydrated groups on the ligand and protein binding pocket are dehydrated to form new bonds, which means that the hydration level of the molecules is reduced upon binding. According to Chen *et al.* model, this would lead to a negative binding volume as is observed for the system in question [89]. The approach by Chalikian *et al.*, which decomposes volume changes into changes in thermal and changes of water volume, does not, in general, contradict the appearance of the negative contribution of solvation effects towards binding volume [5]. Thus hydration is a very likely contributor towards binding volume of this system.

The binding event of sulfonamide inhibitors and CA comes with at least three protonation events [203, 204]. The zinc coordinated hydroxy ion is protonated, the sulfonamide group of the ligand is deprotonated, and excess protons are discarded by protonating the buffer molecules. The volumes of buffer protonation can vary, but in this study, the buffers used were selected by their insignificant deprotonation volumes ($3.1 \, \mathrm{mL \, mol^{-1}}$ – Bis-Tris and $4.8 \, \mathrm{mL \, mol^{-1}}$ – HEPES second protonation) [208]. Therefore buffer protonation likely has a negative but insignificant contribution towards binding volume. Contrary, the volumes of protonation for specific sulfonamide inhibitors and the coordinated water in the CA structure, to my knowledge, are not known. However, most ionization events come with a specific volume change. For example the ionization of water at infinite dilution is $-22 \, \mathrm{mL \, mol^{-1}}$ [212, 213]. In the event of sulfonamide binding, this would mean a positive contribution of the same magnitude. As the volume of a water molecule is around $-18 \, \mathrm{mL \, mol^{-1}}$, this can be counterintuitive, but in reality, the rearrangements of the whole solvent network occur, leading to this value. Therefore we can not compare this value to what the effects of zinc coordinated water protonation would be. Sulfonamide inhibitors often have a p$K_\mathrm{a}$ value towards the basic side [214]. From the general tendencies of buffer p$K_\mathrm{a}$ and deprotonation volume relationship [208], it can be guessed that the deprotonation volume of sulfonamide inhibitors can be small and positive, leading to a small negative contribution in the

binding event. Therefore the net result of ionization effects in sulfonamide binding event is subject to compensatory effects of opposing sign contributions. We can conclude that ionization possibly contributes to the binding volume, yet more experiments in different buffer solutions must be done. Overall the most likely major contributor to the negative binding volume of sulfonamide compounds to CA's is the difference in solvation volume, but void volume changes and volume changes due to ionization events could also contribute to the net result. The contributions of the latter two sources empirically are universal and less dependent on ligand structure. Therefore hydration could be the separating factor between different values for different inhibitors. Hydration volumes could be an explanation for the previously proposed correlation between binding strength and negative binding volume [129]. A more significant negative contribution arising from solvation means a larger contact surface between the ligand and hydrophobic-hydrophilic sides of the binding pockets, forming more favorable contacts.

# Chapter 14

# Summary of oppositely charged poly(amino acid) − surfactant interactions

In this chapter ITC data of charged surfactant binding to oppositely charged amino acid homopolymers is discussed. The ITC data showed that surfactants at this concentration range (5 mM to 20 mM) bind to the oppositely charged moieties of poly(amino acid)s with the charge ratio of 1:1. The slight discrepancies of the stoichiometry ratio can arise from deviations in the concentration of both the poly(amino acid) and surfactant solutions. Previous elemental analysis of the poly(amino acid) showed that up to 20 % of water could be present in these batches [8], which could also affect the binding stoichiometry.

The majority of alkyl sulfate-poly(Arg$^+$) isotherms had a distinct dip in enthalpy (an increase in absolute value towards the negative side) at the charge neutralization point. This additional enthalpy might be a result of aggregate formation or structural rearrangement of the polymer. McCord *et al.* have determined that SDS induces the formation of an ordered polyarginine with an $\alpha$-helix structure at the charge neutralization point. Enthalpy values of an $\alpha$-helix formation known in the literature are in the range of $-2 \, \text{kcal} \, \text{mol}^{-1}$ to $-0.9 \, \text{kcal} \, \text{mol}^{-1}$ per residue[216–218], which is in agreement with our results.

Added sodium chloride increasingly reduced surfactant binding to poly(amino acid)s. Inhibition by salt most likely signifies the importance of electrostatic attraction in poly(amino acid) binding of surfactants. At

high concentrations, sodium and chloride ions possibly compete for the charged groups of poly(amino acid) and surfactants, blocking their ion pair formation. Another way of looking at this phenomenon is that a high added salt concentration lowers the CMC of ionic surfactants. In other words, the combination of tail hydrophobic repulsion from water and head attraction towards it becomes more significant, to the point where micelles independent from polymer become the preferred state instead of binding to the polymer. Dodecyl amine binding to poly(Glu$^-$) was almost completely halted by a 25 mM concentration of NaCl, while SDS binding to poly(Arg$^+$) continued in NaCl conentrations up to 200 mM. Such differences in the concentration of NaCl required to prevent surfactant binding, between poly(Glu$^-$) and poly(Arg$^+$), can be explained by the high affinity of the guanidinium group to sulfates [219].

The CH$_2$ group contribution to enthalpy at 25 °C averaged at 1.7 kJ/mol/CH$_2$, with poly(Arg$^+$) and alkyl sulfate system being significantly higher ($(2.7 \pm 3.0)$ kJ/mol/CH$_2$ and poly(Glu$^-$)-alkylamine system being significantly lower ($(0.92 \pm 2.70)$ kJ/mol/CH$_2$). The nature of these differences is unclear. There seems to be no clear correlation between the CH$_2$ group contributions to the enthalpy and the transitions in secondary structure. According to the literature [215, 220–222], poly(Orn$^+$), poly(Glu$^-$) and poly(Arg$^+$) undergo a coil-to-helix transition after the neutralization point is reached. Poly(Lys$^+$) undergoes a coil-to-$\beta$-sheet transition with all of the tested surfactants except octyl sulfate, while poly(Asp$^-$) does not undergo a transition to the more structured state. Although, some of these transitions may also be too slow to be observed in an ITC experiment [223]. A possible explanation, on the other hand, is differences in energies required to attain specific conformations. For example, possible conformations of poly(Glu$^-$) are calculated to have consistently higher torsional energies of side chains than poly(Asp$^-$) [224].

The negative $\Delta C_p$ values in this study were similar to those of hydrocarbon transfer from water to an organic solvent [21]. This similarity suggests that hydrophobic tail interactions between bound surfactants also play a significant role and plausibly explain the observed enthalpies. A linear increase in the enthalpy contribution towards binding with surfactant chain lengthening was present in all surfactant–poly(amino acid)

pairs, even those with endothermic interaction profiles. Furthermore, the CH$_2$ group contributions to the interaction enthalpy were similar in various systems. Overall the RSO$_4{}^-$–poly(Arg$^+$) system had a significantly larger CH$_2$ contribution to binding, more negative $\Delta C_p$ binding and an isotherm shape that indicated stronger binding from the start of the experiment, whereas in other systems binding was weaker at the start and cooperative effects were more pronounced. These disagreements lead to the conclusion that binding events involving poly(Arg$^+$) and RSO$_4$ have distinct differences from other tested systems. The differences are explainable by the strong affinity between sulfate and guanidinium groups [219], which is also accompanied by a more strict geometry of the salt bridge. A tighter headgroup bond could also induce the higher surfactant's tail contributions, as it could constrain the bound surfactants.

Previous studies have shown that the enthalpy of aliphatic chain interaction between themselves can indicate if the chains aggregate to a liquid phase or a solid phase. The difference in the enthalpies of binding can match the enthalpy of fusion [7, 225–227]. The enthalpy of the CH$_2$ group binding into a liquid form yielded the value of $-1.25$ kJ/mol, enthalpy of aggregation into the solid form was greater and equal to $-5.2$ kJ/mol per CH$_2$ group [226]. Here in this study, association value was in the range of $-2.7$ kJ/mol to $-0.92$ kJ/mol per CH$_2$ group. The absolute magnitude indicates that the phase of the poly(amino acid)-–surfactant complex may be liquid or solid. Only part of the contacts may have formed between the aliphatic chains in the solid because poly(amino acid)s have conformational constraints and would not enable surfactant's aliphatic chains to bind to each other fully. Therefore, it is most likely that the chains only partially interact with each other, and the remaining length of the chains interacts with the amino acids of the polymer.

# Conclusions

- GdmHCl reduces the $p_m$ values of CA I, CA II, and CA XIII linearly at low concentration range. At a higher concentration range $p_m$ values do not decrease linearly due to the GdmHCl-induced unfolding which can occur in either two-state (CA I) or three state (CA II, CA XIII) manner.

- It is possible to determine the binding volumes of tightly binding ligands using FPSA in different denaturant concentrations if changes in $p_m$ values are linear within the tested range.

- Primary sulfonamide inhibitors bind to CA I, CA II, and CA XIII with a negative $\Delta V_b$ value, meaning their binding constant is larger at higher pressure.

- If conditions for exchange rate and binding strength are met, the Gibbs energy of protein-ligand can be determined from a single $^1\text{H} - ^{15}\text{N}$ HSQC NMR spectrum. Extending this method with variable pressure allows relatively fast determination of changes in volume upon protein-ligand binding.

- Charged surfactants bind to oppositely charged poly(amino acid)s with a stoichiometry of one surfactant molecule per amino acid moiety, by forming ion-pairs between the surfactant head group and charged amino acid moiety.

- Addition of a $CH_2$ group on the aliphatic chain of a surfactant leads to a more favorable interaction enthalpy that is similar in value for various oppositely charged model systems.

- Poly($\text{Arg}^+$) exhibits a particularly strong interaction with alkyl sulfate and sulfonate surfactants. This interaction has a differ-

ent binding profile than other poly(amino acid)-ionic surfactant interactions.

# Acknowledgments

# List of Publications

## Publications included in this thesis

- Skvarnavičius, G., Toleikis, Z., Grigaliūnas, M., Smirnovienė, J., Norvaišas, P., Cimmperman, P., Matulis, D. & V Petrauskas. High Pressure Spectrofluorimetry – a Tool to Determine Protein-Ligand Binding Volume. *J. Phys.: Conf. Ser.* **950,** 042001 (2017)

  I have preformed the high pressure spectrofluorimetry experiments, analyzed the data.

- Skvarnavičius, G., Matulis, D. & Petrauskas, V. in *Carbonic Anhydrase as Drug Target: Thermodynamics and Structure of Inhibitor Binding* (ed Matulis, D.) 97–106 (Springer International Publishing, Cham, 2019)

  I have preformed the high pressure spectrofluorimetry experiments, analyzed the data.

- Skvarnavičius, G., Dvareckas, D., Matulis, D. & Petrauskas, V. Thermodynamics of Interactions Between Charged Surfactants and Ionic Poly(Amino Acids) by Isothermal Titration Calorimetry. *ACS Omega* **4,** 17527–17535 (2019)

  I have preformed the ITC experiments, analyzed the data, participated in writing the manuscript.

- Skvarnavičius, G., Toleikis, Z., Michailovienė, V., Roumestand, C., Matulis, D. & Petrauskas, V. Protein–Ligand Binding Volume Determined from a Single 2D NMR Spectrum with Increasing Pressure. *The Journal of Physical Chemistry B* **125,** 5823–5831 (2021)

I have analyzed the $^1$H – $^{15}$N HSQC NMR data, participated in writing the manuscript.

- Skvarnavičius, G., Toleikis, Z., Matulis, D. & Petrauskas, V. Denaturant- or ligand-induced changes in protein volume by pressure shift assay. *Phys Chem Chem Phys* (2022)

  I have preformed the experiments and analyzed the data, writen a major portion of the manuscript.

# Publications not included in this thesis

- Toleikis, Z., Sirotkin, V. A., Skvarnavičius, G., Smirnovienė, J., Roumestand, C., Matulis, D. & Petrauskas, V. Volume of Hsp90 Protein–Ligand Binding Determined by Fluorescent Pressure Shift Assay, Densitometry, and NMR. *The Journal of Physical Chemistry B* **120,** 9903–9912 (2016)

  I have participated in the $^1$H – $^{15}$N HSQC NMR experiments, analyzed the data.

# Conference presentations

- G. Skvarnavičius, Z. Toleikis, P. Cimmperman, D. Matulis, V. Petrauskas. Investigating ligand binding induced changes in protein volume using high pressure spectrofluorimetry. The COINS 2018, Vilnius, 2018 February 28th - March 2nd (oral presentation)

- G. Skvarnavičius, Z. Toleikis, D. Matulis, V. Petrauskas. Fluorescent pressure shift assay – a method to investigate volumetric properties of protein-ligand interaction. 15-oji Lithuanian biochemical sosciety conference, 2018 m. June 26th - 29th Dubingiai, Lithuania (poster presentation).

- G. Skvarnavičius, D. Matulis, V. Petrauskas. Thermodynamics of ionic surfactant–poly(amino acid) interaction. Kalorimetrietage, Braunshweig, 2019 June 12th - 14th (poster presentation).

- G. Skvarnavičius, Z. Toleikis, C. Roumestand, D. Matulis, V. Petrauskas. Protein-ligand Binding Volume by Fluorescent Pressure

Shift Assay and NMR. 10th International Meeting on Biomolecules under Pressure. Dortmundas, 2019m. September 29th - October 3d (oster presentation).

# References

1. Gupta, M., Sharma, R. & Kumar, A. Docking Techniques in Pharmacology: How Much Promising? *Comput. Biol. Chem.* **76,** 210–217 (2018).

2. Klebe, G. Virtual Ligand Screening: Strategies, Perspectives and Limitations. *Drug Discov. Today* **11,** 580–594 (2006).

3. Royer, C. A. Revisiting Volume Changes in Pressure-Induced Protein Unfolding. *Biochimica et Biophysica Acta (BBA) - Protein Structure and Molecular Enzymology* **1595,** 201–209 (2002).

4. Chalikian, T. V. & Filfil, R. How Large Are the Volume Changes Accompanying Protein Transitions and Binding? *Biophys. Chem.* **104,** 489–499 (2003).

5. Chalikian, T. V. & Macgregor, R. B. On Empirical Decomposition of Volumetric Data. *Biophys. Chem.* **246,** 8–15 (2019).

6. Matulis, D., Rouzina, I. & Bloomfield, V. A. Thermodynamics of Cationic Lipid Binding to DNA and DNA Condensation: Roles of Electrostatics and Hydrophobicity. *Journal of the American Chemical Society* **124,** 7331–7342 (2002).

7. Norvaišas, P., Petrauskas, V. & Matulis, D. Thermodynamics of Cationic and Anionic Surfactant Interaction. *The Journal of Physical Chemistry B* **116,** 2138–2144 (2012).

8. Petrauskas, V., Maximowitsch, E. & Matulis, D. Thermodynamics of Ion Pair Formations Between Charged Poly(Amino Acid)s. *The Journal of Physical Chemistry B* **119,** 12164–12171 (2015).

9. Li, T. M., Hook, J. W., Drickamer, H. G. & Weber, G. Effects of Pressure upon the Fluorescence of the Riboflavin Binding Protein and Its Flavin Mononucleotide Complex. *Biochemistry-us.* **15,** 3205–3211 (1976).

10. Gekko, K. & Yamagami, K. Compressibility and Volume Changes of Lysozyme Due to Inhibitor Binding. *Chem. Lett.* **27,** 839–840 (1998).

11. Dubins, D. N., Filfil, R., Macgregor, R. B. & Chalikian, T. V. Role of Water in Protein-Ligand Interactions: Volumetric Characterization of the Binding of 2'-Cmp and 3'-Cmp to Ribonuclease A. *The Journal of Physical Chemistry B* **104,** 390–401 (2000).

12. Oliva, R., Jahmidi-Azizi, N., Mukherjee, S. & Winter, R. Harnessing Pressure Modulation for Exploring Ligand Binding Reactions in Cosolvent Solutions. *The Journal of Physical Chemistry B* **125,** 539–546 (2021).

13. Chaires, J. B. Calorimetry and Thermodynamics in Drug Design. *Annu. Rev. Bioph. Biom.* **37,** 135–151 (2008).

14. Klebe, G. Applying Thermodynamic Profiling in Lead Finding and Optimization. *Nat. Rev. Drug Discov.* **14,** 95–110 (2015).

15. Claveria-Gimeno, R., Vega, S., Abian, O. & Velazquez-Campoy, A. A Look at Ligand Binding Thermodynamics in Drug Discovery. *Expert Opinion on Drug Discovery* **12,** 363–377 (2017).

16. Wiseman, T., Williston, S., Brandts, J. F. & Lin, L. N. Rapid Measurement of Binding Constants and Heats of Binding Using a New Titration Calorimeter. *Anal. Biochem.* **179,** 131–137 (1989).

17. Velazquez-Campoy, A., Todd, M. J. & Freire, E. HIV-1 Protease Inhibitors: Enthalpic versus Entropic Optimization of the Binding Affinity. *Biochemistry-us.* **39,** 2201–2207 (2000).

18. Cabani, S., Gianni, P., Mollica, V. & Lepori, L. Group Contributions to the Thermodynamic Properties of Non-Ionic Organic Solutes in Dilute Aqueous Solution. *J. Solution Chem.* **10,** 563–595 (1981).

19. Stone, M. J. NMR Relaxation Studies of the Role of Conformational Entropy in Protein Stability and Ligand Binding. *Accounts Chem. Res.* **34,** 379–388 (2001).

20. Siebert, X. & Amzel, L. M. Loss of Translational Entropy in Molecular Associations. *Proteins: Structure, Function, and Bioinformatics* **54,** 104–115 (2004).

21. Baldwin, R. L. Temperature Dependence of the Hydrophobic Interaction in Protein Folding. *Proceedings of the National Academy of Sciences* **83,** 8069–8072 (1986).

22. Vega, S., Abian, O. & Velazquez-Campoy, A. On the Link between Conformational Changes, Ligand Binding and Heat Capacity. *Biochimica et Biophysica Acta (BBA) - General Subjects. Microcalorimetry in the BioSciences - Principles and Applications* **1860,** 868–878 (2016).

23. Gallagher, K. & Sharp, K. Electrostatic Contributions to Heat Capacity Changes of DNA-Ligand Binding. *Biophys. J.* **75,** 769–776 (1998).

24. Cooper, A. Heat Capacity Effects in Protein Folding and Ligand Binding: A Re-Evaluation of the Role of Water in Biomolecular Thermodynamics. *Biophys. Chem.* **115,** 89–97 (2005).

25. Lee, B. & Graziano, G. A Two-State Model of Hydrophobic Hydration That Produces Compensating Enthalpy and Entropy Changes. *Journal of the American Chemical Society* **118,** 5163–5168 (1996).

26. Qian, H. Entropy-Enthalpy Compensation: Conformational Fluctuation and Induced-Fit. *The Journal of Chemical Physics* **109,** 10015–10017 (1998).

27. Tellinghuisen, J. & Chodera, J. D. Systematic Errors in Isothermal Titration Calorimetry: Concentrations and Baselines. *Anal. Biochem.* **414,** 297–299 (2011).

28. Exner, O. Entropy–Enthalpy Compensation and Anticompensation: Solvation and Ligand Binding. *Chem. Commun.,* 1655–1656 (2000).

29. Kramer, C., Kalliokoski, T., Gedeck, P. & Vulpetti, A. The Experimental Uncertainty of Heterogeneous Public Ki Data. *J. Med. Chem.* **55,** 5165–5173 (2012).

30. McKenna, R. & Frost, S. C. Overview of the Carbonic Anhydrase Family. *Subcell Biochem* **75,** 3–5 (2014).

31. Frost, S. C. Physiological Functions of the Alpha Class of Carbonic Anhydrases. *Subcell Biochem* **75,** 9–30 (2014).

32. Esbaugh, A. J. & Tufts, B. L. The Structure and Function of Carbonic Anhydrase Isozymes in the Respiratory System of Vertebrates. *Respiratory physiology & neurobiology* **154,** 185–198 (2006).

33. Lönnerholm, G., Wistrand, P. J. & Bárány, E. Carbonic Anhydrase Isoenzymes in the Rat Kidney. Effects of Chronic Acetazolamide Treatment. *Acta Physiol. Scand.* **126,** 51–60 (1986).

34. Bagnis, C., Marshansky, V., Breton, S. & Brown, D. Remodeling the Cellular Profile of Collecting Ducts by Chronic Carbonic Anhydrase Inhibition. *American Journal of Physiology. Renal Physiology* **280,** F437–448 (2001).

35. Ruusuvuori, E. Carbonic Anhydrase Isoform VII Acts as a Molecular Switch in the Development of Synchronous Gamma-Frequency Firing of Hippocampal CA1 Pyramidal Cells. *J. Neurosci.* **24,** 2699–2707 (2004).

36. Lehtonen, J. *et al.* Characterization of CA XIII, a Novel Member of the Carbonic Anhydrase Isozyme Family. *J Biol Chem* **279,** 2719–27 (2004).

37. Patrikainen, M., Pan, P., Kulesskaya, N., Voikar, V. & Parkkila, S. The Role of Carbonic Anhydrase VI in Bitter Taste Perception: Evidence from the Car6-/- Mouse Model. *J. Biomed. Sci.* **21,** 82 (2014).

38. Grincevičienė, Š. & Matulis, D. in *Carbonic Anhydrase as Drug Target: Thermodynamics and Structure of Inhibitor Binding* (ed Matulis, D.) 335–349 (Springer International Publishing, Cham, 2019).

39. Creighton, C. J. *et al.* Genes Regulated by Estrogen in Breast Tumor Cells in Vitro Are Similarly Regulated in Vivoin Tumor Xenografts and Human Breast Tumors. *Genome Biol.* **7,** R28 (2006).

40. Makani, S. *et al.* NMDA Receptor-Dependent Afterdepolarizations Are Curtailed by Carbonic Anhydrase 14: Regulation of a Short-Term Postsynaptic Potentiation. *J. Neurosci.* **32,** 16754–16762 (2012).

41. Boone, C. D., Pinard, M., McKenna, R. & Silverman, D. in *Subcell Biochem* 31–52 (2014).

42. Baranauskienė, L. & Matulis, D. in *Carbonic Anhydrase as Drug Target: Thermodynamics and Structure of Inhibitor Binding* (ed Matulis, D.) 39–49 (Springer International Publishing, Cham, 2019).

43. Verpoorte, J. A., Mehta, S. & Edsall, J. T. Esterase Activities of Human Carbonic Anhydrases B and C. *J. Biol. Chem.* **242,** 4221–4229 (1967).

44. Innocenti, A. *et al.* Investigations of the Esterase, Phosphatase, and Sulfatase Activities of the Cytosolic Mammalian Carbonic Anhydrase Isoforms I, II, and XIII with 4-Nitrophenyl Esters as Substrates. *Bioorg Med Chem Lett* **18,** 2267–71 (2008).

45. Uda, N. R. *et al.* Esterase Activity of Carbonic Anhydrases Serves as Surrogate for Selecting Antibodies Blocking Hydratase Activity. *J Enzyme Inhib Med Chem,* 1–6 (2015).

46. Supuran, C. T. How Many Carbonic Anhydrase Inhibition Mechanisms Exist? *J. Enzym. Inhib. Med. Ch.* **31,** 345–360 (2016).

47. Baranauskienė, L. & Matulis, D. in *Carbonic Anhydrase as Drug Target: Thermodynamics and Structure of Inhibitor Binding* (ed Matulis, D.) 3–14 (Springer International Publishing, Cham, 2019).

48. Krishnamurthy, V. M. *et al.* Carbonic Anhydrase as a Model for Biophysical and Physical-Organic Studies of Proteins and Protein-Ligand Binding. *Chem. Rev.* **108,** 946–1051 (2008).

49. Baranauskienė, L., Petrikaitė, V., Matulienė, J. & Matulis, D. Titration Calorimetry Standards and the Precision of Isothermal Titration Calorimetry Data. *Int. J. Mol. Sci.* **10,** 2752–2762 (2009).

50. Paketurytė, V., Linkuvienė, V., Krainer, G., Chen, W.-Y. & Matulis, D. Repeatability, Precision, and Accuracy of the Enthalpies and Gibbs Energies of a Protein–Ligand Binding Reaction Measured by Isothermal Titration Calorimetry. *Eur. Biophys. J.* **48,** 139–152 (2019).

51. Mickevičiūtė, A. *et al.* in *Carbonic Anhydrase as Drug Target: Thermodynamics and Structure of Inhibitor Binding* (ed Matulis, D.) 15–37 (Springer International Publishing, Cham, 2019).

52. Smirnov, A., Manakova, E., Gražulis, S., McKenna, R. & Matulis, D. in *Carbonic Anhydrase as Drug Target: Thermodynamics and Structure of Inhibitor Binding* (ed Matulis, D.) 179–202 (Springer International Publishing, Cham, 2019).

53. Fisher, Z. *et al.* Neutron Structure of Human Carbonic Anhydrase II: A Hydrogen-Bonded Water Network "Switch" Is Observed between pH 7.8 and 10.0. *Biochemistry-us.* **50,** 9421–9423 (2011).

54. Fisher, S. Z., Aggarwal, M., Kovalevsky, A. Y., Silverman, D. N. & McKenna, R. Neutron Diffraction of Acetazolamide-Bound Human Carbonic Anhydrase II Reveals Atomic Details of Drug Binding. *J. Am. Chem. Soc.* **134,** 14726–14729 (2012).

55. Sethson, I., Edlund, U., Holak, T. A., Ross, A. & Jonsson, B. H. Sequential Assignment of 1H, 13C and 15N Resonances of Human Carbonic Anhydrase I by Triple-Resonance NMR Techniques and Extensive Amino Acid-Specific 15N-labeling. *Journal of biomolecular NMR* **8,** 417–428 (1996).

56. Venters, R. A., Farmer II, B. T., Fierke, C. A. & Spicer, L. D. Characterizing the Use of Perdeuteration in NMR Studies of Large Proteins:13C,15N and1H Assignments of Human Carbonic Anhydrase II. *J. Mol. Biol.* **264,** 1101–1116 (1996).

57. Li, D., Chen, L., Wang, R., Liu, R. & Ge, G. Synergetic Determination of Thermodynamic and Kinetic Signatures Using Isothermal Titration Calorimetry: A Full-Curve-Fitting Approach. *Anal. Chem.* **89,** 7130–7138 (2017).

58. Langevin, D. Polyelectrolyte and Surfactant Mixed Solutions. Behavior at Surfaces and in Thin Films. *Adv. Colloid Interfac.* **89–90,** 467–484 (2001).

59. Taylor, D. J. F., Thomas, R. K. & Penfold, J. The Adsorption of Oppositely Charged Polyelectrolyte/Surfactant Mixtures: Neutron Reflection from Dodecyl Trimethylammonium Bromide and Sodium Poly (Styrene Sulfonate) at the Air/Water Interface. *Langmuir* **18,** 4748–4757 (2002).

60. Kauzmann, W. Some Factors in the Interpretation of Protein Denaturation. *Adv. Protein Chem.* **14,** 1–63 (1959).

61. Baldwin, R. L. The New View of Hydrophobic Free Energy. *FEBS Letters. The Many Faces of Proteins* **587,** 1062–1066 (2013).

62. Wang, H., Wang, Y., Yan, H., Zhang, J. & Thomas, R. K. Binding of Sodium Dodecyl Sulfate with Linear and Branched Polyethyleneimines in Aqueous Solution at Different pH Values. *Langmuir* **22,** 1526–1533 (2006).

63. Kogej, K. Association and Structure Formation in Oppositely Charged Polyelectrolyte–Surfactant Mixtures. *Adv. Colloid Interfac. Polyelectrolytes* **158,** 68–83 (2010).

64. Wang, C. & Tam, K. C. Interaction between Polyelectrolyte and Oppositely Charged Surfactant: Effect of Charge Density. *The Journal of Physical Chemistry B* **108,** 8976–8982 (2004).

65. Chen, Z., Li, X.-W., Zhao, K.-S., Xiao, J.-X. & Yang, L.-K. Dielectric Spectroscopy Investigation on the Interaction of Poly(Diallyldimethylammonium Chloride) with Sodium Decyl Sulfate in Aqueous Solution. *The Journal of Physical Chemistry B* **115,** 5766–5774 (2011).

66. Manning, G. S. Counterion Binding in Polyelectrolyte Theory. *Accounts Chem. Res.* **12,** 443–449 (1979).

67. Santerre, J. P., Hayakawa, K. & Kwak, J. C. T. A Study of the Temperature Dependence of the Binding of a Cationic Surfactant to an Anionic Polyelectrolyte. *Colloid. Surface.* **13,** 35–45 (1985).

68. Chakraborty, T., Chakraborty, I. & Ghosh, S. Sodium Carboxymethylcellulose-CTAB Interaction: A Detailed Thermodynamic Study of Polymer-Surfactant Interaction with Opposite Charges. *Langmuir* **22,** 9905–9913 (2006).

69. Shirahama, K., Takashima, K. & Takisawa, N. Interaction between Dodecyltrimethylammonium Chloride and DNA. *Bulletin of the Chemical Society of Japan* **60,** 43–47 (1987).

70. Lee, J. & Moroi, Y. Binding of Sodium Dodecyl Sulfate to a Cationic Polymer of High Charge Density. *Bulletin of the Chemical Society of Japan* **76,** 2099–2102 (2003).

71. Goddard, E. Polymer—Surfactant Interaction Part II. Polymer and Surfactant of Opposite Charge. *Colloid. Surface.* **19,** 301–329 (1986).

72. Majhi, P. R. & Blume, A. Thermodynamic Characterization of Temperature-Induced Micellization and Demicellization of Detergents Studied by Differential Scanning Calorimetry. *Langmuir* **17,** 3844–3851 (2001).

73. Hayakawa, K. & Kwak, J. C. T. Surfactant-Polyelectrolyte Interactions. 1. Binding of Dodecyltrimethylammonium Ions by Sodium Dextransulfate and Sodium Poly(Styrenesulfonate) in Aqueous Solution in the Presence of Sodium Chloride. *The Journal of Physical Chemistry* **86,** 3866–3870 (1982).

74. Malovikova, A., Hayakawa, K. & Kwak, J. C. T. Surfactant-Polyelectrolyte Interactions. 4. Surfactant Chain Length Dependence of the Binding of Alkylpyridinium Cations to Dextran Sulfate. *The Journal of Physical Chemistry* **88,** 1930–1933 (1984).

75. Hayakawa, K. & Kwak, J. C. T. Study of Surfactant-Polyelectrolyte Interactions. 2. Effect of Multivalent Counterions on the Binding of Dodecyltrimethylammonium Ions by Sodium Dextran Sulfate and Sodium Poly(Styrene Sulfonate) in Aqueous Solution. *The Journal of Physical Chemistry* **87,** 506–509 (1983).

76. Wang, X. *et al.* Salt Effect on the Complex Formation between Polyelectrolyte and Oppositely Charged Surfactant in Aqueous Solution. *The Journal of Physical Chemistry B* **109,** 10807–10812 (2005).

77. Nizri, G., Lagerge, S., Kamyshny, A., Major, D. T. & Magdassi, S. Polymer–Surfactant Interactions: Binding Mechanism of Sodium Dodecyl Sulfate to Poly(Diallyldimethylammonium Chloride). *J. Colloid Interf. Sci.* **320,** 74–81 (2008).

78. Ahmadova, G. A. *et al.* Effect of Head-Group of Cationic Surfactants and Structure of Ionic Groups of Anionic Polyelectrolyte in Oppositely Charged Polymer-Surfactant Complexes. *Colloids and Surfaces A: Physicochemical and Engineering Aspects* **613,** 126075 (2021).

79. Petkova, R., Tcholakova, S. & Denkov, N. D. Role of Polymer–Surfactant Interactions in Foams: Effects of pH and Surfactant Head Group for Cationic Polyvinylamine and Anionic Surfactants. *Colloids and Surfaces A: Physicochemical and Engineering Aspects. A Collection of Papers Presented at the 9th EUFOAM Conference, Lisbon, Portugal, 8-11 July 2012* **438,** 174–185 (2013).

80. Yan, P., Jin, C., Wang, C., Ye, J. & Xiao, J.-X. Effect of Surfactant Head Group Size on Polyelectrolyte-Surfactant Interactions: Steady-State and Time-Resolved Fluorescence Study. *J. Colloid Interf. Sci.* **282,** 188–192 (2005).

81. Goddard, E. D. & Hannan, R. B. Polymer/Surfactant Interactions. *Journal of the American Oil Chemists' Society* **54,** 561–566 (1977).

82. Okuzaki, H. & Osada, Y. Effects of Hydrophobic Interaction on the Cooperative Binding of a Surfactant to a Polymer Network. *Macromolecules* **27,** 502–506 (1994).

83. Wallin, T. & Linse, P. Monte Carlo Simulations of Polyelectrolytes at Charged Micelles. 3. Effects of Surfactant Tail Length. *The Journal of Physical Chemistry B* **101,** 5506–5513 (1997).

84. Kiefer, J. J., Somasundaran, P. & Ananthapadmanabhan, K. P. Interaction of Tetradecyltrimethylammonium Bromide with Poly(Acrylic Acid) and Poly(Methacrylic Acid). Effect of Charge Density. *Langmuir* **9,** 1187–1192 (1993).

85. Li, D. & Wagner, N. J. Universal Binding Behavior for Ionic Alkyl Surfactants with Oppositely Charged Polyelectrolytes. *Journal of the American Chemical Society* **135,** 17547–17555 (2013).

86. Wallin, T. & Linse, P. Monte Carlo Simulations of Polyelectrolytes at Charged Micelles. 1. Effects of Chain Flexibility. *Langmuir* **12,** 305–314 (1996).

87. Ram-On, M., Cohen, Y. & Talmon, Y. Effect of Polyelectrolyte Stiffness and Solution pH on the Nanostructure of Complexes Formed by Cationic Amphiphiles and Negatively Charged Polyelectrolytes. *The Journal of Physical Chemistry B* **120,** 5907–5915 (2016).

88. Richards, F. M. Areas, Volumes, Packing, and Protein Structure. *Annu. Rev. Biophys. Bio.* **6,** 151–176 (1977).

89. Chen, C. R. & Makhatadze, G. I. Molecular Determinant of the Effects of Hydrostatic Pressure on Protein Folding Stability. *Nat. Commun.* **8,** 14561 (2017).

90. Chalikian, T. V. Volumetric Properties of Proteins. *Annu. Rev. Bioph. Biom.* **32,** 207–235 (2003).

91. Ando, N. *et al.* Structural and Thermodynamic Characterization of T4 Lysozyme Mutants and the Contribution of Internal Cavities to Pressure Denaturation. *Biochemistry-us.* **47,** 11097–11109 (2008).

92. Kauzmann, W. Thermodynamics of Unfolding. *Cah. Rev. The.* **325,** 763–764 (1987).

93. Kharakoz, D. P. Partial Molar Volumes of Molecules of Arbitrary Shape and the Effect of Hydrogen Bonding with Water. *J. Solution Chem.* **21,** 569–595 (1992).

94. Chalikian, T. V., Sarvazyan, A. P. & Breslauer, K. J. *Partial Molar Volumes, Expansibilities, and Compressibilities of .Alpha.,.Omega.-Aminocarboxylic Acids in Aqueous Solutions between 18 and 55.Degree.C* https://pubs.acs.org/doi/pdf/10.1021/j100151a061. 2002.

95. Chalikian, T. V., Gindikin, V. S. & Breslauer, K. J. Hydration of Diglycyl Tripeptides with Non-Polar Side Chains: A Volumetric Study. *Biophys. Chem.* **75,** 57–71 (1998).

96. Mitra, L., Rouget, J.-B., Garcia-Moreno, B., Royer, C. A. & Winter, R. Towards a Quantitative Understanding of Protein Hydration and Volumetric Properties. *ChemPhysChem* **9,** 2715–2721 (2008).

97. Rouget, J.-B. *et al.* Size and Sequence and the Volume Change of Protein Folding. *Journal of the American Chemical Society* **133,** 6020–6027 (2011).

98. Lee, S., Heerklotz, H. & Chalikian, T. V. Effects of Buffer Ionization in Protein Transition Volumes. *Biophys. Chem.* **148,** 144–147 (2010).

99. Roche, J. & Royer, C. A. Lessons from Pressure Denaturation of Proteins. *J. R. Soc. Interface* **15,** 20180244 (2018).

100. Kauzmann, W. Volume Changes in Ovalbumin and Bovine Serum Albumin on Adding Acid. *Biochimica et Biophysica Acta* **28,** 87–91 (1958).

101. Rasper, J. & Kauzmann, W. Volume Changes in Protein Reactions. I. Ionization Reactions of Proteins. *Journal of the American Chemical Society* **84,** 1771–1777 (1962).

102. El Kadi, N. *et al.* Unfolding and Refolding of Bovine Serum Albumin at Acid pH: Ultrasound and Structural Studies. *Biophys. J.* **91,** 3397–3404 (2006).

103. Ruan, K. *et al.* Pressure-Exploration of the 33-kDa Protein from the Spinach Photosystem II Particle. *Eur. J. Biochem.* **268,** 2742–2750 (2001).

104. Myers, J. K., Pace, C. N. & Scholtz, J. M. Denaturant m Values and Heat Capacity Changes: Relation to Changes in Accessible Surface Areas of Protein Unfolding. *Protein Science : A Publication of the Protein Society* **4,** 2138–2148 (1995).

105. ŠKerjanc, J. & Lapanje, S. A Dilatometric Study of the Denaturation of Lysozyme by Guanidine Hydrochloride and Hydrochloric Acid. *Eur. J. Biochem.* **25,** 49–53 (1972).

106. ŠKerjanc, J., Doleček, V. & Lapanje, S. The Partial Specific Volume of Chymotrypsinogen A in Aqueous Urea Solutions. *Eur. J. Biochem.* **17,** 160–164 (1970).

107. Herberhold, H., Royer, C. A. & Winter, R. Effects of Chaotropic and Kosmotropic Cosolvents on the Pressure-Induced Unfolding and Denaturation of Proteins: An FT-IR Study on Staphylococcal Nuclease. *Biochemistry-us.* **43,** 3336–3345 (2004).

108. Ravindra, R. & Winter, R. Pressure Perturbation Calorimetic Studies of the Solvation Properties and the Thermal Unfolding of Proteins in Solution. *Zeitschrift für Physikalische Chemie* **217,** 1221–1244 (2003).

109. Pappenberger, G., Saudan, C., Becker, M., Merbach, A. E. & Kiefhaber, T. Denaturant-Induced Movement of the Transition State of Protein Folding Revealed by High-Pressure Stopped-Flow Measurements. *Proceedings of the National Academy of Sciences* **97,** 17–22 (2000).

110. Timasheff, S. N. & Xie, G. Preferential Interactions of Urea with Lysozyme and Their Linkage to Protein Denaturation. *Biophys. Chem. Walter Kauzmann's 85th Birthday* **105,** 421–448 (2003).

111. Smith, P. E. Protein Volume Changes on Cosolvent Denaturation. *Biophys. Chem.* **113,** 299–302 (2005).

112. Sirotkin, V. A. & Winter, R. Volume Changes Associated with Guanidine Hydrochloride, Temperature, and Ethanol Induced Unfolding of Lysozyme. *The Journal of Physical Chemistry B* **114,** 16881–16886 (2010).

113. Xie, G. & Timasheff, S. N. The Thermodynamic Mechanism of Protein Stabilization by Trehalose. *Biophys. Chem. 10 Years of the Gibbs Conference on Biothermodynamics* **64,** 25–43 (1997).

114. Priev, A., Almagor, A., Yedgar, S. & Gavish, B. Glycerol Decreases the Volume and Compressibility of Protein Interior. *Biochemistry-us.* **35,** 2061–2066 (1996).

115. Almagor, A., Priev, A., Barshtein, G., Gavish, B. & Yedgar, S. Reduction of Protein Volume and Compressibility by Macromolecular Cosolvents: Dependence on the Cosolvent Molecular Weight. *Biochimica et Biophysica Acta (BBA) - Protein Structure and Molecular Enzymology* **1382,** 151–156 (1998).

116. Suladze, S., Kahse, M., Erwin, N., Tomazic, D. & Winter, R. Probing Volumetric Properties of Biomolecular Systems by Pressure Perturbation Calorimetry (PPC) – The Effects of Hydration, Cosolvents and Crowding. *Methods. Biocalorimetry* **76,** 67–77 (2015).

117. Arns, L., Schuabb, V., Meichsner, S., Berghaus, M. & Winter, R. The Effect of Natural Osmolyte Mixtures on the Temperature-Pressure Stability of the Protein RNase A. *Zeitschrift für Physikalische Chemie* **232,** 615–634 (2018).

118. Papini, C. M., Pandharipande, P. P., Royer, C. A. & Makhatadze, G. I. Putting the Piezolyte Hypothesis under Pressure. *Biophys. J.* **113,** 974–977 (2017).

119. Wang, S., Tate, M. W. & Gruner, S. M. Protein Crowding Impedes Pressure-Induced Unfolding of Staphylococcal Nuclease. *Biochimica et Biophysica Acta (BBA) - General Subjects* **1820,** 957–961 (2012).

120. Erlkamp, M., Grobelny, S. & Winter, R. Crowding Effects on the Temperature and Pressure Dependent Structure, Stability and Folding Kinetics of Staphylococcal Nuclease. *Phys. Chem. Chem. Phys.* **16,** 5965–5976 (2014).

121. Zhai, Y. & Winter, R. Effect of Molecular Crowding on the Temperature–Pressure Stability Diagram of Ribonuclease A. *ChemPhysChem* **14,** 386–393 (2013).

122. Al-Ayoubi, S. R., Schummel, P. H., Golub, M., Peters, J. & Winter, R. Influence of Cosolvents, Self-Crowding, Temperature and Pressure on the Sub-Nanosecond Dynamics and Folding Stability of Lysozyme. *Phys. Chem. Chem. Phys.* **19,** 14230–14237 (2017).

123. Chalikian, T. V. & Breslauer, K. J. On Volume Changes Accompanying Conformational Transitions of Biopolymers. *Biopolymers* **39,** 619–626 (1996).

124. Son, I., Shek, Y. L., Dubins, D. N. & Chalikian, T. V. Volumetric Characterization of Tri- *N* -Acetylglucosamine Binding to Lysozyme. *Biochemistry-us.* **51,** 5784–5790 (2012).

125. Kamiyama, T. & Gekko, K. Effect of Ligand Binding on the Flexibility of Dihydrofolate Reductase as Revealed by Compressibility. *Biochimica et Biophysica Acta (BBA) - Protein Structure and Molecular Enzymology* **1478,** 257–266 (2000).

126. Filfil, R. & Chalikian, T. V. Volumetric and Spectroscopic Characterizations of Glucose–Hexokinase Association. *FEBS Letters* **554,** 351–356 (2003).

127. Toleikis, Z., Cimmperman, P., Petrauskas, V. & Matulis, D. Determination of the Volume Changes Induced by Ligand Binding to Heat Shock Protein 90 Using High-Pressure Denaturation. *Anal. Biochem.* **413,** 171–178 (2011).

128. Petrauskas, V., Gylytė, J., Toleikis, Z., Cimmperman, P. & Matulis, D. Volume of Hsp90 Ligand Binding and the Unfolding Phase Diagram as a Function of Pressure and Temperature. *Eur. Biophys. J.* **42,** 355–362 (2013).

129. Toleikis, Z. *et al.* Volume of Hsp90 Protein–Ligand Binding Determined by Fluorescent Pressure Shift Assay, Densitometry, and NMR. *The Journal of Physical Chemistry B* **120,** 9903–9912 (2016).

130. Toleikis, Z., Cimmperman, P., Petrauskas, V. & Matulis, D. Serum Albumin Ligand Binding Volumes Using High Pressure Denaturation. *J. Chem. Thermodyn* **52,** 24–29 (2012).

131. Cinar, S. & Czeslik, C. Inhibitor and Peptide Binding to Calmodulin Characterized by High Pressure Fourier Transform Infrared Spectroscopy and Förster Resonance Energy Transfer. *Biochimica et Biophysica Acta (BBA) - Proteins and Proteomics* **1866,** 617–623 (2018).

132. Cinar, S. *et al.* A High Pressure Study of Calmodulin–Ligand Interactions Using Small-Angle X-ray and Elastic Incoherent Neutron Scattering. *Phys. Chem. Chem. Phys.* **20,** 3514–3522 (2018).

133. Oliva, R., Banerjee, S., Cinar, H. & Winter, R. Modulation of Enzymatic Activity by Aqueous Two-Phase Systems and Pressure – Rivalry between Kinetic Constants. *Chem. Commun.* **56,** 395–398 (2020).

134. Oliva, R., Banerjee, S., Cinar, H., Ehrt, C. & Winter, R. Alteration of Protein Binding Affinities by Aqueous Two-Phase Systems Revealed by Pressure Perturbation. *Scientific Reports* **10,** 8074 (2020).

135. Krishnamurthy, V. M. *et al.* Thermodynamic Parameters for the Association of Fluorinated Benzenesulfonamides with Bovine Carbonic Anhydrase II. *Chemistry, an Asian Journal* **2,** 94–105 (2007).

136. Myszka, D. G. *et al.* The ABRF-MIRG'02 Study: Assembly State, Thermodynamic, and Kinetic Analysis of an Enzyme/Inhibitor Interaction. *Journal of Biomolecular Techniques : JBT* **14,** 247–269 (2003).

137. Dudutienė, V. *et al.* 4-Substituted-2,3,5,6-Tetrafluorobenzenesulfonamides as Inhibitors of Carbonic Anhydrases I, II, VII, XII, and XIII. *Bioorganic & Medicinal Chemistry* **21,** 2093–2106 (2013).

138. Rutkauskas, K. *et al.* 4-Amino-substituted Benzenesulfonamides as Inhibitors of Human Carbonic Anhydrases. *Molecules* **19,** 17356–17380 (2014).

139. Skvarnavičius, G. *et al.* Protein–Ligand Binding Volume Determined from a Single 2D NMR Spectrum with Increasing Pressure. *The Journal of Physical Chemistry B* **125,** 5823–5831 (2021).

140. Baranauskienė, L. *et al.* Inhibition and Binding Studies of Carbonic Anhydrase Isozymes I, II and IX with Benzimidazo[1,2-c][1,2,3]Thiadiazole-7-Sulphonamides. *J. Enzyme Inhib. Med. Chem.* **25,** 863–870 (2010).

141. Cimmperman, P. *et al.* A Quantitative Model of Thermal Stabilization and Destabilization of Proteins by Ligands. *Biophys. J.* **95,** 3222–3231 (2008).

142. Sūdžius, J. *et al.* 4-[N-(Substituted 4-Pyrimidinyl)Amino]Benzene sulfonamides as Inhibitors of Carbonic Anhydrase Isozymes I, II, VII, and XIII. *Bioorg. Med. Chem.* **18,** 7413–7421 (2010).

143. Skvarnavičius, G. *et al.* High Pressure Spectrofluorimetry – a Tool to Determine Protein-Ligand Binding Volume. *J. Phys.: Conf. Ser.* **950,** 042001 (2017).

144. Skvarnavičius, G., Matulis, D. & Petrauskas, V. in *Carbonic Anhydrase as Drug Target: Thermodynamics and Structure of Inhibitor Binding* (ed Matulis, D.) 97–106 (Springer International Publishing, Cham, 2019).

145. Tanford, C. in *Advances in Protein Chemistry* (eds Anfinsen, C. B., Edsall, J. T. & Richards, F. M.) 1–95 (Academic Press, 1970).

146. Greene, R. F. & Pace, C. N. Urea and Guanidine Hydrochloride Denaturation of Ribonuclease, Lysozyme, $\alpha$-Chymotrypsin, and $\beta$-Lactoglobulin. *J. Biol. Chem.* **249,** 5388–5393 (1974).

147. Tanford, C. in *Advances in Protein Chemistry* (eds Anfinsen, C. B., Anson, M. L., Edsall, J. T. & Richards, F. M.) 121–282 (Academic Press, 1968).

148. Fan, Y. X., Zhou, J. M., Kihara, H. & Tsou, C. L. Unfolding and Refolding of Dimeric Creatine Kinase Equilibrium and Kinetic Studies. *Protein Science : A Publication of the Protein Society* **7,** 2631–2641 (1998).

149. Teale, F. W. J. & Weber, G. Ultraviolet Fluorescence of the Aromatic Amino Acids. *Biochem. J.* **65,** 476–482 (1957).

150. Royer, C. A. Probing Protein Folding and Conformational Transitions with Fluorescence. *Chem. Rev.* **106,** 1769–1784 (2006).

151. Vivian, J. T. & Callis, P. R. Mechanisms of Tryptophan Fluorescence Shifts in Proteins. *Biophys. J.* **80,** 2093–2109 (2001).

152. Matulis, D., Kranz, J. K., Salemme, F. R. & Todd, M. J. Thermodynamic Stability of Carbonic Anhydrase: Measurements of Binding Affinity and Stoichiometry Using ThermoFluor. *Biochemistry-us.* **44,** 5258–5266 (2005).

153. de Araujo, E. D. *et al.* High-Throughput Thermofluor-Based Assays for Inhibitor Screening of STAT SH2 Domains. *J. Pharmaceut. Biomed.* **143,** 159–167 (2017).

154. Zubrienė, A. *et al.* Measurement of Nanomolar Dissociation Constants by Titration Calorimetry and Thermal Shift Assay – Radicicol Binding to Hsp90 and Ethoxzolamide Binding to CAII. *Int. J. Mol. Sci.* **10,** 2662–2680 (2009).

155. Boivin, S., Kozak, S. & Meijers, R. Optimization of Protein Purification and Characterization Using Thermofluor Screens. *Protein Expres. Purif.* **91,** 192–206 (2013).

156. Ericsson, U. B., Hallberg, B. M., DeTitta, G. T., Dekker, N. & Nordlund, P. Thermofluor-Based High-Throughput Stability Optimization of Proteins for Structural Studies. *Anal. Biochem.* **357,** 289–298 (2006).

157. Reinhard, L., Mayerhofer, H., Geerlof, A., Mueller-Dieckmann, J. & Weiss, M. S. Optimization of Protein Buffer Cocktails Using Thermofluor. *Acta Crystallographica Section F: Structural Biology and Crystallization Communications* **69,** 209–214 (2013).

158. Kazlauskas, E., Petrauskas, V., Paketurytė, V. & Matulis, D. Standard Operating Procedure for Fluorescent Thermal Shift Assay (FTSA) for Determination of Protein–Ligand Binding and Protein Stability. *Eur. Biophys. J.* **50,** 373–379 (2021).

159. Cimmperman, P. & Matulis, D. in *RSC Biomolecular Sciences* (eds Podjarny, A., Dejaegere, A. P. & Kieffer, B.) 247–274 (Royal Society of Chemistry, Cambridge, 2011).

160. Petrauskas, V., Zubrienė, A., Todd, M. J. & Matulis, D. in *Carbonic Anhydrase as Drug Target: Thermodynamics and Structure of Inhibitor Binding* (ed Matulis, D.) 63–78 (Springer International Publishing, Cham, 2019).

161. Matulis, D., Baumann, C. G., Bloomfield, V. A. & Lovrien, R. E. 1-Anilino-8-naphthalene Sulfonate as a Protein Conformational Tightening Agent. *Biopolymers* **49,** 451–458 (1999).

162. Gedgaudas, M., Baronas, D., Kazlauskas, E., Petrauskas, V. & Matulis, D. Thermott: A comprehensive online tool for protein–ligand binding constant determination. *Drug Discovery Today* **27,** 2076–2079 (2022).

163. Newville, M., Stensitzki, T., Allen, D. B. & Ingargiola, A. *LM-FIT: Non-Linear Least-Square Minimization and Curve-Fitting for Python* Zenodo. 2014.

164. Williamson, M. P. Using Chemical Shift Perturbation to Characterise Ligand Binding. *Prog. Nucl. Mag. Res. Sp.* **73,** 1–16 (2013).

165. Fielding, L. NMR Methods for the Determination of Protein–Ligand Dissociation Constants. *Prog. Nucl. Mag. Res. Sp.* **51,** 219–242 (2007).

166. Piotto, M., Saudek, V. & Sklenář, V. Gradient-Tailored Excitation for Single-Quantum NMR Spectroscopy of Aqueous Solutions. *Journal of Biomolecular NMR* **2,** 661–665 (1992).

167. Vranken, W. F. *et al.* The CCPN Data Model for NMR Spectroscopy: Development of a Software Pipeline. *Proteins: Structure, Function, and Bioinformatics* **59,** 687–696 (2005).

168. Venters, R. A., Coggins, B. E., Kojetin, D., Cavanagh, J. & Zhou, P. (4,2)D Projection-Reconstruction Experiments for Protein Backbone Assignment: Application to Human Carbonic Anhydrase II and Calbindin D $_{28K}$. *Journal of the American Chemical Society* **127,** 8785–8795 (2005).

169. Ladbury, J. E. Calorimetry as a Tool for Understanding Biomolecular Interactions and an Aid to Drug Design. *Biochem. Soc. T.* **38,** 888–893 (2010).

170. Keller, S. *et al.* High-Precision Isothermal Titration Calorimetry with Automated Peak Shape Analysis. *Anal. Chem.* **84,** 5066–5073 (2012).

171. Zhao, H., Piszczek, G. & Schuck, P. SEDPHAT – A Platform for Global ITC Analysis and Global Multi-Method Analysis of Molecular Interactions. *Methods* **76,** 137–148 (2015).

172. Jones, E., Oliphant, T., Peterson, P., *et al. SciPy: Open Source Scientific Tools for Python* 2001.

173. Ravindra, R. & Winter, R. On the Temperature–Pressure Free-Energy Landscape of Proteins. *ChemPhysChem* **4,** 359–365 (2003).

174. Canchi, D. R. & García, A. E. Cosolvent Effects on Protein Stability. *Annu. Rev. Phys. Chem.* **64,** 273–293 (2013).

175. Hawley, S. A. Reversible Pressure-Temperature Denaturation of Chymotrypsinogen. *Biochemistry-us.* **10,** 2436–2442 (1971).

176. Makhatadze, G. I. Thermodynamics of Protein Interactions with Urea and Guanidinium Hydrochloride. *The Journal of Physical Chemistry B* **103,** 4781–4785 (1999).

177. Bushmarina, N. A., Kuznetsova, I. M., Biktashev, A. G., Turoverov, K. K. & Uversky, V. N. Partially Folded Conformations in the Folding Pathway of Bovine Carbonic Anhydrase II: A Fluorescence Spectroscopic Analysis. *Chembiochem* **2,** 813–21 (2001).

178. Borén, K., Grankvist, H., Hammarström, P. & Carlsson, U. Reshaping the Folding Energy Landscape by Chloride Salt: Impact on Molten-Globule Formation and Aggregation Behavior of Carbonic Anhydrase. *FEBS Letters* **566,** 95–99 (2004).

179. Hollowell, H. N., Younvanich, S. S., McNevin, S. L. & Britt, B. M. Thermodynamic Analysis of the Low- to Physiological-Temperature Nondenaturational Conformational Change of Bovine Carbonic Anhydrase. *J. Biochem. Mol. Biol.* **40,** 205–211 (2007).

180. Carlsson, U., Henderson, L. E. & Lindskog, S. Denaturation and Reactivation of Human Carbonic Anhydrases in Guanidine Hydrochloride and Urea. *Biochimica et Biophysica Acta (BBA) - Protein Structure* **310,** 376–387 (1973).

181. Wong, K.-P. & Tanford, C. Denaturation of Bovine Carbonic Anhydrase B by Guanidine Hydrochloride: A PROCESS INVOLVING SEPARABLE SEQUENTIAL CONFORMATIONAL TRANSITIONS. *J. Biol. Chem.* **248,** 8518–8523 (1973).

182. Uversky, V. N. & Ptitsyn, O. B. Further Evidence on the Equilibrium "Pre-molten Globule State": Four-state Guanidinium Chloride-induced Unfolding of Carbonic Anhydrase B at Low Temperature. *J. Mol. Biol.* **255,** 215–228 (1996).

183. Gupta, P., Mahlawat, P. & Deep, S. Effect of Disease-Linked Mutations on the Structure, Function, Stability and Aggregation of Human Carbonic Anhydrase II. *Int. J. Biol. Macromol.* **143,** 472–482 (2020).

184. Sasahara, K. & Nitta, K. Pressure-Induced Unfolding of Lysozyme in Aqueous Guanidinium Chloride Solution. *Protein Sci.* **8,** 1469–1474 (1999).

185. Baranauskienė, L., Matulienė, J. & Matulis, D. Determination of the Thermodynamics of Carbonic Anhydrase Acid-Unfolding by Titration Calorimetry. *J. Biochem. Biophys. Met.* **70,** 1043–1047 (2008).

186. Paketurytė, V. *et al.* Uncertainty in Protein–Ligand Binding Constants: Asymmetric Confidence Intervals versus Standard Errors. *Eur. Biophys. J.* (2021).

187. Linkuvienė, V. *et al.* Thermodynamic, Kinetic, and Structural Parameterization of Human Carbonic Anhydrase Interactions toward Enhanced Inhibitor Design. *Q. Rev. Biophys.* **51,** 1–48 (2018).

188. Kitahara, R., Hata, K., Li, H., Williamson, M. P. & Akasaka, K. Pressure-Induced Chemical Shifts as Probes for Conformational Fluctuations in Proteins. *Prog. Nucl. Mag. Res. Sp.* **71,** 35–58 (2013).

189. Wilton, D. J., Tunnicliffe, R. B., Kamatari, Y. O., Akasaka, K. & Williamson, M. P. Pressure-Induced Changes in the Solution Structure of the GB1 Domain of Protein G. *Proteins: Structure, Function, and Bioinformatics* **71,** 1432–1440 (2008).

190. Wilton, D. J., Kitahara, R., Akasaka, K., Pandya, M. J. & Williamson, M. P. Pressure-Dependent Structure Changes in Barnase on Ligand Binding Reveal Intermediate Rate Fluctuations. *Biophys. J.* **97,** 1482–1490 (2009).

191. Williamson, M. P., Akasaka, K. & Refaee, M. The Solution Structure of Bovine Pancreatic Trypsin Inhibitor at High Pressure. *Protein Sci.* **12,** 1971–1979 (2003).

192. Refaee, M., Tezuka, T., Akasaka, K. & Williamson, M. P. Pressure-Dependent Changes in the Solution Structure of Hen Egg-white Lysozyme. *J. Mol. Biol.* **327,** 857–865 (2003).

193. Asakura, T., Taoka, K., Demura, M. & Williamson, M. P. The Relationship between Amide Proton Chemical Shifts and Secondary Structure in Proteins. *Journal of Biomolecular NMR* **6,** 227–236 (1995).

194. Frye, K. J. & Royer, C. A. Probing the Contribution of Internal Cavities to the Volume Change of Protein Unfolding Under Pressure. *Protein Science : A Publication of the Protein Society* **7,** 2217–2222 (1998).

195. Monod, J., Wyman, J. & Changeux, J.-P. On the Nature of Allosteric Transitions: A Plausible Model. *J. Mol. Biol.* **12,** 88–118 (1965).

196. Andersen, B. F., Baker, H. M., Morris, G. E., Rumball, S. V. & Baker, E. N. Apolactoferrin Structure Demonstrates Ligand-Induced Conformational Change in Transferrins. *Cah. Rev. The.* **344,** 784–787 (1990).

197. Williams, D. H., Stephens, E. & Zhou, M. Ligand Binding Energy and Catalytic Efficiency from Improved Packing within Receptors and Enzymes. *J. Mol. Biol.* **329,** 389–399 (2003).

198. Celej, M. S., Montich, G. G. & Fidelio, G. D. Protein Stability Induced by Ligand Binding Correlates with Changes in Protein Flexibility. *Protein Sci.* **12,** 1496–1506 (2003).

199. Fradera, X. *et al.* Ligand-Induced Changes in the Binding Sites of Proteins. *Bioinformatics* **18,** 939–948 (2002).

200. Koch, C., Heine, A. & Klebe, G. Ligand-Induced Fit Affects Binding Modes and Provokes Changes in Crystal Packing of Aldose Reductase. *Biochimica et Biophysica Acta (BBA) - General Subjects* **1810,** 879–887 (2011).

201. Chen, C. R. & Makhatadze, G. I. Molecular Determinants of Temperature Dependence of Protein Volume Change upon Unfolding. *The Journal of Physical Chemistry B* **121,** 8300–8310 (2017).

202. Baker, B. M. & Murphy, K. P. Evaluation of Linked Protonation Effects in Protein Binding Reactions Using Isothermal Titration Calorimetry. *Biophys. J.* **71,** 2049–2055 (1996).

203. Baranauskienė, L. & Matulis, D. Intrinsic Thermodynamics of Ethoxzolamide Inhibitor Binding to Human Carbonic Anhydrase XIII. *BMC biophys.* **5,** 12 (2012).

204. Morkūnaitė, V. *et al.* Intrinsic Thermodynamics of Sulfonamide Inhibitor Binding to Human Carbonic Anhydrases I and II. *J. Enzym. Inhib. Med. Ch.* **30,** 204–211 (2015).

205. Millero, F. J., Hoff, E. V. & Kahn, L. The Effect of Pressure on the Ionization of Water at Various Temperatures from Molal-Volume Data1. *J. Solution Chem.* **1,** 309–327 (1972).

206. Neuman, R. C., Kauzmann, W. & Zipp, A. Pressure Dependence of Weak Acid Ionization in Aqueous Buffers. *The Journal of Physical Chemistry* **77,** 2687–2691 (1973).

207. Olofsson, G. & Hepler, L. G. Thermodynamics of Ionization of Water over Wide Ranges of Temperature and Pressure. *J. Solution Chem.* **4,** 127–143 (1975).

208. Kitamura, Y. & Itoh, T. Reaction Volume of Protonic Ionization for Buffering Agents. Prediction of Pressure Dependence of pH and pOH. *J. Solution Chem.* **16,** 715–725 (1987).

209. Kauzmann, W., Bodanszky, A. & Rasper, J. Volume Changes in Protein Reactions. II. Comparison of Ionization Reactions in Proteins and Small Molecules. *Journal of the American Chemical Society* **84,** 1777–1788 (1962).

210. Liljas, A. Carbonic Anhydrase under Pressure. *IUCrJ* **5,** 4–5 (2018).

211. Singh, H. *et al.* The Active Site of a Prototypical "Rigid" Drug Target Is Marked by Extensive Conformational Dynamics. *Angewandte Chemie International Edition* (2020).

212. Le Noble, W. J. & Kelm, H. Chemistry in Compressed Solutions. *Angewandte Chemie International Edition in English* **19,** 841–856 (1980).

213. Bonetti, G., Vecli, A. & Viappiani, C. Reaction Volume of Water Formation Detected by Time-Resolved Photoacoustics: Photoinduced Proton Transfer between o-Nitrobenzaldehyde and Hydroxyls in Water. *Chem. Phys. Lett.* **269,** 268–273 (1997).

214. Čapkauskaitė, E. *et al.* Thiazole-Substituted Benzenesulfonamides as Inhibitors of 12 Human Carbonic Anhydrases. *Bioorg. Chem.* **77,** 534–541 (2018).

215. McCord, R. W., Blakeney, E. W. & Mattice, W. L. Conformational Changes Induced in Ionized Poly(L-arginine) and Poly(L-histidine) by Sodium Dodecyl Sulfate. *Biopolymers* **16,** 1319–1329 (1977).

216. Scholtz, J. M. *et al.* Calorimetric Determination of the Enthalpy Change for the Alpha-Helix to Coil Transition of an Alanine Peptide in Water. *Proceedings of the National Academy of Sciences* **88,** 2854–2858 (1991).

217. Yang, A.-S. & Honig, B. Free Energy Determinants of Secondary Structure Formation: I. α-Helices. *J. Mol. Biol.* **252,** 351–365 (1995).

218. Lopez, M. M., Chin, D.-H., Baldwin, R. L. & Makhatadze, G. I. The Enthalpy of the Alanine Peptide Helix Measured by Isothermal Titration Calorimetry Using Metal-Binding to Induce Helix Formation. *Proceedings of the National Academy of Sciences* **99,** 1298–1302 (2002).

219. Wernersson, E. *et al.* Effect of Association with Sulfate on the Electrophoretic Mobility of Polyarginine and Polylysine. *The Journal of Physical Chemistry B* **114,** 11934–11941 (2010).

220. Satake, I. & Yang, J. T. Interaction of Sodium Decyl Sulfate with Poly(L-ornithine) and Poly(L-lysine) in Aqueous Solution. *Biopolymers* **15,** 2263–2275 (1976).

221. Satake, I. & Yang, J. T. Effect of Chain Length and Concentration of Anionic Surfactants on the Conformational Transitions of Poly(L-ornithine) and Poly(L-lysine) in Aqueous Solution. *Biochem. Bioph. Res. Co.* **54,** 930–936 (1973).

222. Mattice, W. L., McCord, R. W. & Shippey, P. M. Disorder–Order Transitions Induced in Anionic Homopolypeptides by Cationic Detergents. *Biopolymers* **18,** 723–730 (1979).

223. Hayakawa, K., Murata, H. & Satake, I. Conformational Change of Poly(L-lysine) and Poly(L-ornithine) and Cooperative Binding of Sodium Alkanesulfonate Surfactants with Different Chain Length. *Colloid Polym. Sci.* **268,** 1044–1051 (1990).

224. Yan, J. F., Vanderkooi, G. & Scheraga, H. A. Conformational Analysis of Macromolecules. V. Helical Structures of Poly-L-aspartic Acid and Poly-L-glutamic Acid, and Related Compounds. *The Journal of Chemical Physics* **49,** 2713–2726 (1968).

225. Matulis, D. & Bloomfield, V. A. Thermodynamics of the Hydrophobic Effect. II. Calorimetric Measurement of Enthalpy, Entropy, and Heat Capacity of Aggregation of Alkylamines and Long Aliphatic Chains. *Biophys. Chem.* **93,** 53–65 (2001).

226. Matulis, D. Thermodynamics of the Hydrophobic Effect. III. Condensation and Aggregation of Alkanes, Alcohols, and Alkylamines. *Biophys. Chem.* **93,** 67–82 (2001).

227. Matulis, D. & Bloomfield, V. A. Thermodynamics of the Hydrophobic Effect. I. Coupling of Aggregation and pKa Shifts in Solutions of Aliphatic Amines. *Biophys. Chem.* **93,** 37–51 (2001).

228. Skvarnavičius, G., Dvareckas, D., Matulis, D. & Petrauskas, V. Thermodynamics of Interactions Between Charged Surfactants and Ionic Poly(Amino Acids) by Isothermal Titration Calorimetry. *ACS Omega* **4,** 17527–17535 (2019).

229. Skvarnavičius, G., Toleikis, Z., Matulis, D. & Petrauskas, V. Denaturant- or ligand-induced changes in protein volume by pressure shift assay. *Phys Chem Chem Phys* (2022).

# Santrauka

## Įvadas

Racionalusis vaistų kūrimas yra paremtas žiniomis apie cheminio junginio (ligando) ir baltymo sąveikos fundamentaliuosius parametrus - jungimosi energiją, entalpiją, šiluminę talpą, bei ligando ir baltymo jungimosi sąlygotus tūrio pokyčius. Žinios apie šių parametrų dėsningumus ir galimybės juos prognozuoti yra ribotos, todėl šios disertacijos pagrindinis tikslas yra užpildyti tam tikras žinių apie baltymų-ligandų sąveikas spragas.

Baltymų ir ligandų sąveikos pasekoje atsirandantis tūrio pokytis yra tiriamas keletą dešimtmečių [9–12]. Nepaisant susidomėjimo, rezultatai nėra gausūs ir gauti tik keliose nenuoskliai susijusiose baltymų ir ligandų sistemose. Taip yra daugiausia todėl, kad tūrio pokyčio atsiradusio dėl baltymų-ligandų sąveikos ($\Delta V_\mathrm{b}$) nustatymas yra techniškai sudėtingas ir dažnai reikalauja aukšto slėgio metodų, kurie nėra prieinami daugumai tyrėjų. Šiame darbe pristatomas $\Delta V_\mathrm{b}$ tyrimas karboanhidrazių (CA) ir pirminių sulfonamidų sistemose. Šios sistemos yra plačiai tyrinėjamos nustatant įvairius sąveikos aspektus ir todėl gali būti pagrįstai laikomos modeline baltymo-ligando sistema $\Delta V_\mathrm{b}$ reikšmės tyrimui. Disertacijoje ištirtas guanidinio hidrochlorido (GdmHCl), dažnai naudojamos destabilizuojančios medžiagos slėginės denatūracijos tyrimuose, poveikis. CA XIII denatūracijos su GdmHCl eiga buvo nustatyta pirmą kartą. Trims CA izoformoms (CA I, CA II, CA XIII) įvertintas lydymosi slėgio ($p_\mathrm{m}$) poslinkio tiesiškumas didinant GdmHCl koncentraciją. Šių tyrimų rezultatai leido sukurti stipriai sąveikaujančių baltymų ir ligandų $\Delta V_\mathrm{b}$ nustatymo metodą, naudojant fluorescencinį slėginį poslinkį (*angl.* fluorescent pressure shift assay (FPSA)) esant skirtingoms GdmHCl ir ligandų koncentracijoms. Pirminių sulfonamidų ir CA izoformų I ir II $\Delta V_\mathrm{b}$ nustatymui panaudotas branduolių magnetinio rezonanso (BMR) aukštame slėgyje metodas. BMR duomenys taip pat atskleidė išsamią informaciją apie tai, kurias baltymo aminorūgštis paveikia ligando prisijungimas ir slėgis. Pirmą kartą buvo aprašytas metodas, skirtas nustatyti $\Delta V_\mathrm{b}$ iš vienos BMR spektrų serijos.

Dėl baltymų-ligandų sistemų sudėtingumo joninio ryšio susidarymo indėlis į šias sąveikas taip pat nėra iki galo ištirtas. Norint nustatyti joninio ryšio susidarymo indėlį į baltymų-ligandų sąveiką, buvo naudojama modelinė sistema, susidedanti iš priešingai įkrautų aminorūgščių homopolimerų ir paviršinio aktyvumo medžiagų (PAR). Alkilo grandinės pailgėjimo ir joninio ryšio sudarymo indėlis į entalpiją ir sąveikos šiluminę talpą pirmą kartą buvo nustatytas priešingai įkrautų poli(amino rūgščių) (PAR)-PAM sistemoje.

**Disertacijos tikslai:**

- Ištirti sulfonamidinių slopiklių prisijungimo sąlygotus tūrio pokyčus trijose karboanhidrazių šeimos baltymų sistemose.

- Ištirti jonų porų susidarymo termodinaminius parametrus baltymų-ligandų modelinėje sistemoje, sudarytoje iš krūvį turinčių poli(amino rūgščių) ir priešingą krūvį turničių paviršinio aktyvumo medžiagų.

**Disertacijos užduotys:**

- Tobulinti FPSA metodiką $\Delta V_b$ parametrų nustatymui stipriai sąveikaujančių baltymų-ligandų sistemose.

- Nustatyti tūrio pokyčius, atsirandančius dėl sąveikos tarp karboanhidrazės šeimos baltymų ir pirminių sulfonamidų, naudojant FPSA ir aukšto slėgio branduolių magnetinio rezonanso metodus.

- Įvertinti $\Delta V_b$ nustatymo metodų privalumus ir trūkumus.

- Remiantis literatūros žiniomis, pateikti $\Delta V_b$ verčių fizikinę interpretaciją CA-sulfonamidų sistemose.

- Atlikti izoterminės titravimo kalorimetrijos (*angl.* isothermal titration calorimetry (ITC)) eksperimentus su priešingai įkrautomis PAR-PAM sistemomis, varijuojant paviršiaus aktyviosios medžiagos grandinės ilgį, temperatūrą ir joninę jėgą.

- Išanalizuoti ir susisteminti ITC duomenis ir nustatyti krūvį turinčių cheminių grupių indėlį į bendrą sistemos sąveikos energiją.

**Ginamieji teiginiai:**

- Mažos GdmHCl koncentracijos tiesiškai sumažina karboanhidrazių lydimosi slėgių ($p_m$) vertes. Šiame koncentracijų intervale gautas $p_m$ vertes galima naudoti stipriai sąveikaujančių baltymų-ligandų $\Delta V_b$ nustatymui FPSA metodu.

- BMR aukštame slėgyje gali būti naudojamas norint nustatyti tūrio pokyčius dėl baltymų ir ligandų sąveikos, ne tik sąveikoms kurių greitis BMR laiko skalėje yra greitas, bet ir toms kurių greitis yra lėtas.

- Baltymo ir ligando sąveikos sąlygotus tūrio pokyčius galima apskaičiuoti iš vienos BMR spektrų serijos, tiriant vienos baltymo-ligando poros BMR spektrus užrašytus skirtinguose slėgiuose, jeigu sąveikos disociacijos konstanta yra panašiame verčių intervale kaip ir naudojama baltymo koncentracija.

- Karboanhidrazių sąveika su sulfonamidiniais slopikliais turi mažą neigiamą $\Delta V_b$ vertę.

- Įkrautos aktyviosios paviršiaus medžiagos jungiasi prie priešingai įkrautų PAR, sudarydamos jonų poras santykiu vienas su vienu tarp paviršiaus aktyviosios medžiagos joninės grupės ir įkrautų polimero aminorūgščių liekanų.

- Prie polimero prisijungusių paviršinio aktyvumo medžiagų alkilo grandinių sąveika tarpusavyje yra svarbus sąveikos veiksnys ir priklauso nuo grandinės ilgio.

- Jungimasis tarp paviršinio aktyvumo medžiagos joninės grupės ir PAR įkrautos liekanos skiriasi prieklausomai nuo įkrautų grupių cheminės struktūros, tuo tarpu alifatinės grandinės pailgėjimo sąlygota palankesnė sąveikos entalpija yra vienoda įvairiose PAA-PAM sistemose.

# Medžiagos ir metodai

## 1 Medžiagos

**Ligandai.** Šiame darbe naudotų karboanhidrazių slopiklių struktūros yra pavaizduotos paveikse 5.1. Junginiai: **1** – 4-Aminobenzensulfonamidas (sulfanilamidas) [135], **2** – p-karboksibenzensulfonamidas (karzenidas) [136], **3** – acetazolamidas buvo nusipirkti iš Sigma-Aldrich. Junginių: **4** – 4-pakeisto benzensulfonamido ir **5** – analogiško 2,3,5,6-tetrafluor benzensulfonamido sintezė yra aprašyta Dudutienės ir kt. [137]. Junginio **6** – 4-amino pakeisto benzensulfonamido sintezė yra aprašyta Rutkausko ir kt. [138].

**Baltymai.** $^{15}$N žymėtų baltymų, rekombinantinių žmogaus CA I ir CA II raišką ir biomasės auginimą atliko Vaida Juozapaitienė ir Aurelija Mickevičiūtė. Baltymai buvo išreikšti *E.coli* kamiene BL21(DE). Kultūra buvo auginta per naktį (10 mL) LB terpėje su 0.060 mM ZnCl$_2$, tuomet surinkta centrifūgavimo būdu sukant (5 min, 4000 × G), ir suspenduota M9 minimalioje terpėje su žymėtu amonio chloridu (42.2 mM (6 g L$^{-1}$) Na$_2$HPO$_4$, 22 mM (3 g L$^{-1}$) KH$_2$PO$_4$, 2 mM MgSO$_4$, 1 g L$^{-1}$ NH$_4$Cl ir metalų mišinys), 4 g L$^{-1}$ D-gliukozės, 0.06 mM ZnCl$_2$, ir 0.1 g L ampicilino. kultūra buvo auginta 37 °C temperatūroje, maišant 220 rpm apie 6 valandas iki optinis tankis ties 600 nm pasiekė nuo 0.6 iki 0.8. Baltymo raiška buvo indukuota su 0.20 mM izopropiltio-$\beta$-galaktozidu, taip pat pridėta 0.4 mM ZnCl$_2$. Kultūra buvo surinkta centrifūgavimo būdu praėjus 16 h po baltymo raiškos esant 20 °C temperatūrai ir maišant 220 rpm.

Nežymėtų baltymų raišką atliko Zigmantas Toleikis. Baltymų raiška buvo atlikta *E.coli* kamiene BL21(DE). Kultūra buvo auginta per naktį LB terpėje su 0.060 mM ZnCl$_2$.kultūra buvo auginta 37 °C temperatūroje, maišant 220 rpm apie šešias valandas iki optinis tankis ties 600 nm pasiekė nuo 0.6 iki 0.8. Baltymų raiška buvo indukuota su 0.20 mM izopropiltio-$\beta$-galaktozidu, taip pat pridėta 0.4 mM ZnCl$_2$. Kultūra buvo surinkta centrifūgavimo būdu praėjus 16 h po baltymo raiškos esant 20 °C temperatūrai ir maišant 220 rpm.

$^{15}$N žymėtus baltymus, CA I ir CA II, išgrynino Vilma Michailovienė taip kaip aprašyta publikacijoje [139].

Nežymėtas CA I, CA II ir CA XIII taip pat išgrynino Vilma Michailovienė. Tai buvo atlikta naudojantis giminingumo chromatografija naudojant imobilizuotus metalo jonus (chelatuojanti sefarozė Fast Flow) ir jonų mainų chromatografija (SP-sefarozės kolonėlė CA I ir CM-sefarozė CA II ir CA XIII) taip kaip aprašyta publikacijose [140–142].

# 2 Aukšto slėgio fluorescencijos spektroskopija

## 2.1 Slėginio poslinkio metodas

Fluorescent pressure shift assay (FPSA) yra skirtas baltymų-ligandų $\Delta V_b$ nustatymui ir yra paremtas baltymų stabilizavimu prieš slėginę denatūraciją ligandais [127–130, 143, 144].

FPSA eksperimentai kuriuose tirta CA I sąveika su junginiu **1**, ir CA II sąveika su junginiais **5** ir **4** buvo atlikti 20 mM HEPES buferiniame tirpale pH 7.5, su nuo 1.2 M iki 1.5 M GdmHCl ir 2 % tūrio DMSO. Baltymų koncentracija buvo 5 µM. Eksperimentai kuriuose tirta CA II sąveika su junginiais **3** ir **2** buvo atlikti 10 mM Bis-Tris buferiniame tirpale pH 7.0 su nuo 0 M iki 1.5 M GdmHCl ir 2 % tūrio DMSO. CA II koncentracija buvo 3 µM.

**Eksperimentinė įranga.** Aukšto slėgio fluorescencijos spektroskopijos eksperimentai buvo atlikti su ISS PC1 fotonus skaičiuojančiu spektrofluorimetru turinčiu aukšto slėgio celę. Stiklinė kiuvetė yra pripildoma su mėginiu ir uždengiama tvirta plėvele. Kiuvetė yra patalpinama į aukšto slėgio celę, kuri yra užpildoma dejonizuotu vandeniu. Aukšto slėgio celė turi safyrinius langus kurie atlaiko iki 380 MPa slėgį. Slėgis sukuriamas rankine hidrostatine pompa. Per celės korpusą yra išvedžioti vamzdeliai, jais teka vanduo iš termostato kuris užtikrina norimą temperatūrą. Šviesą generuoja ksenono arkinė lempa. Šviesa praeina pro monochromatorių ir 2 mm pločio plyšius.

**Baltymų išvyniojimas aukštu slėgiu.** Baltymų išvyniojimas slėgiu yra supaprastinamas kaip grįžtamas dviejų būsenų virsmas tarp natyvios (N) ir išsivyniojusios (U) būsenų:

$$N \rightleftharpoons U \tag{14.1}$$

Kaip aprašyta Tanford [145], dviejų būsenų virsmui, kuriame abi stadijos turi išskirtinį fluorescencijos profilį, bendras ryšys tarp fluorescencijos ir slėgio gali būti išreiškiamas lygtimi:

$$f(p) = f_s(p - p_0) + f_N + \frac{f_U - f_N}{1 + \exp(\Delta G_u^\circ / RT)} \qquad (14.2)$$

Čia, $f_N$ ir $f_U$ yra fluorescencijos parametrai reiškiantys N ir U baltymo formas. Šie parametrai šiame darbe atitinka triptofano fluorescencijos spektro masių centrą ($\lambda_{csm}$). $f_s$ tai parametras kuris apibrėžia nedidelį, tiesinį fluoresencijos poslinkį nuo slėgio, kuris gali būti stebimas dėl fluoroforo vidinių reiškinių. Lygtyje (14.2) $R$ yra universalioji dujų konstanta ir $T$ yra eksperimentinė temperatūra, o $\Delta G_u^\circ$ yra išsivyniojimo laisvoji Gibso energija ir jos priklausomybė nuo slėgio išreiškiama:

$$\Delta G_u^\circ = \Delta G_{u,0}^\circ + \Delta V_u(p - p_0) + \frac{\Delta \beta_u}{2}(p - p_0)^2 \qquad (14.3)$$

Čia, $\Delta G_{u,0}^\circ$ Yra Gibso laisvoji energija standartinėse sąlygose, $\Delta V_u$ yra tūrio pokytis atsirandantis baltymui išsivyniojant (išsivyniojimo tūris), $\Delta \beta_u$ yra suspaudžiamumo pokytis baltymui išsivyniojant. Pagal šį modelį, iš virsmo tarp natyvios ir išsivyniojusios būsenų vidurio taško, skaičiuotas baltymo lydymosi slėgis – $p_m$.

**Dozavimo modelis.** Šiame darbe $p_m$ vertės iš slėginės denatūracijos eksperimentų ir ligando koncentracija susietos lygtimi:

$$L_t = (\exp(-\Delta G_u^\circ / RT) - 1) \times \left( \frac{P_t}{2 \exp(-\Delta G_u^\circ / RT)} + \frac{1}{\exp(-\Delta G_b^\circ / RT)} \right), \qquad (14.4)$$

kur $L_t$ yra bendra ligando koncentracija ir $P_t$ yra bendra baltymo koncentracija. $\Delta G_b^\circ$ yra jungimosi laisvoji Gibso energija išreiškiama:

$$\Delta G_b^\circ = \Delta G_{b,0}^\circ + \Delta V_b(p - p_0) + \frac{\Delta \beta_b}{2}(p - p_0)^2, \qquad (14.5)$$

kur $\Delta G_{b,0}^\circ$ yra jungimosi laisvoji Gibso energija atmosferos slėgyje, $\Delta V_b$ yra jungimosi tūris ir $\Delta \beta_b$ yra suspaudžiamumo pokytis dėl ligando prisijungimo prie baltymo.

## 2.2 Baltymų išvyniojimas denatūrantais

**Matematinis modelis.** Denatūracijos su GdmHCl eksperimentuose fluorescencija su baltymo būsenų populiacijomis susieta naudojantis lygtimi [145]:

$$f([\text{GdmHCl}]) = f_N + \frac{f_U - f_N}{1 + e^{\Delta G_u^\circ / RT}}. \tag{14.6}$$

Čia $f_N$ ir $f_U$ atitinka eksperimentiškai matuojamus signalus, kurie atitinkamai priklauso išvyniotai ir natyviai būsenoms. $\Delta G_u^\circ$ yra išsyviniojimo laisvoji Gibso energija. Parametrai $f_U$ ir $f_N$ šioje disertacijoje yra triptofano fluorescencijos spektro masių centras ($\lambda_{\text{csm}}$).

**Eksperimentinė įranga ir sąlygos.** Cheminės denatūracijos eksperimentai buvo atlikti su Varian Cary Eclipse fluorescencijos spektrofluorimetru. Sužadinimo bangos ilgis buvo 295 nm. Eksperimentai buvo atlikti 10 mM Bis-Tris buferiniame tirpale su 2 % tūrio DMSO.

# 3 Terminio poslinkio metodas

**Procedūra ir įranga.** Terminio poslinkio metodui (*angl.* thermal shift assay (TSA)) šiame darbe naudotas Corbett Rotor-Gene 6000 (QIAGEN Rotor-Gene Q) instrumentas. Kiekvienai baltymo-ligando porai, toje pačioje GdmHCl koncentracijoje, buvo paruošta aštuonių mėginių serija (įskaitant ir kontrolę). Mėginiai buvo paruošti sumaišant pradinį tirpalą kuris susideda iš buferio (50 mM fosfato buferis pH 7.0 su 50 mM NaCl), GdmHCl (nuo 0.2 M iki 1.2 M), DMSO (2 % tūrio) ir 400 µM ligando. Taip pat paruoštas identiškas skiedimo tirpalas kuriame nebuvo tik ligando. Mėginiai 2-7 buvo paruošti atliekant seriją 2 kartų skiedimų (1.5 karto ligandui **2**). Skiedimas buvo atliktas sumaišant mėginį santykiu 1:1 su skiedimo tirpalu. Taip paruoštas mėginys buvo naudojamas sekančiam skiedimui. Taip įskaitant neskiestą mėginį ir skiedimo tirpalą gaunami aštuoni mėginiai su ligando koncentracijomis nuo 0 µM iki 400 µM. 10 µL kiekvieno mėginio buvo patalpinta į 0.2 mL mgintuvėlius. Atskiras tirpalas susidedantis iš to paties buferinio tirpalo bei priedų, bet su 20 µM CA II ir 200 µM 8-anilinonaftalensulfonrūgšties. 10 µL šio baltymo tirpalo buvo įpiltą į prieš tai ruoštus mėginius 0.2 mL mėgintuvėliuose. Taip gauti aštuoni mėginiai kiekviename iš kurių buvo nuo 0 µM iki 200 µM ligando ir 10 µM baltymo. Mėginiai sudėti į instru-

mentą ir kaitinti nuo $25\,°C$ iki $99\,°C$ vieno laipsnio per minutę greičiu. Fluorescencija kiekviename mėginyje buvo sužadinta su $(365 \pm 15)\,nm$ bangos ilgio šviesa, detekcija vyko $(460 \pm 15)\,nm$ bangos ilgyje.

**Duomenų analizė.** Neapdorotų duomenų analizė buvo atlikta Thermott programa. Dozavimo kreivės buvo analizuotos naudojant globalią analizę atliktą su Python "lmfit" paketu [163].

# 4 BMR aukštame slėgyje

**Eksperimentinės sąlygos.** BMR spektroskopijos neapdoroti duomenys buvo gauti Centre de Biochimie Structurale, University of Montpellier, Zigmanto Toleikio ir Christian Roumestand [139]. Baltymų mėginiai ($0.52\,mM$ ar $0.43\,mM$ CA I ir ($0.34\,mM$ CA II) buvo paruošti buferniame tirpale ($10\,mM$ Bis-Tris, $50\,mM$ NaCl, $10\,\%$ $D_2O$, $4\,\%$ DMSO, pH $6.2$ CA I ir pH $6.4$ for CA II) su skirtingomis ligandų **1** ar **6** koncentracijomis, kurie buvo ištirpinti gryname DMSO. BMR spektroskopija aukštame slėgyje buvo panaudota užrašyti 2D $^1H-^{15}N$ HSQC CA I ir CA II spektrams skirtinguose slėgiuose. $0.33\,mL$ baltymo tirpalo buvo įpilta į keramikinį mėgintuvėlį ($5\,mm$ išorinio ir $3\,mm$ vidinio diametro) iš Daedelus Innovations (Aston, PA, USA). Hidrostatinis slėgis mėginyje buvo sukeltas tiesiogiai magneto viduryje, per plieno vamzdelį pripildytą mažo tankio parafino aliejumi (Sigma), naudojantis Xtreme Syringe pompa iš Daedelus Innovations. 2D $^1H-^{15}N$ HSQC spektrai buvo užrašyti $25\,°C$ temperatūroje ir aštuoniuose skirtinguose slėgiuose nuo $5\,MPa$ iki $210\,MPa$, su Bruker AVANCE III $600\,MHz$ turinčiu $5\,mm$ Z-gradient TXI zondo galvą. Vandens nuslopinimas buvo atliktas WATERGATE metodu [166]. $^1H$ cheminiai poslinkiai buvo tiesiogiai atskaityti į vandens rezonansą ($4.7\,ppm$), o $^{15}N$ cheminiai poslinkiai buvo atskaityti netiesiogiai į $^{15}N/^1H$ absoliučių dažnių santykius. Vandens rezonansas kaip atskaitos taškas buvo panaudotas todėl, kad dažniausiai naudojamas atskaitos junginys DSS (natrio trimetilsililpropan sulfonatas) gali slopinti CA I ir CA II. Visi BMR eksperimentai buvo apdoroti su TOPSPIN programine įranga (Bruker), spektrai buvo analizuoti su CcpNmr Analysis V2 programa [167]. Pilnas vieno mėginio spektrų rinkinys, visame slėgių intervale, buvo užrašytas per maždaug $20\,h$ su CA I baltymu, ir $30\,h$ su CA II

baltymu.

Žmogaus CA I rezonansų priskirimas buvo nustatytas pagal literatūros duomenis [55] ir paimtas iš Biological Magnetic Resonance Data Bank (įrašo numeris: 4022, doi:10.13018/BMR4022). CA II rezonansų priskyrimu pasidalino Ronald A. Venter iš Duke University BMR centro [168].

# 5 Izoterminio titravimo kalorimetrija

**ITC eksperimentai.** ITC eksperimentuose, PAR koncentracija buvo išreikšta vienam monomerui. PAR koncentracijos buvo nustatytos taip kaip aprašyta ankstesnėje publikacijoje [8]. Dauguma eksperimentų buvo atlikta su TA Instruments Nano ITC kalorimetru kurio celės ir švirkšto tūriai yra atitinkamai $1.00\,mL$ ir $250\,\mu L$. Celė dažniausiai buvo užpildoma su nuo $0.5\,mM$ iki $2\,mM$ koncentracijos PAR tirpalu, o švirkštas su $3.25\,mM$ iki $20\,mM$ priešingą krūvį turinčios linijinės PAM tirpalu. Tipinis titravimas susidėjo iš dvidešimt penkių $10\,\mu L$ injekcijų su nemažesniais kaip $3\,min$ intervalais ir 200 sūkių per minutę maišymo greičiu. Bent $3\,min$ duomenys buvo surenkami prieš pirmąją injekciją, kad įsitikinti bazinės linijos stabilumu. Prieš eksperimentą, kalorimetro celė buvo nuplauta miliQ vandeniu ir praskalauta su celės mėginio tirpalu. Eksperimentinė temperatūra buvo nuo $13\,°C$ iki $61\,°C$. Eksperimentai buvo pakartoti nuo dviejų iki dešimties kartų.

**Duomenų analizė.** Duomenys buvo apdoroti su NITPIC programine įranga [170]. Entalpijos vertės visiems eksperimentams buvo nustatytos integruojant plotą po kreive, tai buvo padaryta naudojantis "trapz" funkcija iš SciPy Python 3 [172].

# Rezultatai

## 1 Tūrio pokyčio dėl baltymo-ligando jungimosi apskaičiavimas FPSA pagalba

### 1.1 Karboanhidrazių stabilumas GdmHCl tirpaluose ir aukštame slėgyje

Trijų karboanhidrazių (CA) izoformų, I, II ir XIII (CA I, CA II, CA XIII), fluroescencijos spektrai buvo registruoti tirpaluose su iki 3.75 M GdmHCl. GdmHCl koncentracijos didinimas sukėlė fluorescencijos spektrų poslinkius į raudonos šviesos pusę visoms CA izoformoms. $\lambda_{csm}$ vertės buvo apskaičiuotos bangos ilgiams nuo 320 nm iki 400 nm. Išsivyniojimo kreivės buvo gautos atidedant $\lambda_{csm}$ vertes nuo GdmHCl koncentracijos (paveikslas 10.2). CA I išvyniojimas su GdmHCl geriausiai buvo apibūdinamas su dviejų būsenų virsmo modeliu (lygtis (6.6)), CA II ir CA XIII atitiko trijų būsenų modelį su stabilia tarpine būsena (lygtis (6.8)). Atitinkami modeliai buvo pritaikyti duomenims. Modelių rezultatai pateikti lentelėje 10.1. Šios disertacijos duomenimis, tarpinė būsena pasižymi 354.2 nm $\lambda_{csm}$ verte tiek CA I, tiek CA XIII izoformoms. Virsmo iš tarpinės į išsivyniojusią būseną parametrai ($\Delta G^{\circ}_{0,I\rightarrow U}$, $m_{I\rightarrow U}$) taip pat yra panašūs abejoms izoformoms, tai reiškia jog tarpinė būsena yra mažiau specifiška CA izoformoms.

### 1.2 CA išvyniojimas slėgiu GdmHCl tirpaluose

CA I, CA II ir CA XIII buvo išvyniotos slėgiu, tirpaluose su skirtingomis GdmHCl koncentracijomis. Pavyzdinės išvyniojimo kreivės yra atvaizduotos paveiksle 10.3. GdmHCl koncentracijos iki 0.8 M stumia išsivyniojimo kreivę į žemesnio slėgio ruožą, nepakeičiant $f_N$ ir $f_U$ parametrų ar kreivės formos. Pridėjus 1 M GdmHCl išsivyniojimo kreivė praranda savo sigmoidinę formą ir prasideda ties didesne $\lambda_{csm}$ verte. Šie požymiai, kartu su išvyniojimo su GdmHCl rezultatais, rodo, kad šiose sąlygose nėra dominuojančios baltymo būsenos, visos trys būsenos egzistuoja vienu metu. Iš išvyniojimo su GdmHCl duomenų žinoma, kad esant 1.2 M GdmHCl dominuoja tarpinė būsena. Tarpinę būseną patvirtina ir išvyniojimo aukštu slėgiu duomenys, kadangi, šiose sąly-

gose išsivyniojimo kreivė atgauna savo sigmoidinę formą ir prasideda su $\lambda_{\text{csm}}$ verte panašia į tarpinės būsenos nustatyta išvyniojimo GdmHCl eksperimente ($f_i$). Visuose bandytose GdmHCl koncentracijose, CA II išvyniojimas slėgiu vyko kaip dviejų būsenų virsmas.

Paveiksle 10.4, $p_m$ vertės buvo atidėtos kaip priklausomybė nuo GdmHCl koncentracijos. Iš išsivyniojimo modelio kreivių vidurio taškų gautos lydymosi slėgio vertės, pavaizduotos paveiksle 10.4. Šių modelių parametrai yra pateikti lentelėje 10.2. Keturios globalios analizės buvo atliktos skirtingiems duomenų rinkiniams: CA I, CA II, CA II tarpinė būsena ir CA XIII pirmasis virsmas. $\Delta G^{\circ}_{\text{u,0}}$ ir $\Delta V_{\text{u}}$ parametrai buvo palikti kisti kiekvienam eksperimentui atskirai (lokalūs), kadangi $\Delta G^{\circ}_{\text{u,0}}$ turi kisti priklausomai nuo GdmHCl koncentracijos, o GdmHCl efektas $\Delta V_{\text{u}}$ parametrui nėra gerai ištirtas. $\Delta \beta_{\text{u}}$ parametras buvo fiksuotas ties 0.

Paveiksle 10.4, $p_m$ mažėja tiesiškai didinant GdmHCl koncentraciją iki pasiekiama 0.8 M koncentracija CA II baltymui ar 1.2 M CA I ir CA XIII baltymams. Šiame paveiksle $p_m$ vertės išsidėlioja toje pačioje tiesėje kaip ir išvyniojimo su GdmHCl atmosferos slėgyje vidurio taškai (juodi žymenys). Tai patvirtina tiesinę priklausomybę (lygtis (6.7)) šiame koncentracijų intervale. Tiesės buvo pratęstos į nulinę GdmHCl koncentraciją, taip suskaičiuotos $p_m$ vertės be GdmHCl ($p_m(\text{H}_2\text{O})$). $p_m$ vertės eksperimentuose su CA II, esant GdmHCl koncentracijoms didesnėms nei reikalingos pirmajam virsmui (1.0 M), yra toje pačioje tiesėje kaip ir antrojo virsmo atmosferiniame slėgyje taškas. Ši tiesė turi mažesnį polinkį ($-89\,\text{MPa/M}_{\text{[GdmHCl]}}$) lyginant su tiesėmis esant mažesnei GdmHCl koncentracijai ($-522\,\text{MPa/M}_{\text{[GdmHCl]}}$). Tiesių polinkiai yra tiesiogiai proporcingi denatūrantų $m$ vertėms.

## 1.3 Ligandų jungimosi prie CA GdmHCl tirpaluose matavimai TSA metodu

Tam, kad patikrinti kaip GdmHCl veikia CA sąveikos su slopikliais termodinaminius parametrus, TSA eksperimentai buvo atlikti tirpaluose su GdmHCl. CA II izoforma ir trys junginiai—**2**, **3**, **5**—turintys skirtingas jungimosi konstantas buvo ištirti GdmHCl koncentracijose iki 1.2 M. TSA yra pagrįstas baltymų termine denatūracija ir ligandų savybe stabilizuoti baltymus. GdmHCl pridėjimas sumažino CA II lydymosi temperatūros ($T_m$) vertes. CA II išvyniojimo tranzicijos negalėjo būti ste-

bimos GdmHCl koncentracijose didesnėse nei 1 M. Tokiose sąlygose $T_m$ vertės per žemos, kad jas būtų galima nustatyti. Tai sufleruoja, jog CA II, esant tiek GdmHCl, yra praradusi natyvią struktūrą jau kambario temperatūroje. Paveikslas 10.5 rodo CA II išsivyniojimo kreives su ir be ligando **5**. Duomenims pritaikytas matematinis modelis iš lygties (7.4) (pilnoje disertacijoje). Kuoment ligando **5** yra mažiau nei baltymo, matomi du išsivyniojimo pikai. Tokiais atvejais pritaikytas modelis iš šaltinio [154].

Dozavimo kreivės su 0.2 M ir 0.8 M GdmHCl pavaizduotos paveiksle 10.6. Analizės rezultatai pateikti lentelėje 10.3. Pridėjus iki 0.8 M GdmHCl Baltymų-ligandų jungimosi konstantos, $K_b$, paklaidų ribose liko panašios, $K_b$ vertės TSA metode gali kisti $\pm$ du kartus [186]. Rezultatai patvirtina, jog CA II jungimasis su sulfonamidais reikšmingai nesikeičia GdmHCl koncentracijose iki 1 M, rezultatai sutinka su literatūroje žinomais aktyvumo matavimais [180, 183].

## 1.4 Baltymų stabilizavimas ligandais prieš denatūraciją sukeltą GdmHCl ir aukšto slėgio.

CA II slėginės denatūracijos eksperimentai atlikti 1.2 M GdmHCl tirpale su ligandais **4** ir **5**, kurie su CA II jungiasi skirtingu stiprumu. Gautos išsivyniojimo kreivės atvaizduotos paveiksle 10.7. Esant 1.2 M GdmHCl koncentracijai, dominuoja tarpinė CA II būsena. Nesant pridėto ligando, stebimas dviejų būsenų virsmas tarp tarpinės ir pilnai išsivyniojusių būsenų. Kuomet yra pridedama ligando, išsivyniojimo kreivės paveiksle 10.7 A prasideda su žemesnėmis $\lambda_{csm}$ vertėmis iki kol pasiekiama $\lambda_{csm}$ vertė būdinga natyviai CA II. Esant didelėms ligando koncentracijoms, stebimas dviejų būsenų virsmas iš natyvios į pilnai išsivyniojusią būseną, t.y. slėginės denatūracijos metu nėra stebima stabili tarpinė būsena net ir esant aukštoms GdmHCl koncentracijoms. Paveiksle 10.7 B CA II $\lambda_{csm}$ vertės atmosferos slėgyje yra atidėtos kaip priklausomybė nuo ligando koncentracijos. $\lambda_{csm}$ vertės žemėja iki pasiekiama natyvaus CA II baltymo $\lambda_{csm}$ vertė. Vertės stabilizuojasi kuomet baltymas yra prisotintas ligandu. Eksperimento sąlygose, ligandas **5** jungiasi prie CA II stipriau nei ligandas **4**, todėl $\lambda_{csm}$ vertės su ligandu **4** stabilizuojasi esant didesnėms jo koncentracijoms. Iš šių eksperimentų galima daryt išvadą, kad stipriai besijungiantys ligandai stabilizuoja CA II struktūrą esant aukštoms GdmHCl koncentracijoms, kuriose CA II priešingu atvejų būtu

išsivyniojusi.

Denatūracijos su GdmHCl eksperimentai buvo atlikti esant skirtingoms ligando **3** koncentracijoms (paveikslas 10.8). Modelio aprašomo (6.8) lygtimi pritaikymo rezultatai yra pateikti lentelėje 10.4. Esant didesnėms ligando **3** koncentracijoms, reikėjo daugiau GdmHCl, kad denatūruoti CA II, tai pasireiškė $\Delta G^{\circ}_{0,N\rightarrow I}$ parametro kitimu. Skirtumas tarp CA II be ligando ir CA II-**3** komplekso $\Delta G^{\circ}_{0,N\rightarrow I}$ verčių yra panašus į jungimosi Gibbso energiją $(-43.5\,\text{kJ/M})$. Šio skyrelio rezultatai patvirtina jog ligandai stabilizuoja CA II prieš išvyniojimą ir su GdmHCl, ir su aukštu slėgiu. Todėl, slėginės denatūracijos eksperimentai esant ligandui gali būti atliekami didesnėse GdmHCl koncentracijose, tokiose kur baltymas be ligando būtų jau išsivyniojęs esant atmosferos slėgiui.

## 1.5 Tūrio pokyčio dėl baltymo-ligando jungimosi matavimas vienoje GdmHCl koncentracijoje

Atlikti dviejų baltymų-ligandų porų tyrimai taikant FPSA. CA I ir ligando **1** sąveika tirta esant 1.5 M GdmHCl, CA II ir **2** sąveika tirt esant 0.8 M GdmHCl. CA I-**1** tyrimo rezultatai pavaizduoti paveiksle 10.9. Iš dozavimo kreivės analizės apskaičiuoti šie parametrai: $\Delta G^{\circ}_{b} = 20\,\text{kJ}\,\text{mol}^{-1}$ ir $\Delta V_{b} = -27\,\text{mL}\,\text{mol}^{-1}$. $\Delta G^{\circ}_{b}$ vertė yra panaši į literatūroje žinomą [187]. Apskaičiuota $\Delta V_{b}$ vertė yra panaši į vertę gautą aukšto slėgio BMR metodu [139], kuri lygi $(-23 \pm 3)\,\text{mL}\,\text{mol}^{-1}$.

Ligando **2** jungimasis prie CA II buvo tirtas esant 0.8 M GdmHCl (paveikslas 10.10). Šiuo atveju, esant tai pačiai GdmHCl koncentracijai nebuvo įmanoma gauti išsivyniojimo kreivių pakankamai plačiame ligando koncentracijų intervale. Net 10 µM ligando koncentracija buvo pakankama paslinkti išsivyniojimo kreivę į nepasiekiamą slėgį. Ligandas **2** yra pakankamai silpnai besijungiantis $(K_{d} = 10\,\text{µM})$. Silpnas jungimasis ir didelis $p_{m}$ poslinkis sufleruoja didelę neigiamą $\Delta V_{b}$ vertę. Pritaikius modelį šios vertės apskaičiuotos kaip: $\Delta V_{b} = -48\,\text{mL}\,\text{mol}^{-1}$ ir $\Delta G^{\circ}_{b} = -25\,\text{kJ}\,\text{mol}^{-1}$.

## 1.6 $\Delta V_b$ verčių nustatymas iš eksperimentų su skirtinga GdmHCl koncentracija

Dėl prieš tai nustatytos, $p_m$ verčių tiesinės priklausomybės nuo GdmHCl koncentracijos, jos gali būti ekstrapoliuotos į sąlygas be GdmHCl, kad gauti $p_m$ vertes be GdmHCl ($p_m(H_2O)$). CA II išvyniojimo slėgiu eksperimentai buvo atlikti su ligandu **3** ir GdmHCl koncentracijomis nuo 0.35 M iki 1.20 M. Gautos $p_m$ vertės atvaizduotos paveiksle 10.11. Išsivyniojimo kreivėms buvo pritaikytas modelis naudojant tuos pačius apribojimus kaip ir CA II pirmajam virsmui skyriuje 1.2. Išsivyniojimo kreivių analizės rezultatai yra pateikti 10.5. Priklausomai nuo GdmHCl koncentracijos, $p_m$ vertės kito tiesiškai esant ligandui **3**, todėl buvo galima apskaičiuoti $p_m(H_2O)$ vertes. Įdomu tai, kad ligando **3** pridėjimas pakeitė $m$ vertes, ką galima matyti iš tiesių polinkio kampo. Iš suskaičiuotų $p_m(H_2O)$ verčių buvo gauta dozavimo kreivė, ji pateikta paveiksle 10.11 B. Iš dozavimo kreivės analizės gauta $\Delta V_b = -8\,\text{mL}\,\text{mol}^{-1}$. Neigiama $\Delta V_b$ vertė taip pat stebima ir iš $\Delta V_u$ verčių lentelėje 10.5. $\Delta V_u$ vertės CA II-**3** kompleksui buvo mažesnės nei CA II be ligando.

# 2 Aukšto slėgio BMR

## 2.1 CA II su ir be ligando NMR spektrai

BMR spektroskopija buvo panaudota trijų baltymų-ligandų porų (CA I-**1**, CA I-**6** ir CA II-**1**) sąveikai tirti. $^1\text{H}-^{15}\text{N}$ HSQC BMR spektrai (pav. 11.1) parodė, kad visų porų sąveikos greitis buvo lėtas (mainų greitis žymiai mažesnis nei rezonanso dažnių skirtumas). Viename spektre galima stebėti du vienos aminorūgšties signalus, vieną iš būsenos be ligando ir vieną iš su ligandu susijungusios būsenos, pvz. Tyr 194 signalas (pav. 11.2). Didėjančios ligandų koncentracijos (11.2 paveikslo kairė dalis) padidino smailės, atitinkančios ligandą prisijungusios CA I, intensyvumą. Ligandų koncentracijos padidėjimas nepakeitė smailių padėties. Dešinioji 11.2 paveikslo dalis rodo Tyr 194 smailės elgseną esant skirtingam slėgiui ir fiksuotai ligando koncentracijai. Didėjant slėgiui, ligandą prisijungusios būsenos smailės intensyvumas didėja ir abi smailės slenka išilgai $\delta(^1\text{H})$ ir $\delta(^{15}\text{N})$ ašims $^1\text{H}-^{15}\text{N}$ HSQC spektruose.

## 2.2 Tūrio pokyčio dėl CA I-ligando 1 sąveikos skaičiavimas

Tūrio pokytis jungiantis baltymui su ligandu pastovioje temperatūroje, $T$, yra

$$\Delta V_{\mathrm{b}} = \left(\frac{\Delta G_{\mathrm{b}}^{\circ}}{p}\right)_T \tag{14.7}$$

kur $p$ reiškia slėgį, o $\Delta G_{\mathrm{b}}^{\circ}$ yra standartinės (1 baro slėgis, dalyvaujančių medžiagų koncentracija $1\,\mathrm{mol}\,\mathrm{L}$, aktyvumo koeficientai lygūs 1) Gibso jungimosi energijos pokytis. Ši lygtis rodo, kad norėdami gauti $\Delta V_{\mathrm{b}}$, turime nustatyti $\Delta G_{\mathrm{b}}^{\circ}$ reikšmes esant skirtingam slėgiui. $\Delta G_{\mathrm{b}}^{\circ}$ reikšmes galima apskaičiuoti iš disociacijos konstantos ($K_{\mathrm{d}}$) reikšmių, naudojant lygtį $\Delta G_{\mathrm{b}}^{\circ} = \mathrm{R}T\ln K_{\mathrm{d}}$. Su ligandu susijungusio baltymo dalį ($\theta$) galima gauti iš smailių tūrių verčių. $\theta$ vertės buvo apskaičiuotos iš amidų kryžminių smailių, priklausančių būsenoms prisijungus ligandą ir ne, tūrių, naudojant lygtį (8.7).

Siekiant didesnio tikslumo, analizėje naudojamos kelios aminorūgščių smailės. Tolesnei analizei buvo atrinktos tik liekanos, kurios visame slėgio diapazone turėjo aiškias, nepersidengiančias smailes. CA I-**1** šios liekanos buvo: Ile 59, Gly 104, Gly 111, Leu 131, Tyr 194, Gly 196, Thr 208, Ile 211 ir His 243. CA I-**6** liekanos buvo: Gly 104, Gly 107, Gly 111, Ser 136, Gly 145, Tyr 194, Gly 196, Tyr 204, Thr 208. CA II-**1**: Ile 33, Gly 82, Phe 93, Trp 97, His 107, Ala 116, Val 142, Trp 208. Dauguma pasirinktų aminorūgščių yra arti CA izoformų ligandų prisijungimo kišenės. Tačiau greičiausiai dėl baltymo trimatės (3D) struktūros pertvarkymų jungiantis su ligandais, kai kurios tolimesnės aminorūgščių liekanos taip pat turėjo su ligandu susieto baltymo smailę $^1\mathrm{H}-{}^{15}\mathrm{N}$ HSQC spektre. Šių aminorūgščių rinkinių $\theta$ vertės buvo suvidurkintos į vieną reikšmę:

$$\theta = \frac{1}{n}\sum_{i}^{n}\theta(i). \tag{14.8}$$

Čia $\theta(i)$ yra $\theta$ vertė, apskaičiuota iš $i$-osios aminorūgšties smailių. Šios vidutinės soties reikšmės, apskaičiuotos pagal lygtį 14.8, buvo naudojamos visai tolesnei analizei.

Paveiksle 11.4 vidutinės baltymų įsotinimo reikšmės buvo pavaizduotos kaip priklausomybė nuo bendros ligando koncentracijos ($L_{\mathrm{t}}$).

$K_d$ reikšmės buvo apskaičiuotos esant skirtingam slėgiui iki $180\,\mathrm{MPa}$, atliekant duomenų nelinijinę regresinę analizę pagal modelį lygtyje (8.10). Šios $K_d$ reikšmės buvo transformuotos į $\Delta G_b^\circ$ reikšmes su lygtimi:

$$K_{eq} = \frac{[B]}{[A]} = \mathrm{e}^{-\Delta G^\circ RT} \tag{14.9}$$

ir atidėtos pagal slėgį 11.4 B paveiksle. $\Delta G_b^\circ$ reikšmės mažėjo tiesiškai didėjant slėgiui, tai reiškia, kad suspaudžiamumas yra nereikšmingas, todėl $\Delta V_b$ reikšmes galima apskaičiuoti iš tiesės aprašomos lygtimi (14.7) nuolydžio. Apskaičiuota CA I-**1** $\Delta V_b$ vertė lygi $(-23 \pm 3)\,\mathrm{mL\,mol^{-1}}$.

## 2.3  $\Delta V_b$ skaičiavimai iš vienos $^1\mathrm{H}-{}^{15}\mathrm{N}$ HSQC BMR spektrų serijos esant tai pačiai ligando koncentracijai ir varijuojant slėgį

Lėtųjų mainų režimas stebimas karboanhidrazėms CA I, CA II prisijungiant ligandus **1** ir **6** leido naudoti alternatyvų $K_d$ nustatymo būdą, naudojant vieną baltymo ir ligando koncentraciją. $K_d$ iš vieno spektro gali būti apskaičiuojamas išreiškiant $K_d = \frac{[P][L]}{[PL]}$ per ligandą prisijungusios ir laisvos baltymo būsenų santykį. Tai galima padaryti pertvarkant masės balanso lygtis:

$$P_t = [P] + [PL], \tag{14.10}$$
$$L_t = [L] + [PL].$$

Gaunama išraiška:

$$K_d = \frac{[P]}{[PL]} \left( L_t - \frac{P_t}{1 + \frac{[P]}{[PL]}} \right). \tag{14.11}$$

Šioje lygtyje baltymo be ligando ir su ligandu susijungusio baltymo $\frac{[P]}{[PL]}$ santykis gali būti pakeistas atitinkamos smailės intensyvumo (tūrio) santykiu ir tai veda į lygtį, naudojamą apskaičiuojant $K_d$ iš BMR spektro, gauto esant vienai baltymo ir ligando koncentracijai:

$$K_d = \frac{I_P}{I_{PL}} \left( L_t - \frac{P_t}{1 + \frac{I_P}{I_{PL}}} \right). \tag{14.12}$$

Norint įvertinti $K_d$ apskaičiavimo iš vieno $^1\text{H}-^{15}\text{N}$ HSQC spektro netikslumus, $K_d$ reikšmės iš kelių eksperimentų su skirtingomis ligandų koncentracijomis buvo apskaičiuotos iš spektrų skirtinguose slėgiuose, naudojant lygtį (14.12) (lentelė 11.1) ir palygintos su $K_d$ reikšmėmis iš titravimo atitikmenų (11.5 pav.). Tiksliausi rezultatai buvo apskaičiuoti iš spektrų su 0.70 mM ligando, kur egzistuoja panašus kiekis baltymo su ligandu ir baltymo be ligando.

## 2.4  $\Delta V_b$ verčių iš BMR eksperimentų palyginimas

Remiantis ankstesniame skyriuje aprašytu skaičiavimo metodu. $\Delta V_b$ buvo apskaičiuota CA I-**6** ir CA II-**1** baltymų-ligandų poroms. Rezultatai pateikti paveiksle 11.6. Iš tiesinio modelio pritaikymo paveiksle 11.6 apskaičiuotos $\Delta V_b$ vertės lygios $(-22 \pm 4)$ ml/mol CA I–**1** , $(-26 \pm 4)$ ml/mol CA I–**6** ir $(-28 \pm 4)$ ml/mol CA II –**1**. Paklaidos, pateiktos šalia $\Delta V_b$ verčių, rodo standartinį nuokrypį, kuris buvo įvertintas lyginant $\Delta V_b$ reikšmes esant skirtingoms pridėto ligando koncentracijoms. Baltymų ir ligandų porų jungimosi konstantos vertės išsidėsto ta pačia tvarka, kaip tikėtasi iš literatūros [187]. CA I-**1** $\Delta V_b$ reikšmė yra paklaidos ribose nuo tos, kuri nustatyta FPSA, esant 1.5 M GdmHCl (skyrius 1.5). Šiuo metu nėra kitų duomenų apie $\Delta V_b$ CA I-**6** arba CA II-**1** sistemose, tačiau šių porų $\Delta V_b$ verčių tvarka atitinka anksčiau pastebėtą koreliaciją tarp surišimo stiprumo ir $\Delta V_b$ [129].

## 2.5  Skirtingas baltymo ir baltymo-ligando komplekso atsakas į slėgį

BMR metodu galima pastebėti nedidelius baltymų būsenos populiacijų pokyčius [188]. Pasirinktų aminorūgščių $^1\text{H}$ ir $^{15}\text{N}$ cheminiai poslinkiai pateikti 11.7 paveiksle. Straipsnyje, paremtame šia disertacija [139], CA I aminorūgščių atsaką į slėgį suskirstėme į tris pagrindines kategorijas.

Kai kurios aminorūgštys, pvz., Ile 59 ir Tyr 204, parodė skirtingą tiesinį atsaką į slėgį ligandą prisijungusio ir laisvo baltymo būsenose. Šių aminorūgščių smailės turėjo didesnį cheminio poslinkio pokytį esant slėgiui nei visų aminorūgščių vidurkis. Šių aminorūgščių būsenos be ligando smailių cheminio poslinkio pokytis, $^{15}\text{N}$ dimensijoje, esant 210 MPa, buvo didesnis nei būsenos su ligandu. CA I-**1** komplekso Ile 59

$\Delta\delta$ ($^{15}$N) pokytis buvo maždaug dešimt kartų mažesnis nei būsenos be ligando, Tyr 204 atitinkamai 3 kartus mažesnis. Panašus elgesys buvo pastebėtas su CA II Ile 33 ir Phe 93 aminorūgščių liekanomis. Linijiniai cheminio poslinkio pokyčiai atsiranda dėl susivyniojusio baltymo struktūrinių svyravimų.

Arg 89 paveiksle 11.7 yra antrojo tipo atsako pavyzdys. Arg 89, Val 62, Leu 147 rodė didžiausią tiesinį $\Delta\delta$, tačiau jų atsakas į slėgį buvo panašus tiek CA I būsenoje susijungusioje su ligandu, tiek būsenoje be ligando. Šios tendencijos rodo, kad šiose srityse vyksta svyravimai aukštame slėgyje, tačiau jų nevaržo prie CA I prisijungęs junginys **1**. Val 62 poslinkis yra netiesinis iki 220 MPa slėgio. Netiesiškumas dažnai yra konformacinių pokyčių požymis ir galbūt šios aminorūgšties liekanos sužadintos būsenos populiacija padidėja esant aukštam slėgiui.

His 94 ir His 119 yra ypač svarbios šioje sistemoje. Šios aminorūgštys kartu su His 96 koordinuoja cinko jonus CA I ir CA II aktyviuose centruose. Šios aminorūgštys parodė trečiąjį atsako į aukštą slėgį tipą. Amido azoto $\Delta\delta$ vertės His 94 CA I-**6** komplekse ir His 119 CA I-**1** komplekse buvo šiek tiek didesnės esant aukštam slėgiui, palyginti su baltymo būsena be ligando. Šis padidėjimas rodo, kad peptidinės jungties dviplokščių kampų pokytis gali būti didesnis su ligandu susijungusioje būsenoje. Nors padidėjimas nebuvo aiškus CA I-**1** komplekso His 94 atvejui. Šių aminorūgščių cheminio poslinkio pokyčiai buvo artimi vidutiniams ($\Delta\delta$ ($^{15}$N = 0.4 ppm ties 210 MPa), todėl aminorūgštys nebuvo ypač jautrios slėgiui. Įdomus reiškinys buvo pastebėtas His 94 ir Tyr 204 protonų cheminiuose poslinkiuose. Didėjant slėgiui, su ligandu susijungusios būsenos poslinkiai judėjo link didesnių ppm verčių, priešingai nei CA I būsenos be ligandų. Toks elgesys gali reikšti, kad šių amido grupių vandenilio ryšiai pailgėja esant slėgiui su ligandu susijungusioje būsenoje ir trumpėja, kai ligando nėra [193].

# 3 Polimerų ir paviršinio aktyvumo medžiagų sąveika

Polimerų ir PAM poros, naudojamos šiame tyrime gali būti suskirstytos į dvi pagrindines grupes:

A Teigiamai įkrautas polimeras su neigiamai įkrautu PAM. Šios poros sudarytos iš teigiamą krūvį turinčių aminorūgščių homopolimerų

(poliarginino [poly(Arg$^+$)], polilizino [poly(Lys$^+$)], polironitino [poly(Orn$^+$)] ir neigiamai įkrautų PAM – skirtingo ilgio alkil sulfatų ir alkil sulfonatų (natrio oktil sulfatas, decil sulfatas, undecilsulfatas, dodecil sulfatas (SDS), oktil sulfonatas, nonil sulfonatas, ir decil sulfonatas).

B Neigiamai įkrautas polimeras su teigiamą krūvį turinčiais PAM. Šios poros sudarytos iš teigiamą krūvį turinčių amino rūgščių homopolimerų (poliasparto rūgšis [poly(Asp$^-$)], poliglutamo rūgštis [poly(Glu$^-$)]) ir teigiamai įkrautų PAM – skirtingo ilgio alkil aminų (decilamino, undecilamino, dodecilamino, ir tridecilamino).

## 3.1 Sąveikos stechiometrija ir joninės jėgos įtaka

Paveiksle 12.2 atvaizduoti neapdoroti ITC duomenys (**A, C**) ir izotermės (**B, D**) gautos tiriant SDS jungimąsi su poly(Arg$^+$) (**A, B**) ir dodecilamino jungimąsi su poly(Glu$^-$) (**C, D**) esant $T = 25\,°\text{C}$.

Eksperimentai atvaizduoti paveiksle 12.2 turėjo stechiometrijos parametrą $n$ apytikriai lygų vienam. Tai pasikartojo visiems eksperimentams atliktiems vandenyje. Sąveika tarp PAM ir PAR šilumos išskleidimu ar sugertimi iki krūvių neutralizacijos taško, po kurio stebimos tik skiedimo šilumos. Sąveikos tarp PAR ir PAM buvo tirtos keičiant NaCl koncentracijas. Duomenys paveiksle 12.3 rodo jog $50\,\text{mM}$ ir $200\,\text{mM}$ natrio chlorido vis labiau mažino sąveikos stechiometrijos parametrą $n$. NaCl koncentracijos virš $1\,\text{M}$ visiškai sustabdė SDS jungimąsi prie poly(Arg$^+$).

## 3.2 Jungimosi entalpija kaip PAM alifatinės grandinės funkcija

Tam, kad ištirti alifatinės grandinės reikšmę sąveikoje, buvo atliktos eksperimentų serijos naudojant PAM turinčius įvairaus ilgio alifatines grandines. Rezultatai atvaizduoti paveiksle 12.4 ir pateikti lentelėse 12.2, 12.3, 12.4, ir 12.5. Alkil sulfatų jungimosi prie teigiamo krūvio PAR entalpija beveik visada buvo teigiama, išskyrus oktilsulfato jungimąsi prie poly(Lys$^+$) ir poly(Orn$^+$). Atvirkščia, alkilaminų jungimosi prie poly(Asp$^-$) ir poly(Glu$^-$) sistema, pagrinde pasižymėjo teigiamomis jungimosi entalpijomis. Visos tirtos sistemos pasižymėjo jungimosi entalpijos priklausomybe nuo PAM grandinės ilgio. Paveikslo 12.4 **A**

ir **B** dalyse atvaizduota išmatuotų PAM-PAR sąveikos $\Delta H°$ verčių priklausomybė nuo PAM alifatinėje grandinėje esančių anglies atomų skaičiaus - $m$. $CH_2$ grupės pridėjimas prie hidrofobinės PAM grandinės turėjo neigiamą įnašą į sąveikos entalpiją. Šios priklausomybės buvo tiesinės, $CH_2$ grupės įnašas į įvairių PAM–PAR sistemų sąveiką, esant $25°C$, pateiktos lentelėje 12.1. Visų eksperimentų izotermių formos rodo aukštą kooperatyvumo laipsnį. Daugeliu atvejų reakcija tapo egzotermiškesnė, kuomet titravimas artėjo prie krūvio neutralizavimo taško. Tai nebuvo pastebėta endoterminėms sąveikoms, pvz., $C_{10}H_{21}NH_3^+$ prisijungime prie poly($Asp^-$) ir poly($Glu^-$), reakcija tapo labiau endoterminė link neutralizacijos taško. Kooperatyvumas buvo mažiau ryškus eksperimentuose, kuriuose alkilo sulfatas prisijungia prie poly($Arg^+$). Alkilsulfatų ir poly($Arg^+$) jungimasis pasižymėjo žymiai didesniu $\Delta H°$ ir statesne jungimosi izoterme nei visos kitos sąveikos. Šie skirtumai rodo, kad poly($Arg^+$)-$RSO_4^-$ sąveikoje krūvį turinčių grupių giminiškumas vaidina svarbesnį vaidmenį, todėl titravimo eiga skiriasi.

## 3.3 Sąveikos entalpijos priklausomybė nuo temperatūros

ITC eksperimentai su skirtingomis PAR-PAM poromis buvo atlikti įvairiuose temperatūrų diapazonuose. Krūvį turinčios PAM, prisijungimas prie priešingo krūvio PAR, aukštesnėje temperatūroje buvo vis labiau egzoterminis.

Entalpijos, kaip temperatūros funkcijos, grafikai buvo naudojami reakcijos pastovaus slėgio šiluminės talpos pokyčiui apskaičiuoti ($\Delta C_p^\circ$). Tai buvo atlikta taikant tiesinius modelius ir darant prielaidą, kad $\Delta C_p^\circ$ yra nepriklausoma nuo temperatūros tiriamame temperatūrų diapazone. Sistemose su poly($Glu^-$) ir poly($Asp^-$) $\Delta C_p^\circ$ vertės buvo neigiamesnės ilgesnių alifatinių grandinių alkilaminams (lentelės 12.4,12.5). Šiek tiek kitokios tendencijos pastebėtos $RSO_4^-$–poly($Arg^+$) sistemoje. Nustatyta $\Delta C_p^\circ$ vertė lygi $(-0.18\pm0.04)\,kJ/mol/K$ $C_8H_{17}SO_4^-$–poly($Arg^+$) sistemai. Padidintas grandinės ilgis padidino absoliučią $\Delta C_p$ vertę ir paklaidų ribose išliko panašus kitose ilgesnės grandinės alkilsulfatų serijose (lentelė 12.2).

## 3.4 Alkil sulfatų ir sulfoninių rūgščių jungimosi prie PAR skirtumai

Alkilo sulfato, prisijungusio prie poly(Arg$^+$), entalpijos buvo labiau neigiamos nei sulfoninių rūgščių, kai alifatinės grandinės ilgis tas pats. Duomenys rodo, kad sąveikos tarp poly(Arg$^+$) ir alkilsulfoninės rūgšties, kurios alifatinėje grandinėje yra $m$ anglies atomų entalpija, yra maždaug lygi sąveikos entalpijai tarp poly(Arg$^+$) ir alkilsulfato, turinčio vienu anglies atomu mažiau (pav. 12.8). Šis rezultatas rodo, kad paviršiaus aktyviosios medžiagos grandinės pailgėjimas dėl deguonies tarp sulfato sieros ir anglies atomų, atlieka panašų vaidmenį kaip papildoma CH$_2$ grupė alifatinėje grandinėje. Toks pokrypio kampas nepasitvirtino atliekant sulfonato prisijungimo prie kitų katijoninių PAR eksperimentų, kur jungimosi su poly(Lys$^+$) arba poly(Orn$^+$) entalpijos. Šiuose eksperimentuose entalpijos buvo artimos nuliui, todėl neaišku, ar tai anomalija, ar eksperimentinė klaida.

## 3.5 PAM jungimosi prie PAR pastovaus slėgio šiluminės talpos pokytis

$\Delta H^\circ$ temperatūros priklausomybės leido įvertinti sąveikų pastovaus slėgio šilumines talpas ($\Delta C_p^\circ$). Paveiksle 12.9 parodytos $\Delta C_p^\circ$ vertės, gautos taikant tiesinius $\Delta H^\circ$ priklausomybės nuo temperatūros modelius. Visi išmatuoti šiluminės talpos pokyčiai buvo neigiami ir padidėjo absoliučia verte padidinus PAM grandinės ilgį. $\Delta C_p^\circ$ priklausomybės nuo grandinės ilgio buvo tiesinės, išskyrus poly(Arg$^+$) sistemą. $\Delta C_p^\circ$-grandinės ilgio priklausomybei buvo pritaikytos tiesės, iš kurių polinkio kampų buvo apskaičiuotas papildomos CH$_2$ grupės įnašas į $\Delta C_p^\circ$ vertę. Šie įnašai buvo nuo $-0.10\,\mathrm{kJ\,mol^{-1}\,K^{-1}}$ iki $-0.061\,\mathrm{kJ\,mol^{-1}\,K^{-1}}$ (pav. 12.9). Reikšmės išsibarsčiusios paklaidų ribose, todėl galima priimti vidutinę reikšmę lygią $(-0.092 \pm 0.018)\,\mathrm{kJ\,mol^{-1}\,K^{-1}}$.

# Išvados

- GdmHCl tiesiškai sumažina CA I, CA II ir CA XIII $p_m$ vertes esant žemai denatūranto koncentracijai. Esant didesniam koncentracijos diapazonui, $p_m$ vertės keičiasi netiesiškai dėl GdmHCl sukelto išsivyniojimo, kuris gali vykti kaip dviejų būsenų (CA I) arba trijų būsenų (CA II, CA XIII) procesas.

- Naudojant FPSA skirtingose GdmHCl koncentracijose, galima nustatyti stipriai besijungiančių ligandų $\Delta V_b$, jei $p_m$ reikšmių pokyčiai yra tiesiniai tiriamame GdmHCl koncentracijų diapazone.

- Pirminiai sulfonamidai jungiasi prie CA I, CA II ir CA XIII su neigiama $\Delta V_b$ verte, o tai reiškia, kad jų prisijungimo konstanta yra didesnė esant didesniam slėgiui.

- Esant tinkamam mainų greičiui, baltymo-ligando jungimosi Gibso energiją galima nustatyti iš vieno $^1\text{H}-^{15}\text{N}$ HSQC NMR spektro. Šį metodą taikant įvairiuose slėgiuose galima santykinai greitai nustatyti $\Delta V_b$.

- Įkrautos paviršinio aktyvumo medžiagos jungiasi su priešingai įkrautomis poli(aminorūgštimis), sudarant jonų poras tarp paviršinio aktyvumo medžiagos "galvos" ir įkrautos aminorūgšties liekanos, santykiu – viena aktyviosios paviršiaus medžiagos molekulė prie vienos aminorūgšties šoninės grandinės.

- $\text{CH}_2$ grupės pridėjimas prie alifatinės paviršiaus aktyviosios medžiagos grandinės lemia neigiamesnę sąveikos entalpiją, kurios vertė yra panaši įvairioms priešingai įkrautų PAR-PAM modelinėms sistemoms.

- Poly($\text{Arg}^+$) pasižymi ypač stipria sąveika su alkil sulfatais ir alkilsulfoninėmis rūgštimis. Ši sąveika skiriasi nuo kitų PAR-joninių paviršinio aktyvumo medžiagų sąveikų.

# Curriculum vitae

**Išsilavinimas**

| | |
|---|---|
| 2017/10 – 2021/10 | Vilniaus universitetas, Gyvybės mokslų centras, cheminės inžinerijos doktorantūra. |
| 2010/09 – 2014/06 | Vilniaus universitetas, Chemijos fakultetas, chemijos **magistro** kvalifikacinis laipsnis. |
| 2010/09 – 2014/06 | Vilniaus universitetas, Chemijos fakultetas, biochemijos **bakalauro** kvalifikacinis laipsnis. |

**Darbo patirtis**

| | |
|---|---|
| 2021/11 – dabar | MTEP vadovas, UAB Bioapplications. |
| 2018/07 – 2021/10 | Jaunesnysis mokslo darbuotojas, Biotechnologijos institutas, Biotermodinamikos ir vaistų tyrimų laboratorija. |
| 2016/05 – 2017/10 | Jaunesnysis technologas, UAB "TEVA Sicor Biotech", Vilnius, Lietuva. |
| 2014/03 – 2016/05 | Laborantas, Biotechnologijos institutas, Biotermodinamikos ir vaistų tyrimų laboratorija. |

# Publikacijų sąrašas

## Į disertaciją įtrauktos publikacijos

- Skvarnavičius, G., Toleikis, Z., Grigaliūnas, M., Smirnovienė, J., Norvaišas, P., Cimmperman, P., Matulis, D. & V Petrauskas. High Pressure Spectrofluorimetry – a Tool to Determine Protein-Ligand Binding Volume. *J. Phys.: Conf. Ser.* **950,** 042001 (2017)

  Atlikau aukšto slėgio fluorimetrijos eksperimentus, išanalizavau duomenis.

- Skvarnavičius, G., Matulis, D. & Petrauskas, V. in *Carbonic Anhydrase as Drug Target: Thermodynamics and Structure of Inhibitor Binding* (ed Matulis, D.) 97–106 (Springer International Publishing, Cham, 2019)

  Atlikau auškto slėgio fluorimetrijos eksperimentus, išanalizavau duomenis.

- Skvarnavičius, G., Dvareckas, D., Matulis, D. & Petrauskas, V. Thermodynamics of Interactions Between Charged Surfactants and Ionic Poly(Amino Acids) by Isothermal Titration Calorimetry. *ACS Omega* **4,** 17527–17535 (2019)

  Atlikau ITC eksperimentus, išanalizavau duomenis, rašiau tekstą.

- Skvarnavičius, G., Toleikis, Z., Michailovienė, V., Roumestand, C., Matulis, D. & Petrauskas, V. Protein–Ligand Binding Volume Determined from a Single 2D NMR Spectrum with Increasing Pressure. *The Journal of Physical Chemistry B* **125,** 5823–5831 (2021)

  Analizavau $^1$H$-^{15}$N HSQC BMR duomenis, prisidėjau prie teksto rašymo.

- Skvarnavičius, G., Toleikis, Z., Matulis, D. & Petrauskas, V. Denaturant- or ligand-induced changes in protein volume by pressure shift assay. *Phys Chem Chem Phys* (2022)

  Atlikau eksperimentus ir išanalizavau duomenis. Parašiau didžiąją dalį teksto.

# Į disertaciją neįtrauktos publikacijos

- Toleikis, Z., Sirotkin, V. A., Skvarnavičius, G., Smirnovienė, J., Roumestand, C., Matulis, D. & Petrauskas, V. Volume of Hsp90 Protein–Ligand Binding Determined by Fluorescent Pressure Shift Assay, Densitometry, and NMR. *The Journal of Physical Chemistry B* **120,** 9903–9912 (2016)

  Prisidėjau prie $^1H - {}^{15}N$ HSQC BMR eksperimentų, analizavau duomenis.

# Pranešimai konferencijose

- <u>G. Skvarnavičius</u>, Z. Toleikis, P. Cimmperman, D. Matulis, V. Petrauskas. Investigating ligand binding induced changes in protein volume using high pressure spectrofluorimetry. The COINS 2018, Vilnius, 2018 m. Vasario 28 d. - Kovo 2 d. (žodinis pranešimas).

- <u>G. Skvarnavičius</u>, Z. Toleikis, D. Matulis, V. Petrauskas. Fluorescent pressure shift assay – a method to investigate volumetric properties of protein-ligand interaction. 15-oji Lietuvos biochemikų draugijos konferencija, 2018 m. biržerlio 26 - 29 d. Dubingiai, Lietuva (stendinis pranešimas).

- <u>G. Skvarnavičius</u>, D. Matulis, V. Petrauskas. Thermodynamics of ionic surfactant–poly(amino acid) interaction. Kalorimetrietage, Braunšveigas, 2019 m. birželio 12 - 14 d. (stendinis pranešimas).

- <u>G. Skvarnavičius</u>, Z. Toleikis, C. Roumestand, D. Matulis, V. Petrauskas. Protein-ligand Binding Volume by Fluorescent Pressure Shift Assay and NMR. 10th International Meeting on Biomolecules under Pressure. Dortmundas, 2019m. rugsėjo 29d. - spalio 3d. (stendinis pranešimas).

# UŽRAŠAMS